International Conference on Mechanical, Industrial and Materials Engineering 2015 (ICMIME2015)
11-13 December, 2015, RUET, Rajshahi, Bangladesh.

Paper ID: AM-01

SOUND SOURCE RECOGNITION FOR INTELLIGENT SURVEILLANCE

Md. Rokunuzzaman*[1], Lutfun Nahar Nipa[1], Tamanna Tasnim Moon[1], Shafiul Alam[1]
[1]Department of Mechanical Engineering, Rajshahi University of Engineering & Technology (RUET), Bangladesh.
*E-mail of the corresponding author: rzaman.mte@ruet.ac.bd

Abstract

In surveillance, most of the systems aiming to automatically detect abnormal situations are only based on visual clues while, in some situations, it may be easier to detect a given event using the audio information. A new platform for sustainable development of automatic surveillance is introduced based on sound recognition which gathers information of human behavior, activities and environmental changes. The present research deals with audio events detection in noisy environments for surveillance application. The increasing availability of forensic audio surveillance recordings covering days or weeks of time makes human audition impractical and error prone. The ability of a normal human listener to recognize objects in the environment from only the sounds they produce is extraordinarily robust even in adverse acoustic conditions. In this research, we have developed an intelligent surveillance system which recognizes sound sources and detect events. This system can cover large area which is cost efficient. Sound sources can be recognized by comparing the frequency of sounds. This proposed intelligent surveillance system can recognize different sound sources accurately in real time and pretty much quick.

Keywords: *intelligent surveillance; sound recognition; event detection*

1. Introduction

When the vision system is unable to detect events occurring at a high speed, sound is an important cue for perception. To become intelligent, systems or robots should have to understand situation, make decisions and interact accordingly. Vision system is susceptible to adverse conditions like fog, mist, rain, dark etc. In these conditions sound system can be very effective. If a camera can be made by an intelligent system to respond accordingly for specific sound recognition, an event can be detected instantly. If an intelligent sound system is introduced, it will be easy to detect an event of any unnatural sound for the operator and take actions accordingly. The perspective of using such a recognition system in surveillance and security applications is therefore possible, on the condition that sound class models could be learned and built at the place to control. Long-term audio surveillance recordings may contain speech information and also non-speech sounds such as environmental noise, audible warning and alert signals, footsteps, mechanical sounds, gunshots, and other acoustic information of potential forensic interest. Security system should focus on the robustness of the detection against variable and adverse conditions which is particularly important in surveillance applications. Research in the area of automatic surveillance systems is mainly focused on detecting abnormal events based on the acquired video information [1, 2]. In addition to the traditional video cameras, the use of audio sensors in surveillance and monitoring applications is becoming increasingly important. Audio based surveillance has been studied earlier for detecting various types of acoustic events such as human's coughing in the office environment [3], impulsive sounds like gunshot detection [4], glass breaks, explosions or door alarm [5].

Sound effected camera control is the technology to detect sound sources with the help of the installed sensors in a definite platform and orient the camera accordingly to the direction from where the sound is created or occurred [6, 7]. According to sound events camera movement is controlled and sound source is localized automatically [8, 9]. Our approach to sound classification is inspired by the human auditory system in that we extract auditory features as known from auditory scene analysis from the input signal [10]. At the highest level, all sound recognition systems contain two main modules feature extraction and feature matching [11] Feature extraction plays a very important in the sound recognition process. This is basically a process of dimension reduction or feature reduction as this process eliminates the irrelevant data present in the given input while maintaining important information [12]. The whole process is divided into two stages: training phase and testing phase. Detection is the first step of sound analysis

system and is necessary to extract the significant sounds before initiating the classification step. The classification stage uses a Gaussian Mixture Model classifier with classical acoustical parameters like MFCC [13]. This paper investigates techniques to recognize environmental sounds and their direction, with the purpose of using intelligent techniques in an autonomous mobile surveillance robot.

2. System architecture

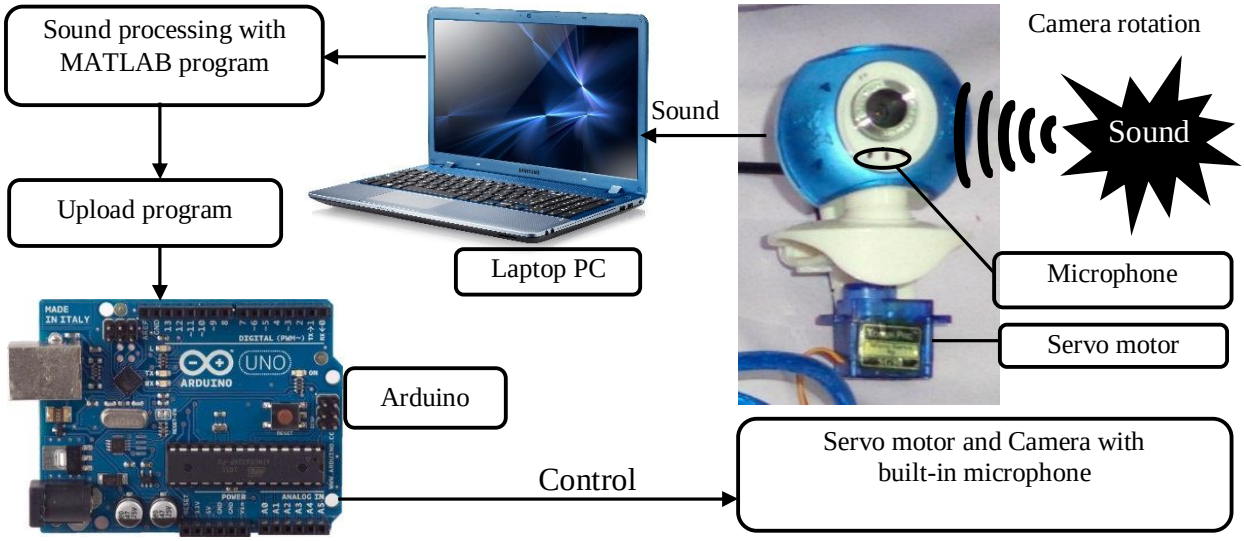

Figure 1: System architecture for development of intelligent surveillance

Figure 1 shows the system architecture for development of intelligent surveillance. When a sound event happens, then it is captured by built-in micro-phone of the camera. The sound signal is passed to the laptop for processing. The sound is processed by the algorithms discussed in section 1 and implemented with MATLAB. The program is then uploaded to an Arduino board. The output signal of the arduino is then fed to the servo motor input to control the movement of the camera toward the sound source.

2.1 Configuration & Position of Sound Source

Three sound input are taken for experiments and their position including camera position with specific angle and room layout are shown in Figure 2.

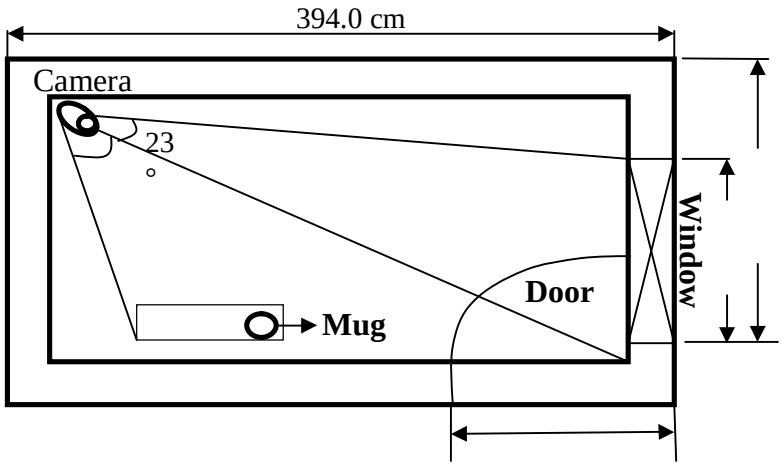

Figure 2: Project room layout

2.2 Intelligent surveillance algorithm

The intelligent surveillance algorithm is based on sound recognition and pointing of the camera towards the recognized sound to track objects. The sound recognition is based on feature matching of sound signals between trained signals and input sound. The feature extraction, training and matching is done through a series of operations namely MFCC computation, Vector Quantization and LBG Design algorithms [14]. Figure 3 shows the complete flow chart of the intelligent surveillance algorithm.

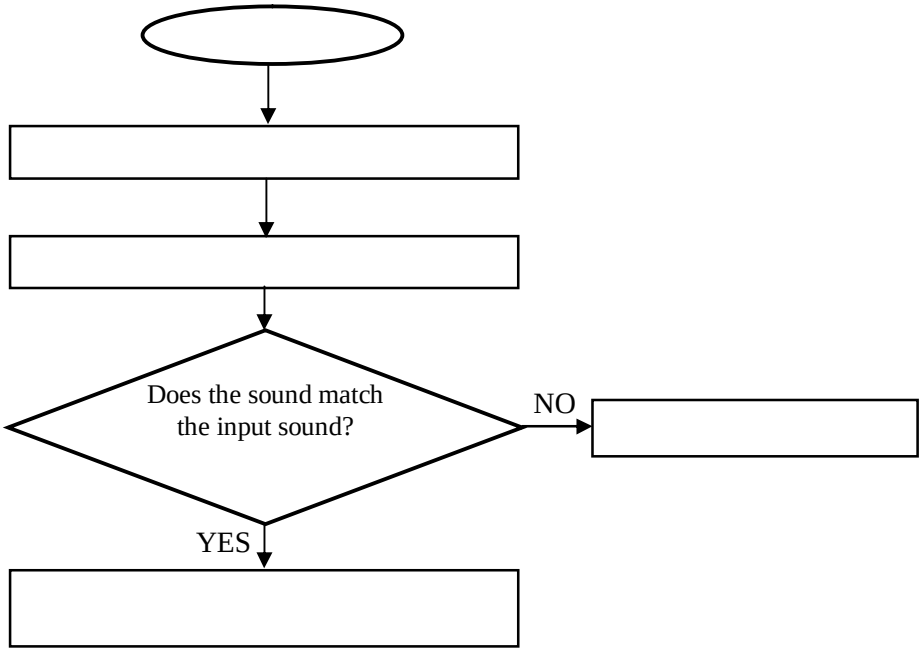

Figure 3: Flow chart of the intelligent surveillance algorithm

2.3 Camera movement

After recognition of sound, the recognized signal is transmitted from serial port of PC to Arduino. According to the configuration and position of sound source as shown in figure 2, the Arduino computes the required angle and rotates the camera with the help of a servomotor.

3. Results

Different types of sounds from objects have been tested for recognition. The results have been shown in Table1. For each type of sound from object, 5 trials have been taken and success rates have been calculated. The success rate is defined by Equation (1) as

$$Success\ rate\ (\%) = \frac{No.\ of\ trials\ of\ sucessful\ detection}{Total\ no.\ of\ trials} \times 100\% \quad \text{.....(1)}$$

Table 1: Success Rates of 3 different sounds

Sound from Object	Successful detection (Y/N)	Success rate (%)
Door	Yes	100
	Yes	
	Yes	
	Yes	
	Yes	
Window	Yes	80
	Yes	
	Yes	
	Yes	
	No	
Plastic mug	Yes	100
	Yes	
	Yes	
	Yes	
	Yes	

Table 2: Recognition time and Success Rates of different sounds

Objects	Average Response Time (s)	Success Rate (100 %)
Door	5	100
Window	5	80
Plastic Mug	5	100

The response times of camera in recognizing specific sound source and the success rates of sound source detection of the system are shown in Table 2. Sample sounds of door, window and mug were tested for several times and response time was recorded using stop watch. The obtained average response time is 5 seconds which means it will take 5 seconds to response after the actual sound detection from environment. Success rate of plastic mug is 100% as its sound is different from door and window. As the sound of door and window is similar so success rate of window was not 100%.

Moreover, it is tested that if two sounds occurred at the same time then sound of maximum intensity was detected. Such as when sound of door and mug or window and mug were occurred simultaneously then sound of mug was detected always due to its high intensity. Similarly when sound of door and window were recorded at the same time then door was detected as the sound of door has higher intensity than window.

Table 3: Identification rates of different sounds with code size book

Code size book	Hamming
1	57.14
2	85.7
4	90.47
8	95.24

16	100
32	100
64	100

The identification rates are shown when hamming window is used for framing in a linear frequency scale. Table 3 clearly shows that as codebook size increases, the identification rate for each of the three cases increases when code book size is 16, 32 and 64.

4. Conclusion

Hearing is an important part of normal human interaction, yet we understand surprisingly little about how our brains make sense of sound. This project is driven by the desire to understand how human auditory perception works. This is also to identify the nature of sound and focus the camera directly on the sound source. The time wasted to search the source of the sound will be saved in this project. So this project is more intelligent and efficient from conventional security system. However, the system can be far developed by reducing the response time of camera and more sound can be stored to the system so that it can recognize variety of sounds from the environment. Though the system should have been more robust, the performance of our developed system is quite satisfactory. This project can play an important role in intelligent security system.

References:

[1] Harma, A, McKinney, M. F, Skowronek, J, Automatic surveillance of the acoustic activity in our living environment, *IEEE International Conference on Multimedia and Expo*, July 2005:1-4.

[2] Michael Cowling. Non- speech environmental sound classification system for autonomous surveillance, *PhD Thesis, Griffith University, Gold Coast Campus*, March 2004

[3] Clavel, C, Ehrette, T, Richard, G, Events detection for an audio-based surveillance system, *IEEE International Conference on Multimedia and Expo*, July 2005: 1306-1309

[4]Valenzise, G, Gerosa, L, Tagliasacchi, M, Antonacci, F, Sarti, A, Scream and Gunshot Detection and Localization for Audio-Surveillance Systems, *IEEE Conference on Advanced Video and Signal Based Surveillance*, September 2007: 21-26

[5] Dufaux, A, Besacier, L, Ansorge, M, Pellandini, F, Automatic sound detection and recognition for noisy environment, *Proc. of the X European Signal Processing Conference*, September, 2000

[4] Brandstein, M. S, Adcock, J. E, Silverman, H. F, A localization-error-based method for microphone-array design, *Proceedings IEEE International Conference on Acoustics, Speech, and Signal Processing*, May 1996 ; 2: 901- 904

[6] Wang, H, Chu, P, Voice source localization for automatic camera pointing system in videoconferencing, *IEEE International Conference on Acoustics, Speech, and Signal Processing*, April 1997; 1: 187-190

[7] Cornaz, C, Hunkeler, U, Velisavljevic, V, An automatic speaker recognition system, *Digital Signal Processing Laboratory*, Federal Institute of Technology, Lausanne, Switzerland, 2003

[8] Allegro, S, Buchler, M, Launer, S, Automatic sound classification inspired by auditory scene analysis, *Eurospeech*, Aalborg, Denmark, September 2001

[9] Vacher, M, Istrate, D, Serignat, J. F, Sound detection and classification through transient models using wavelet coefficient trees, *12th European Signal Processing Conference*, September 2004

[10] Zhong-Xuan Yuan, Bo-Ling Xu, Chong-Zhi Yu, Binary Quantization of Feature Vectors for Robust Text-Independent Speaker Identification, *IEEE Transactions on Speech and Audio Processing*, January 1999; 7(1):70-78

[11] Gupta, S, Jaafar, J, Fatimah, W, Bansal, A, Feature extraction using MFCC, *Signal & Image Processing: An International Journal (SIPIJ)*, August 2013; 4(4): 101-108

[12] Soong, F, Rosenberg, E, Juang, B, Rabiner, L, A Vector Quantization Approach to Speaker Recognition, *AT&T Technical Journal*, March/April 1987; 66: 14-26

[13] Bala A, Kumar A, Birla N, Voice Command Recognition System based on MFCC and DTW, *International Journal of Engineering Science and Technology*, 2010; 2 (12): 7335-734

[14] Pal, A, Kumar and Sar Anup, An efficient codebook initialization Approach for LBG algorithm, *International Journal of Computer Science, Engineering and Applications (IJCSEA),* August 2011; 1(4):72-80

International Conference on Mechanical, Industrial and Materials Engineering 2015 (ICMIME2015)
11-13 December, 2015, RUET, Rajshahi, Bangladesh

Paper ID: AM-02

Effect of Feedforward Control on the Dynamics of a Zero-power Controlled Zero-compliance System

M. M. Zaglul Shahadat[1], T. Mizuno[1], Y. Ishino[2], and M. Takasaki[1]
[1] Graduate School of Science & Engineering, Saitama University
[2] Department of Mechanical Engineering, Saitama University
E-mail: shahadat230@yahoo.com

Abstract

A horizontal single-axis zero-compliance system using zero-power control is studied both analytically and experimentally. The zero-compliance system is obtained by series combination of positive and negative stiffness isolators of equal absolute stiffness, in which negative stiffness isolator is obtained by a zero-power controlled voice coil motor (VCM) as a system with zero-power control behaves as if it has negative stiffness. The positive stiffness isolator in the experimental system is obtained by a PD controlled VCM. Nevertheless, it is noticed that the transient responses of the experimental system are unpleasant and do not match the objective function of a zero-compliance system. In order to suppress these unpleasant transient responses, a feedforward (FF) control is added to the zero-power controller in this study. Several experiments have been conducted to measure the performance of the zero-compliance system with the feedforward control. It is observed that the experimental zero-compliance system suppresses the transient peak significantly without deteriorating the zero-power characteristic of the system; an improved dynamic of the experimental system are confirmed with feedforward control.

Keywords: *Zero-power control, Negative Stiffness, Infinite stiffness, Zero compliance.*

1. Introduction

A zero-compliance system possesses the characteristic of zero displacement to disturbance and is one of the effective approaches to suppress disturbances [1-2]. The integral control is the most usual approach to obtain zero-compliance to direct disturbance; however an integral control provides zero-compliance to disturbance at the cost of increasing of control current. Moreover, conventional integral controlled systems are not suitable for vibration control as they transmit directly the ground vibration to the isolation table. In addition, position accuracy in Hi-tech micro manufacturing and high precision measuring processes has turned into submicron even nanometer range from micrometer range during the last two decays. Thus researches on zero-compliance system have been the focuses of different research groups with increasing emphasis [2-4]. In these regards, the authors have proposed an effective approach that is a series combination of positive and negative stiffness isolators of equal absolute magnitude to obtain a zero-compliance system with the capability of suppressing ground vibrations as well [4].

In the previous study, the authors have implemented this concept (zero-compliance mechanism) to develop the vibration isolation systems, where proper negative stiffness controlled pneumatic actuator are used as negative stiffness isolators and connected in series with mechanical springs [5]. It is observed that the developed vibration isolation system suppresses both direct and ground vibration sufficiently; however, the system consumes power even in the steady states. In contrast, a zero-power controller which has power saving characteristic converges current into zero at steady states. In this study, a zero-power controlled system is employed instead as it behaves if it has negative stiffness. The zero-power control was originally invented to use in the active magnetic bearings [6-7]. Because a zero-power controlled system converges current to zero in the steady states, a zero-power control system needs a passive isolator and this study uses permanent magnet as passive isolator. Therefore, in principle of the proposed method, the zero-power controlled VCM is connected in series with a PD controlled VCM, to obtain a zero-compliance system, in which the ferromagnetic isolation platform of the developed system is placed in between two permanent magnets fixed to the base.

The series combination of negative and positive stiffnesses of equal magnitude is in theory a convenient and easy to understand method to realize a zero-compliance system [4]. However, the transient displacement of this zero-compliance system are often unpleasant and does not satisfy the objective function required to have for using in high-precision micro-manufacturing processes. The higher gain of the closed-loop system in designing

the controller is one of the approaches to overcome this problem but practically it is problematic [8]. Therefore, in this paper, feedforward (FF) control is added with zero-power controller to shorten the transient displacement as well as to improve the dynamics of the system. In a previous research, a feedforward control is added with negative stiffness control system used for vibration isolation [9]. In this research, feedforward control is added to the zero-power control system actuated with linear actuator (voice coil motor, VCM), and a new control network is considered so that the proposed controller does not hamper the power saving characteristic of a zero-power controller. This zero-power control system with feedforward control is connected in series with a positive stiffness system to obtain a zero-compliance system. Theoretically and experimentally, it is shown that the feedforward control with proposed control approach can suppress the transient displacement sufficiently.

2. Zero-compliance System

The aim of this section is to show how zero-compliance to direct disturbance can be realized by two series-connected isolators, where one of them has positive stiffness and the other has negative stiffness of equal absolute magnitude. Two series-connected isolators with stiffness coefficients, k_1 and k_2, provide a combined stiffness, k_c, (see Fig. 1) that can be expressed as follows:

$$k_c = \frac{k_1 k_2}{k_1 + k_2}. \tag{1}$$

This combined stiffness would be infinite if one of the isolators has negative stiffness and both of them are equal in absolute magnitude, which is shown in below:

$$|k_c| = \left| \frac{(-k_2)k_2}{-k_2 + k_2} \right| = \infty. \tag{2}$$

In a consequent, the relative displacement of the upper table (Fig. 1) against a direct disturbance becomes zero, which is shown as follows:

$$k_1 = -k_2 \Rightarrow \frac{F_0}{x_m - x_b} = -\frac{F_0}{x_u - x_m} \Rightarrow x_u - x_b = 0, \tag{3}$$

where F_0 is the disturbance applied on the upper table, and x_m, x_u and x_b denote the displacements of the middle mass, the upper table and the base, respectively. This study uses the concept mentioned above to develop a horizontal zero-compliance system to direct disturbance, in which zero-power control and PD (proportional derivative) control are applied to realize negative and positive stiffness isolators, respectively.

3. Negative stiffness isolator

Basic equation

To realize a negative stiffness isolator, a ferromagnetic stage of mass m between two permanent magnets is actuated by a VCM with zero-power control which is shown in Fig. 2. The permanent magnets provide bias force in the steady states, whereas the VCM (voice coil motor) provides control force to operate the stage along the horizontal direction (translation motion) in the transient states. It is assumed that there is no magnetic force on the stage at zero position; hence, the motion equation of the stage can be presented as follows:

$$m\ddot{x}(t) = k_s x(t) + k_i i(t) + f_d(t), \tag{4}$$

where x: displacement of the stage, k_s: gap-force coefficient of the permanent magnets, k_i: coefficient of the VCM, i: control current, f_d: disturbance acting on the stage. The Laplace transform of Eq. (4) is given in below:

$$X(s) = \frac{1}{s^2 - a}\left(bI(s) + dF_d(s)\right), \tag{5}$$

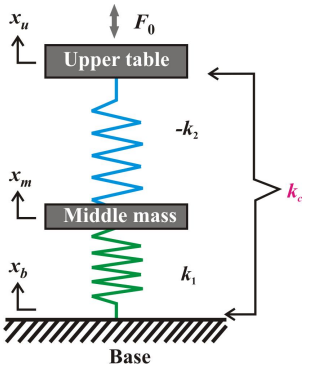

Fig. 1 Series connected isolators

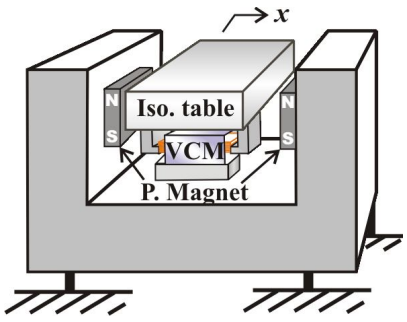

Fig. 2 Horizontal suspension system

where $a=\frac{k_s}{m}$, $b=\frac{k_i}{m}$, $d=\frac{1}{m}$, and each Laplace transform variable is denoted by its capital.

Zero-power controlled suspension

The basic characteristics of a zero-power control magnetic suspension system are shown in Fig. 3. The suspended object moves upward to a new equilibrium position after adding load, and in the steady states the control current converges to zero; the permanent magnets solely provide balancing force in the steady states. In this study, the same concept is applied to obtain a horizontal suspension system actuated by VCM, and a typical block diagram of a Zero-power controlled system (table) is shown in Fig. 4. The controller parameters are determined so that the system shown in Fig. 2 is stable under the zero-power controller which possesses the control current expressed by the following Laplace transform:

$$I(s)=-\frac{\left(P_d s+P_v s^2\right)}{s-P_i}X(s)\,, \tag{6}$$

where P_d, P_v and P_i denote the proportional derivative and local current integral feedback gains of the controller, respectively. Substituting Eq. (6) into Eq. (5) yields the transfer function representation of the system's dynamics under zero-power control as a function of the displacement to direct disturbance; the results is as follows:

$$\frac{X(s)}{F_d(s)}=\frac{d(s-P_i)}{s^3+s^2(bP_v-P_i)+s(bP_d-a)+aP_i}\,. \tag{7}$$

To estimate the steady-state displacements of the stage in response to a direct disturbance, it is assumed that the disturbance, F_d, is stepwise, and there is no ground vibration (X_0=0). The steady-state displacement of the stage is as follows:

$$\frac{x(\infty)}{F_0}=\lim_{s\to 0}\frac{X(s)}{F_d(s)}=\frac{-dP_i}{aP_i}=-\frac{1}{k_s}\,. \tag{8}$$

Equation (8) indicates that the stage has steady-state negative displacement in response to a direct disturbance, and this displacement depends on the gap-force coefficient of the permanent magnet attached in the system (see Fig. 2). Inherently, the stage with zero-power controller behaves as a negative stiffness system; and, in the principle of proposed approach, this negative stiffness system is connected in series with a positive stiffness isolator to obtain a zero-compliance system.

Similarly, to estimate the steady-state current consumption to the stage, the disturbance is assumed stepwise. Substituting Eq. (7) into Eq. (6) yields the current consumption behaviors in response to a direct disturbance; and at steady state, the result is as follows:

$$\frac{i(\infty)}{F_0}=\lim_{s\to 0}\frac{I(s)}{F_d(s)}=\frac{0}{aP_i}=0\,. \tag{9}$$

Equation (8) indicates that the steady-state current consumption to the stage is zero against a direct disturbance applied to it. Inherently, it is confirmed theoretically that the zero-power controlled horizontal system can hold a negative displacement without consuming power in the steady states.

Zero-power controlled suspension with Feedforward control

In this study, to improve the transient displacement as well as the dynamics of the zero-power controlled suspension system (see Fig. 2), a feedforward control is proposed with its original controller (zero-power). A block diagram of the proposed Zero-power controller which contains a Feedforward control is shown in Fig. 5. The displacement is assumed to be a feedback parameter, and the parameters of the proposed controller are determined so that the system is stable. The control current for the proposed controller is expressed by the

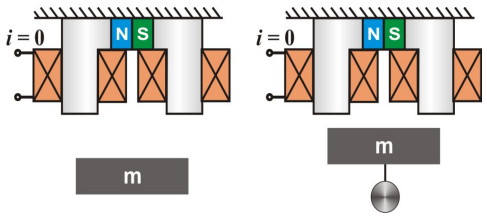

Fig. 3 Concept of zero-power control suspension

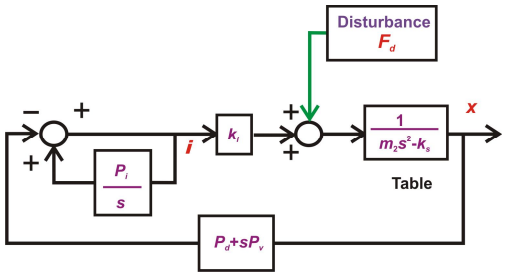

Fig. 4 Block diagram of zero-power control suspension

following Laplace transform:

$$\hat{I}(s) = \frac{-\left(P_d s + P_v s^2\right) X(s) + F_d H(s) s}{s - P_i}, \tag{10}$$

where $H(s)$ is transfer function for the feedforward controller and the other symbols have the same meaning as they did in the earlier sections. Substituting Eq. (10) into Eq. (5) yields the transfer function representation of the system's dynamics under the proposed zero-power control as a function of the displacement to direct disturbance; the results is as follows:

$$\frac{X(s)}{F_d(s)} = \frac{d\{s(1+k_i H) - P_i\}}{s^3 + s^2(bP_v - P_i) + s(bP_d - a) + aP_i}. \tag{11}$$

The dynamics shown by Eqs. (7) and (11) indicate that the characteristic equations of the zero-power controlled system with and without feedforward control are identical; however, the numerator parts that define the transient peak differ from each other. Moreover, by selecting appropriate feedforward gain, $H(s)$, in Eq. (11), the numerator parts with feedforward control can be made smaller compared to that of without feedforward control. It is theoretically confirmed that the transient peak as well as the dynamic behaviors of the zero-power controlled system improves sufficiently while a feedforward control involves in the controller with the gain given in below:

$$H(s) = -\frac{1}{k_i}. \tag{12}$$

In the same way mentioned in the earlier section, the steady-state displacement of the stage in response to a stepwise direct disturbance with respect to the proposed control approach is determined as follows:

$$\frac{x(\infty)}{F_0} = \lim_{s\to 0} \frac{X(s)}{F_d(s)} = \frac{-dP_i}{aP_i} = -\frac{1}{k_s}. \tag{13}$$

Eq. (13) states that, the adding of feedforward controller does not change the stiffness of the stage. It means, the stage has the same negative steady state displacements for both with and without feedforward control to the zero-power controller. In addition, substituting Eq. (11) into Eq. (10) yields the current consumption characteristics in response to a direct disturbance under the proposed control approach (zero-power with feedforward); and at steady state, the result is as follows:

$$\frac{\hat{i}(\infty)}{F_0} = \lim_{s\to 0} \frac{\hat{I}(s)}{F_d(s)} = \frac{0}{-aP_i^2} = 0. \tag{14}$$

Equation (14) indicates that the steady-state current consumption to the stage is zero; inherently, it is theoretically confirmed that a system with the proposed zero-power control approach does not hamper the characteristics that are associated to a conventional zero-power control system. However, the system utilizing the proposed control approach possesses an improved dynamic.

4. Experiment

Experimental zero-compliance system

With respect to the proposed zero-compliance system, a zero-power controlled system is connected in series with a positive stiffness system of equal stiffness. Therefore, the developed horizontal zero-compliance

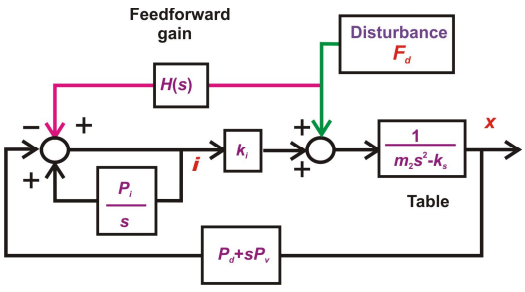

Fig. 5 Block diagram of zero-power with FF control suspension

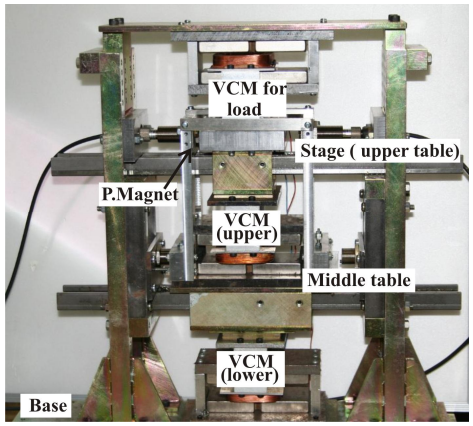

Fig. 6 Concept of zero-power control suspension

system consists of two suspension systems, in which the upper table (stage) suspended with zero-power controlled VCM behaves as a negative stiffness system and the middle table suspended with PD controlled VCM behaves as a positive stiffness system and they are connected in series. A photograph of the experimental zero-compliance system is shown in Fig. 6. The upper table is placed at the top of these two series connected isolators (VCMs) and the middle table is placed in between these two isolators which acts as a mechanical filter to suppress disturbances from base. Since the magnitude of positive stiffness in a PD controlled system varies with the varying of P_d gain, the positive stiffness of the middle table in the developed system is adjusted and made equal to magnitude of negative stiffness in the upper table by varying the P_d gain.

The two permanent magnets provide bias force to the upper table in the steady states, which are attached with respect to the middle and made of NdFeB with dimension 20 x 20 x 2 mm^3. The two VCMs which derive the upper table and middle table have nearly the same dimensions including permanent magnets. The average thrust coefficient of the VCMs is 16 N/A. Eddy-current gap sensors are used to detect the relative displacements of the tables. The power amplifiers manufactured by *Takasago Co. Ltd.* are used to supply current to the VCMs according to the command signals. The designed control algorithm is implemented with a digital controller DS 1105 manufactured by dSPACE^{TM}.

Experimental results:

Several experiments have been conducted to confirm the improvement of the dynamic behavior of the experimental zero-compliance system with feedforward control. The dynamic behaviors of the system with and without feedforward control are measured experimentally against direct static and dynamic disturbances. The direct disturbances were generated by an additional VCM that was mounted on the upper table and fixed with respect to the base. The VCM used to generate disturbances was operated independently from those used to control the motion of the tables. To find the comparative features between with and without feedforward control, the dynamic behaviors of the system are drawn in the same graph. The magnitude of disturbance and maximum stroke length in the upper table are respectively considered 5 N and ± 1.5 mm, respectively.

Figure 6 illustrates the comparative step responses of the upper table in the experimental zero-compliance system with and without feedforward control. In these experiments, the magnitude of disturbances applied to the

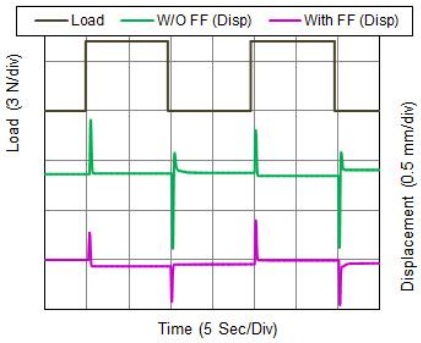

Fig. 7 Displacement of the upper table in the experimental system to stepwise direct disturbance

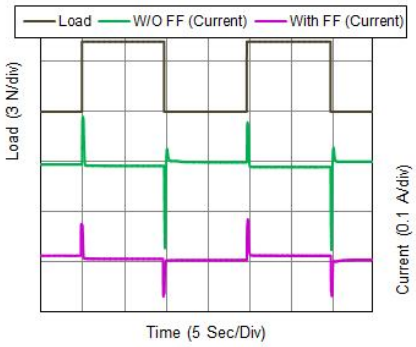

Fig. 8 Current to the upper actuator in the experimental system to stepwise disturbance

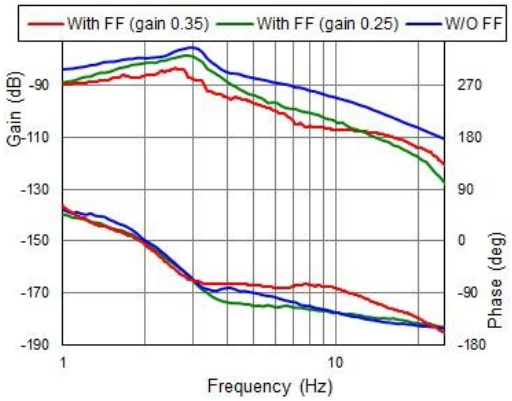

Fig. 9 Frequency response of the upper table's displacement to direct disturbance

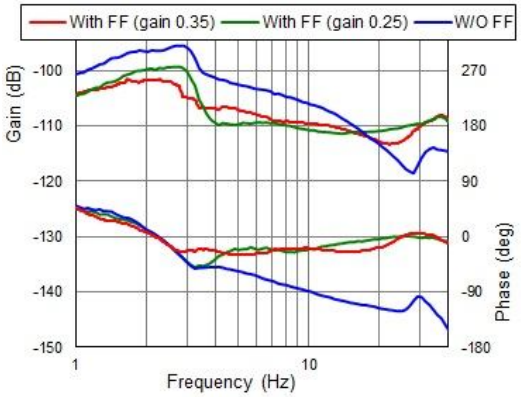

Fig. 10 Frequency response of current to upper actuator to direct disturbance

upper table is kept the same for both with and without feedforward control. It is observed that the upper table resumes its original position and maintains this position in the steady states; hence, zero-compliance characteristic in the experimental system is confirmed. Nevertheless, it is noticed that the step responses contain larger transient peaks (green line) at the beginning of step in and step out of step disturbance. This phenomenon occurs because active feedback control may not accomplish sufficiently fast responses as delays are contained in the control scheme. In this study, these unpleasant transient peaks are reduced by adding feedforward control with respect to disturbance in the original controller (pink line in Fig. 6), as the numerator part of the upper table's dynamics, Eq. (11), becomes smaller with feedforward control that is shown theoretically in section 3. Similarly, the behaviors of current consumption of the upper actuator in response to direct stepwise disturbance are measured with and without feedforward control and shown together in Fig. 7. Figure 7 reveals that the experimental zero-compliance system has the zero-power characteristic either with or without feedforward control. In addition, a shorter transient peak of control current is observed with feedforward control compared to without feedforward control for the same magnitude of disturbance.

The frequency responses to direct disturbance of the upper table in the experimental system with and without feedforward control are measured. The swept sinusoidal direct disturbance is applied on the upper table; the swept sinusoidal signal is generated by digital signal analyzer. The frequency responses of the upper table with and without feedforward control are shown together in Fig. 8 where the applied direct disturbances and the corresponding displacements of the upper table were the input and output signals, respectively; and log of output to input ratios are shown over the frequency of swept direct disturbance. The results showed that displacement gain is lowered sufficiently with feedforward control compared to that without feedforward control. Similarly, the control current to upper actuator in response to dynamic disturbances is measured experimentally and shown in Fig 9, in which the effect of feedforward control on the behavior of control current to upper actuator is illustrated. It is apparent in this figure that the behavior of current consumption with feedforward control improves sufficiently with shorter resonance peak.

5. Conclusions

An active zero-compliance system was developed by using a zero-power controlled VCM connected in series with a positive stiffness system. The behaviors of the developed system were investigated with and without feedforward control associated to disturbance. The experimental results showed that the experimental system with feedforward control, utilizing the control network proposed in this study, suppresses the transient peak of displacement and current consumption significantly compared to that without feedforward control. The reducing of transient peaks with feedforward control was also confirmed theoretically. In addition, the dynamic behaviors of the experimental zero-compliance system were enhanced by feedforward control.

6. References

[1] M. Jaensch, & Lamperth, M.U, "Development of a multi-degree-of-freedom micro positioning, vibration isolation and vibration suppression system," *Smart Materials and Structures*, 16(2), 409-417, 2007.

[2] T. Mizuno, T. Furushima, Y. Ishino, and M. Takasaki, "Realization of zero-compliance system by using displacement cancellation control," *Journal of Vibration and Control*, vol. 16(4), pp. 585-599, 2010.

[3] H. Yoshioka, Y. Takahashi, K. Katayama, T. Imazawa, and N. Murari, "An Active Micro-vibration Isolation System for Hi-Tech Manufacturing Facilities," *ASME Journal of Vibration and Acoustics*, vol. 123, pp. 269-275, 2001.

[4] T. Mizuno, M. Takasaki, D. Kishita, and K. Hirakawa, "Vibration Isolation System Combining Zero-power Magnetic Suspension with Springs", *Control Engineering Practice*, vol. 15, pp. 187-196, 2007.

[5] A.V. Sabnis, J. B. Dendy, and F. M. Schmitt, " A Magnetically Suspended Large Momentum Wheel", *Journal of Spacecraft and Rockets*, vol. 12, no. 7, pp. 420-427, 1975.

[6] M. Morishita, T. Azukizawa, S. Kanda, N. Tamura, and T. Yokoyama, "A new Maglev system for magnetically levitated carrier system", *IEEE Transaction of Vehicle Technology*, vol. 38, no. 4, pp. 230-236, 1989.

[7] T. Mizuno, M. Murashita, M. Takasaki, and Y. Ishino, "Pneumatic Three-axis Vibration Isolation System Using Negative Stiffness", *44th IEEE Conference on decision and Control*, 8254-8259, 2005.

[8] K. K. Hassan, "A note on the Robustness of High-gain-observer-based Controller to Unmolded Actuator and Sensor Dynamics," *Automatica*, vol. 41 (10), pp. 1821-1824, 2005.

[9] M.M.Z. Shahadat, T. Mizuno, Y. Isino, and M. Takasaki, "Improvement of Transient Characteristics of Negative Stiffness Control System by Feedforward Control," *Journal of JSAEM*, vol 20(3), pp. 619-625, 2012.

Paper ID: AM-05

Nonlocal Elasticity Theory for Lateral Torsional Buckling of Nanobeam

M. Zahurul Islam
Department of Applied Mathematics
Faculty of Science, University of Rajshahi, Rajshahi-6205, Bangladesh
Email: islam1977@ru.ac.bd; jahurul_lec_ap@yahoo.com

Abstract:

In this study, lateral torsional buckling instability of nanobeam is performed in the presence of external bending moment, based on the nonlocal elasticity theory and thin beam theory. At the beginning of the study, total energy (strain energy and potential energy) expressions of nanobeam having doubly cross-sectional symmetry are derived in detail. The variational energy principle is applied to the derived energy expressions to obtain the governing differential equations and boundary conditions. To study the nonlocal nanoscale effect on critical buckling moment, the derived equations of motion are solved for exact solutions and the critical instability buckling moments for various end constrains are presented and discussed in detail. It is observed from the analytical solutions that the critical buckling moment decreases with increasing nonlocal nanoscale and scale free classical model over estimates the critical buckling moment.

Keywords: *Nonlocal elasticity, Nanoscale, Lateral torsional buckling, Critical moment*

1. Introduction

The frequent use of advanced materials and structures in a minute length scale (i.e. micro- or nano-scale) has become the root or progress in nanotechnology. Micro-electromechanical-systems (MEMS) and Nano- electromechanical-systems (NEMS) have great influence in modern world because of its specific and interesting properties and also the reduction of production cost and energy consumption. Due to the reduction of device size into micro- and nano-scale, the scale free classical models and theories are unable to predict the increasingly prominence of size effects [1,2].

There are typically three approaches in the study of size effects in nanomechanics, i.e. experiments [3], numerical atomic-scale simulation [4] and scale dependent continuum mechanics model [5-8]. Among the theories, the scale dependent continuum mechanics models have become frequently used technique not only to its simplicity but also promise to predict accurate analytical results because control experiments in nano-scale are very difficult and numerical atomic-simulations are highly computationally expensive. Based on nonlocal elastic stress approach developed by Eringen and his associate [7,8], a series of research on buckling of nanotubes [9-11] has been conducted recently. In particular, Sudak [9] presented column buckling of MWCNTs. Ru [10] developed multiple shell model to study the buckling of CNTs. This model was further extended to study the thermal effect and van der Waals forces between inner and outer nanotubes by Xiaohu and Qiang [11] for axially compressed MWCNTs. All the above studies, partial nonlocal stress model was conducted to obtain the governing differential equation of equilibrium with nanoscale effect. In this aspect, Lim [12,13] presents a new variational consistent approach for bending of nanobeams based on nonlocal elasticity theory of Eringen [9]. For further study, the author is suggested to see the following articles [14,15].

A plenty of research on bending, buckling, vibration and wave propagation has been found; very limited studies on torsional or lateral torsional behaviors in NEMS are available at present. The aim of this article is to study lateral torsional buckling of nanobeam under external bending moment, based on new nonlocal elasticity theory [12,13] and thin beam theory.To study the effect of nanoscale,a reduced higher-order governing differentialequation is simplified and solved to obtainthe critical buckling loads and deflection of nanobeam for different boundary conditions.

2. Nonlocal modeling and formulation

2.1. Kinematics

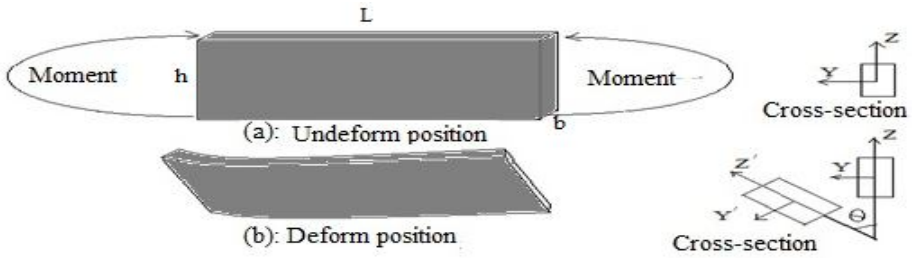

Fig.1. Continuum mode: (a) Undeformed and (b) deformed shape of a doubly symmetric nanobeam loaded to bend about its major axis Y.

Consider a nanobeam of length L, weight b and height h which is shown in **Fig.1**. Let X axis be the beam axis and Y and Z axes are the principle axes of rectangular cross-section. The coordinate of the shear center are generally represented by (y_0, z_0); v and w are the components of displacement of shear center parallel to the rotated axes Y' and Z'; θ is the angle of twist with respect to longitudinal axis X. Let us assume that the bending rigidity of the beam about Y axis is quite large as compared to Z axis. Thus, deflection w in the plane of applied moment is small compared to v and θ. Based on the thin beam theory, the strain displacement relation can be expressed in the following way:

$$\varepsilon_{xx} = y\frac{d^2v}{dx^2} \tag{1}$$

where ε_{xx} is normal strain, y the transverse coordinate measured from the mid-plane, and v the lateral displacement. Considering the relation between the classical shear stress and shear strain, we get

$$\gamma = r\frac{d\theta}{dx} \tag{2}$$

2.1.1. Constitutive relation

For linear, homogeneous and isotropic solids, unlike the classical theory, the nonlocal stress at a point depends not only on the strain at that point but also on the strain at all other points within the continuum. Consequently, in the constitutive relation of nonlocal elasticity theory Hook's law (for local theory) is replaced by an integration which governs the nonlocal material behavior and its relation can be expressed in the following expression [17]

$$t_{i,j}(\mathbf{x}) = \int_V \alpha\left(|\mathbf{x}' - \mathbf{x}|, \tau\right)\sigma_{i,j}(\mathbf{x}')dV(\mathbf{x}')\left(\tau = \frac{e_0 a}{L} = \frac{\mu}{L}\right) \tag{3}$$

where e_0 is a material constant; a is an internal characteristic length such as lattice parameter or granular distance while L is an external characteristic length; $\mathbf{x}$ is a reference point; $\sigma_{i,j}$ is the local or classical stress tensor; and $\alpha(|\mathbf{x}' - \mathbf{x}|, \tau)$ is a kernel function. Eq. (3) is an integro-partial differential equation and it is extremely difficult mathematically to obtain the solutions in terms of displacement field in nonlocal elasticity due to the presence of spatial derivatives inside the integral. However, by using Green's function with certain approximation error, Eringen [17] transformed the Eq. (3) into second order partial differential equation in the form

$$t_{i,j} - \mu^2\nabla^2 t_{i,j} = \sigma_{i,j} \tag{4}$$

where ∇^2 is a Laplacian operator and for one-dimensional thin structure, Eq. (4) can be written as

$$t_{i,j} - \mu^2\frac{d^2 t_{i,j}}{dx^2} = \sigma_{i,j} \tag{5}$$

For the analysis of nanobeam, the constitutive relation in Eq. (5) for bending and torsion becomes

$$\sigma_{xx} - \mu^2\frac{d^2\sigma_{xx}}{dx^2} = Ey\frac{d^2v}{dx^2}; \sigma_{rr} - \mu^2\frac{d^2\sigma_{rr}}{dx^2} = Gr\frac{d\theta}{dx} \tag{6a,b}$$

2.2. Bending strain energy

Reasonable solution of Eq. (6a) can be written as

$$\sigma_{xx} = Ey\sum_{n=1}^{\infty}\mu^{2n-2}\frac{d^{2n}v}{dx^{2n}} \tag{7}$$

As the bending moment is $M_{xx}=\int_A \sigma_{xx} y dA$, the nonlocal moment can be expressed as

$$M_{xx} = EI\sum_{n=1}^{\infty}\mu^{2n-2}\frac{d^{2n}v}{dx^{2n}} \tag{8}$$

where I is the second moment of area. The bending strain energy of the beam is given by

$$U_B = \frac{1}{2}\int_V \sigma_{xx}\varepsilon_{xx}dV = \frac{EI}{2}\sum_{n=1}^{\infty}\mu^{2n-2}\int_0^L \frac{d^{2n}v}{dx^{2n}}\frac{d^2v}{dx^2}dx \tag{9}$$

and the variation of strain energy yields

$$\delta U_B = EI\begin{bmatrix}\int_0^L\sum_{n=1}^{\infty}\mu^{2n-2}\frac{d^{2n+2}v}{dx^{2n+2}}\delta v dx-\left[\sum_{n=1}^{\infty}\mu^{2n-2}\frac{d^{2n+1}v}{dx^{2n+1}}\delta v\right]_0^L \\ +\left[\sum_{n=1}^{\infty}\mu^{2n-2}\frac{d^{2n}v}{dx^{2n}}\delta\left(\frac{dv}{dx}\right)\right]_0^L-\frac{1}{2}\left[\sum_{n=1}^{\infty}\mu^{2n}\frac{d^{2n+1}v}{dx^{2n+1}}\delta\left(\frac{d^2v}{dx^2}\right)\right]_0^L+\cdots\end{bmatrix} \tag{10}$$

2.3. Torsional strain energy

Similar to Eqs. (7-10), the variation of torsional strain energy is

$$\delta U_T = GJ\begin{bmatrix}-\int_0^L\sum_{n=1}^{\infty}\mu^{2n-2}\frac{d^{2n}v}{dx^{2n}}\delta\theta dx+\left[\sum_{n=1}^{\infty}\mu^{2n-2}\frac{d^{2n-1}\theta}{dx^{2n-1}}\delta\theta\right]_0^L \\ -\frac{1}{2}\left[\sum_{n=1}^{\infty}\mu^{2n}\frac{d^{2n}\theta}{dx^{2n}}\delta\left(\frac{d\theta}{dx}\right)\right]_0^L+\frac{1}{2}\left[\sum_{n=1}^{\infty}\mu^{2n}\frac{d^{2n-1}\theta}{dx^{2n-1}}\delta\left(\frac{d^2\theta}{dx^2}\right)\right]_0^L+\cdots\end{bmatrix} \tag{11}$$

where $J=\int_A r^2 dA$ is the polar moment of and $T_{rr}=\int_A \sigma_{rr} r dA$ is the torsional moment. Hence, the variation of total strain energy is

$$\delta U = \delta U_B + \delta U_T \tag{12}$$

where δU_B and δU_T are given by Eq. (10) and Eq. (11) respectively. In the presence of external moment M exerted at the end of nanobeam, the variation of work done on the nanobeam is

$$\delta W = M\left\{\left[\frac{dv}{dx}\delta\theta\right]_0^L-\int_0^L\frac{d^2v}{dx^2}\delta\theta dx\right\}+M\left\{\left[\frac{d\theta}{dx}\delta v\right]_0^L-\int_0^L\frac{d^2\theta}{dx^2}\delta v dx\right\} \tag{13}$$

3. Governing equations and boundary conditions

The principle of virtual displacement states that if a body is in equilibrium, we must have

$$\delta(U-W)=0 \tag{14}$$

Substituting the values of δU and δW into Eq. (14) and since δv, $\delta\left(\frac{dv}{dx}\cdots\right)$, and $\delta\theta$, $\delta\left(\frac{d\theta}{dx}\right)\cdots$ cannot vanish, Eq. (14) yields

$$EI\sum_{n=1}^{\infty}\mu^{2n-2}\frac{d^{2n+2}v}{dx^{2n+2}}+M\frac{d^2\theta}{dx^2}=0 \tag{15}$$

with

$$\begin{aligned}&EI\sum_{n=1}^{\infty}\mu^{2n-2}\frac{d^{2n+1}v}{dx^{2n+1}}+M\frac{d\theta}{dx}=0 \text{ or } v=0 \text{ at } x=0,L \\ &EI\sum_{n=1}^{\infty}\mu^{2n-2}\frac{d^{2n}v}{dx^{2n}}=0 \text{ or } \frac{dv}{dx}=0 \text{ at } x=0,L\end{aligned} \tag{16}$$

and

$$-GJ\sum_{n=1}^{\infty}\mu^{2n-2}\frac{d^{2n}\theta}{dx^{2n}}+M\frac{d^2v}{dx^2}=0 \tag{17}$$

with

$$\begin{aligned} GJ\sum_{n=1}^{\infty}\mu^{2n-2}\frac{d^{2n-1}\theta}{dx^{2n-1}}-M\frac{dv}{dx}=0 \text{ or } \theta=0 \; at \; x=0,L \\ \frac{GJ}{2}\sum_{n=1}^{\infty}\mu^{2n}\frac{d^{2n}\theta}{dx^{2n}}=0 \text{ or } \frac{d\theta}{dx}=0 \; at \; x=0,L \end{aligned} \tag{18}$$

Let us define new parameters α_1 and α_2 as

$$\alpha_1=(M/EI);\alpha_2=(M/GJ) \tag{19a,b}$$

Therefore, Eq. (16) and Eq. (18) can be written as

$$\sum_{n=1}^{\infty}\mu^{2n-2}\frac{d^{2n+2}v}{dx^{2n+2}}+\alpha_1\frac{d^2\theta}{dx^2}=0;-\sum_{n=1}^{\infty}\mu^{2n-2}\frac{d^{2n}\theta}{dx^{2n}}+\alpha_2\frac{d^2v}{dx^2}=0 \tag{20a,b}$$

which represent the higher order equations lateral torsional buckling of nanobeam and the corresponding boundary conditions can be expressed as

$$\left.\begin{aligned} &\frac{dM_{xx}}{dx}+M\frac{d\theta}{dx}=0 \text{ or } v=0 \; at \; x=0,L \\ &M_{xx}=0 \text{ or } \frac{dv}{dx}=0 \; at \; x=0,L \\ &\frac{dM_{xx}}{dx}=0 \text{ or } \frac{d^2v}{dx^2}=0 \, at \; x=0,L \end{aligned}\right\} \tag{21}$$

and

$$\left.\begin{aligned} &\frac{dT_{rr}}{dx}-M\frac{dv}{dx}0 \text{ or } \theta=0 \; at \; x=0,L \\ &T_{rr}=0 \text{ or } \frac{d\theta}{dx}=0 \; at \; x=0,L \end{aligned}\right\} \tag{22}$$

For simplicity, $n=2$ is chosen in Eqs. (20a,b) and the reduced order governing equations can be written as

$$\mu^2\frac{d^6v}{dx^6}+\frac{d^4v}{dx^4}+\alpha_1\frac{d^2\theta}{dx^2}=0;-\mu^2\frac{d^4\theta}{dx^4}-\frac{d^2\theta}{dx^2}+\alpha_2\frac{d^2v}{dx^2}=0 \tag{23a,b}$$

It is clear that both Eqs. (23a,b) contains nonlocal nanoscale effect. Now substituting $\frac{d^2\theta}{dx^2}=\alpha_2\frac{d^2v}{dx^2}$ (from Eq. (23b)without nonlocal effect) into Eq. (23a) yields

$$\mu^2\frac{d^6v}{dx^6}+\frac{d^4v}{dx^4}+\alpha\frac{d^2\theta}{dx^2}=0 \tag{24}$$

where α is defined as

$$\alpha=\alpha_2\alpha_2=\left(M^2/EIGJ\right) \tag{25}$$

Substituting $v=Ce^{\lambda x}$ into Eq. (24), one gets

$$\mu^2\lambda^6+\lambda^4+\alpha\lambda^2=0 \tag{26}$$

which is six-order polynomial equation and the roots are given by

$$\lambda_1=\lambda_2=0;\lambda_{3,4}=\pm i\sqrt{\left(1-\sqrt{1-4\mu^2\alpha}\right)/\left(2\mu^2\right)};\lambda_{5,6}=\pm i\sqrt{\left(1+\sqrt{1-4\mu^2\alpha}\right)/\left(2\mu^2\right)} \tag{27}$$

Hence, the general solution of Eq. (24) can be written as

$$v=C_1+C_2x+C_3\sin\Lambda_1x+C_4\cos\Lambda_1x+C_5\sin\Lambda_2x+C_6\cos\Lambda_2x \tag{28}$$

where $C_i\left(i=1,2,\cdots,6\right)$ are the six unknown constants which are determined from appropriate boundary conditions (Eq. (21) and / Eq. (22)) and Λ_1 and Λ_2 are defined as

$$\Lambda_1=\left|\lambda_{3.4}\right|=\sqrt{\left(1-\sqrt{1-4\mu^2\alpha}\right)/\left(2\mu^2\right)};\Lambda_2=\left|\lambda_{5,6}\right|=\sqrt{\left(1+\sqrt{1-4\mu^2\alpha}\right)/\left(2\mu^2\right)} \tag{29a,b}$$

4. Examples of nanobeam

4.1 Simply supported nanobeam

For a simply supported nanobeam, six boundary conditions are chosen as

$$v = 0;\ \frac{d^2v}{dx^2} = 0;\ M_{xx} = 0 \text{ at } x = 0, L \tag{30}$$

Substituting Eq. (28) into Eq. (30)yields

$$C_1 = C_2 = C_3 = C_4 = C_6 = 0 \text{ and} \sin(\Lambda_2 L) = 0 \text{ or } \Lambda_2 = (k\pi/L)(k = 1, 2, \cdots) \tag{31}$$

Hence, the instability deflection can be given by

$$v = C_5 \sin(k\pi/L)x \tag{32}$$

Further, substituting $\Lambda_2 = \frac{k\pi}{L}$ into Eq. (29b), the instability lateral torsional buckling moment for simply supported beam is given by

$$R = (M_{nl}/M_l) = \sqrt{\{1 - \mu^2 (k\pi/L)^2\}} \tag{33}$$

where $M_l = (k\pi/L)\sqrt{EIGJ}$ is the critical buckling moment[17] for a classical column simply supported at both ends.

4.2 Fully Clamped nanobeam

For a fully clamped nanobeam, six boundary conditions are chosen as

$$v = 0;\ \frac{dv}{dx} = 0;\ \frac{dM_{xx}}{dx} = 0 \text{ at } x = 0, L \tag{34}$$

Substituting into Eq. (28) into Eq. (34) yields

$$\begin{aligned} &C_2 = C_3 = C_4 = C_5 = 0;\ C_1 + C_6 = 0;\ \sin(\Lambda_2 L) = 0;\ \cos(\Lambda_2 L) = 1 \\ &\text{or } \Lambda_2 = (2k\pi/L)(k = 1, 2, \cdots) \end{aligned} \tag{35}$$

Hence, the instability deflection can be given by

$$v = C_1\{1 - \cos(2k\pi/L)x\} \tag{36}$$

Further, substituting $\Lambda_2 = (2k\pi/L)$ into Eq. (29b), the instability lateral torsional buckling moment for simply supported beam is given by

$$R = (M_{nl}/M_l) = \sqrt{\{1 - \mu^2 (2k\pi/L)^2\}} \tag{37}$$

where $M_l = (2k\pi/L)\sqrt{EIGJ}$ is the critical buckling moment for a classical column fully clamped at both ends.The analytical expressions in Eq. (33) for simply supported and in Eq. (37) for fully clamped boundary conditions are presented in **Fig. 2**.

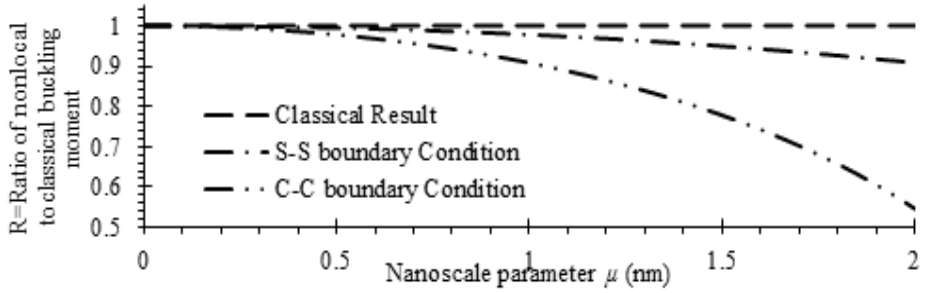

Fig.2: The effect on nanoscale parameter μ on R (for first mode ($k = 1$) in Eq. (34) and Eq. (38)) or the ratio of nonlocal to classical buckling moment for simply supported (S-S) and both side clamped (C-C) boundary conditions for $L = 15\,nm$ with corresponding classical result ($\mu = 0$).

5. General Discussions

The effects of nonlocal nano-scale parameter μ on the ratio of nonlocal to classical buckling moment for s-s and c-c nanobeam for first mode (i.e. $k = 1$) are presented in **Fig. 2**. From the **Fig. 2**, it is

demonstrated that the nonlocal nano-scale reduces buckling moment in both cases compared to the classical result as the nonlocal model contains the nanoscale parameter μ in Eq. (33) and Eq. (37).The classical result overestimates the buckling moment presented in **Fig.2**which can be obtained by dropping the nonlocal terms containing μ in Eq. (33) and Eq. (37). It is also noted that buckling moment for c-c nanobeam decreases more rapidly than that of s-s nanobeam. Similar predictions on bending, bucklingand vibration were reported by using nonlocal shell model [10,18,19], nonlocal Timoshenko beam model [20,21],and molecular dynamic simulation [22].The present trend is consistent with the existing results on nanostructures [9-12, 18-22] obtained by different method.

6. Conclusion

Based on the nonlocal constitutive relation developed by Eringen [16], the nonlocal nanoscale size effect for simply supported and fully clamped nanobeam in the presence of external moment is investigated. The nonlocal equations of motion and boundary conditions are developed by means of variational principle. Analytical expressions for s-s and c-c boundary conditions are established and discussed. It is concluded that the analytical nonlocal model captures nanoscale effects and consequently, proposed model predicts that the lateral torsional buckling moment decreases with increasing nonlocal nanoscale parameter. The classical solutions are recovered in the limit of vanishing nonlocal nanoscale and the validity of the present model is validated.

References:

[1] H. Gleiter, "Nanocristalline materials", *Progress Mater Sci.*, Vol. 33, No. 4, pp. 223-315, 1989.

[2] M.L. Gurtin and A. Murdoch, "A continuum theory of elastic material surfaces", *Arch. Ration Mech. Anal.*, Vol. 57, pp. 291-323, 1975.

[3] S. Iijima, "Helical micro tubules of graphitic carbon", *Nature*, Vol. 354, pp. 56–58, 1991.

[4] G. Dereli and C. Ozdogan, "Structural stability and energies of single-walled carbon nanotubes under uniaxial strain", *Phys. Rev. Lett. B*, Vol. 67, 035416 (6 pages), 2003.

[5] R.D. Mindlin, "Influence of couple-stress on stress concentrations", *Experimental Mechanics*, Vol.3,No. 1, pp. 1-7, 1963.

[6] E.C. Aifantis, Strain gradient interpretation of size effects, *Int. J. Fracture*, Vol. 95, 299-314, 1999.

[7] A.C. Eringen, Nonlinear Theory of Continuous Media, Mc Grew-Hill, New York 1962.

[8] A.C. Eringen and D.G.B. Edelen, On nonlocal elasticity, *Int. J. Eng. Sci. 10*, pp. 233-248,1972.

[9] L.J. Sudak, "Column buckling of multiwalled carbon nanotubes using nonlocal continuum mechanics", *J. Appl. Phys*. Vol.94, pp. 7281–7287, 2003.

[10] C.Q. Ru, "Effect of van der Waals forces on axial buckling of a double walled carbon nanotube", ", *J. Appl. Phys*, Vol. 87, 7227-7231, 2000.

[11] Y. Xiaohu, H Qiang, "Investigation of axially compressed buckling of a multi-walled carbon nanotube under temperature field" *Comp. Scie. and Technl.*, Vol. 67, pp. 125-134 2007.

[12] C.W. Lim, "Equilibrium and static deflection for bending of a nonlocal nanobeam" *Adv. Vib. Eng.* Vol. 8, pp. 277-300, 2009.

[13] C.W. Lim, J.C. Niu, and Y.M. Yu, "Nonlocal Stress theory for buckling instability of Nanotubes: New predictions on stiffness strengthening effects of nanoscales" *J. Com.. Theor. Nanos.* Vol. 7, pp. 1-8, 2010.

[14] CY. Wang, Y.Y. Zhang, C.M. Wang and V.B.C. Tan, "Buckling of carbon nanotubes: A literature survey", *J. Nanoscience and Nanotechlogy*, Vol. 7, pp. 4221-4247, 2007.

[15] A.R. Hall, S. Paulson, T. Cui, J.P. Lu, L-C Qin and S. Washburn, "Torsional electromechanical systems based on carbon nanotubes, *Rep. Prog. Phys*, Vol. 75, 116501, 2012.

[16] A.C. Eringen,, "On differential equations of nonlocal elasticity and solutions of screw dislocation and surface waves" *J. Applied Physics*, Vol. 54, pp. 4703-4710, 1983.

[17] S. Pinarbasi, "Lateral torsional buckling of rectangular beam using variational iteration method", *Scientific research and essays*, Vol. 6, pp. 1445-1457, 2011.

[18] F. Khademolhosseini, R.K.N.D. Rajapakse and A. Nojeh, "Torsional buckling of carbon nanotubes based on nonlocal elasticity shell models", *Computational Materials Science*, Vol. 48, pp. 736-742, 2010

[19] M.J. Hao, X.M. Guo and Q. Wang, "Small-scale effect on torsional buckling of multi-walled carbon nanotubes", *Europ. J. Mechanics A/Solids*, Vol. 29, pp. 49-55, 2010.

[20] C.M. Wang, Y.Y. Zhang, S.S. Ramesh, and S. Kitipornchai, " Buckling analysis of micro-and nano-rods/tubes based on nonlocal Timoshenko beam theory, *J. Phys.D. Appl. Phys.*, Vol. 39, pp. 3904-3909, 2006.

[21] H.T. Thai, "A nonlocal beam theory for bending, buckling, and vibration of nanobeams", *Int. J. Engineering Science*, Vol. 52, pp. 56-64, 2012.

[22] F. Khademolhosseini,A.S. Phani, A. Nojeh and R.K.N.D. Rajapakse and, Nonlocal continuum modeling and molecular dynamics simulation of torsional vibration of carbon nanotubes, *Nanotechnology, IEEE Trans*., Vol. 11, pp. 34-43, 2012.

International Conference on Mechanical, Industrial and Materials Engineering 2015 (ICMIME2015)
11-13 December, 2015, RUET, Rajshahi, Bangladesh.

Paper ID: AM-08

Automatic Exploration of Object from Partial Region of Interest (ROI)

Md. Rokunuzzaman*[1], S. Mandal[1], Md. Kamrul Islam[1] and Basu Deb[1]
[1]Departmentof Mechanical Engineering, Rajshahi University of Engineering & Technology (RUET), Bangladesh
Email: rzaman.mte@ruet.ac.bd

Abstract

Intelligent system tries to explore things when it finds insufficient or partial information. The reason behind this behavior is curiosity. Usually curiosity drives the intelligent system to uncover the truth by searching and exploring. This paper is an attempt to observe this behavior with a simple experiment using vision system. In this experiment, a database has been prepared with features of some simple desktop objects. A web camera has been mounted on the top of an experimental base to capture the image of the simple objects. For processing the image and extraction of features of the observed object, OpenCV library has been used. A simple probability of recognition algorithm has been proposed using feature matching. The web camera has been fixed with a rack and pinion mechanism so that it can move up and down to explore the object according to the probability of recognition. The camera explores the object by moving itself up and down until it finds the maximum probability of recognition. The system then identifies the object and displays its name. This type of system is helpful in autonomous searching of objects, exploring un-identified objects, inspecting of products, collecting information from database and investigating of intelligent behavior in the research area of Artificial Intelligence (AI).

Keywords: Automatic exploration; Image Processing; Partial ROI.

1. Introduction

Robot object detection is concerned with determining the identity of an object being observed in the image from a set of known labels. Central to robot object recognition systems is how the consistency of an image, taken under different lighting and positions, is extracted and recognized. To work, algorithms are made to adopt certain representations or models, either in 2D or 3D, to capture these characteristics, which then facilitate procedures to tell their identities. The recognition process, which could be generative or discriminative, is then carried out by matching the test image against the stored object representations or models in the database. With more reliable representation schemes and recognition algorithms being developed, more progress continues to be made towards recognizing objects even under variations in viewpoint, illumination and under partial occlusion.

An image may be considered to contain sub-images sometimes referred to as regions-of-interest, ROIs, or simply regions. This concept reflects the fact that images frequently contain collections of objects each of which can be the basis for a region. In a sophisticated image processing system it should be possible to apply specific image processing operations to selected regions.

Automatic exploration is a built-in ability of intelligent systems. This ability gives a driving force to extract information from unknown environment. After extracting information, the intelligent system analyzes it and makes decision about the next task. To make such systems, many researches has been carried out in the field of object learning through curiosity [1] or active exploration [2], object detection from partially occluded objects[3], object detection by partial shape matching [4], recognition by components[5], object recognition from Nearest Neighbor Classification technique[6], object recognition from Bayesian inference where geometric primitives are used as prior knowledge for probabilistic integration[7][8], image searching from large database [9], automatic object detection and shape analysis[10] and so on. Although these researches are very relevant, our research is unique in terms of novelty and simplicity of its approach.

2. Experimental set up

Figure 1 shows the experimental setup for automatic exploration of object from partial ROI. The setup consists of a laptop, a web camera, rack-pinion mechanisms for webcam movement and controller circuits with a stepper motor.

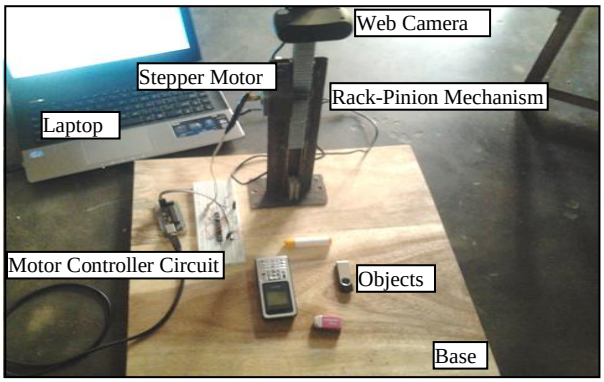

Fig 1: Experimental Setup

3. Methodology

3.1 Input

In this system, four simple desktop objects are selected to test our approach. These are computer, mobile phone, pen and pen-drive.

3.2 Tools and Platform

We have utilized the following state of the art tools and platform to implement our system:

- Software tools and Platforms: Open CV 2.4.5, Code::Blocks 10.05, C make 2.8
- Hardware Tools: Laptop: Pentium Core-2 Duo, 2GB Memory, Webcam: USB2.0 VGA UVC Webcam

3.3 Flow Diagram

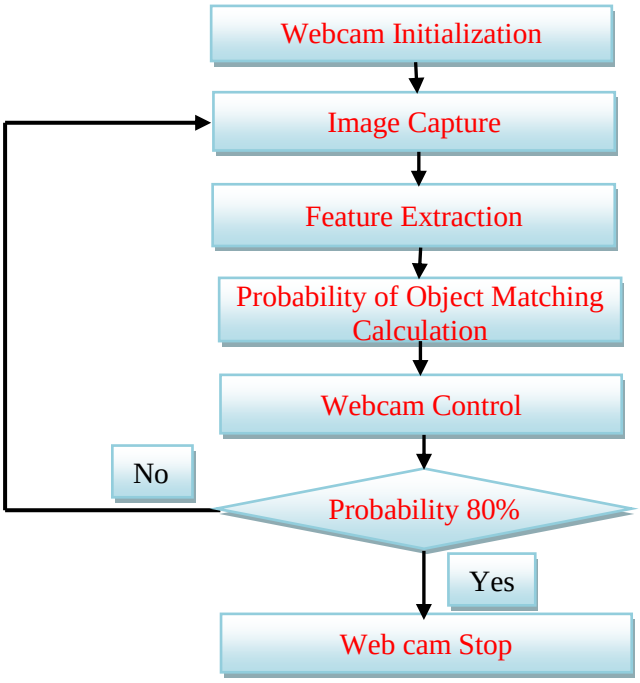

Fig 2: Flow diagram for automatic exploration of objects from partial ROI

Figure 2 shows the flow diagram for automatic exploration of objects from partial ROI. In this process, the webcam is initialized and object is placed on the base of the setup. Then the image of the object is captured and processed by using an image processing function developed by OpenCV [11]. After processing the image, features are extracted and probability of recognition is calculated. The details of feature extraction and probability calculation are stated in the following paragraphs:

3.3.1 Feature Extraction

A feature is an interesting part of an image, such as a corner, blob, edge, or line. Feature extraction process involves mathematical operation which produces feature vectors from input image. To identify an object, geometrical shape is an important parameter and can be easily evaluated by its area, perimeter, bounding box

area, bounding box ratio, density etc. Therefore we have calculated these features using mathematical formulas. The process of feature extraction is depicted in figure 3.

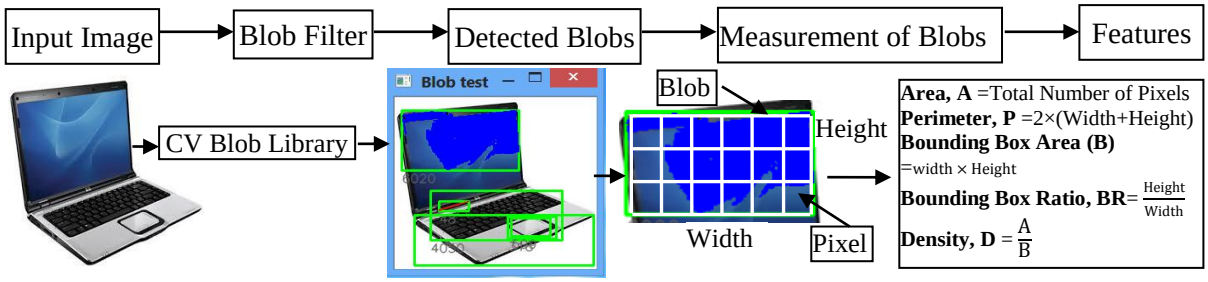

Fig 3: Feature extraction process

In the feature extraction process the image (here laptop) is processed by a Blob filter and detects Blobs (Binary large objects). In the field of computer vision, blob detection refers to mathematical methods that are aimed at detecting regions in a digital image that differ in properties, such as brightness or color, compared to areas surrounding those regions. Informally, a blob is a region of a digital image in which some properties are constant or vary within a prescribed range of values; all the points in a blob can be considered in some sense to be similar to each other. To implement blob detection, we have used CV Blob library for this purpose. The blob detection algorithm can be summarized as follows [12]:

Algorithm for extracting blobs from an image:

1. Convert the source image to binary images by applying thresholding with several thresholds from minThreshold (inclusive) to maxThreshold (exclusive) with distance thresholdStep between neighboring thresholds.
2. Extract connected components from every binary image by findContours and calculate their centers.
3. Group centers from several binary images by their coordinates. Close centers form one group that corresponds to one blob, which is controlled by the minDistBetweenBlobs parameter.
4. From the groups, estimate final centers of blobs and their radiuses and return as locations and sizes of keypoints.

This class performs several filtrations of returned blobs. One should set filterBy* to true/false to turn on/off corresponding filtration. Available filtrations:

- **By color**. This filter compares the intensity of a binary image at the center of a blob to blobColor. If they differ, the blob is filtered out. Use blobColor = 0 to extract dark blobs and blobColor = 255 to extract light blobs.
- **By area**. Extracted blobs have an area between minArea (inclusive) and maxArea (exclusive).
- **By circularity**. Extracted blobs have circularity ($4*\pi*Areaperimeter*perimeter$) between minCircularity (inclusive) and maxCircularity (exclusive).
- **By ratio of the minimum inertia to maximum inertia**. Extracted blobs have this ratio between minInertiaRatio (inclusive) and maxInertiaRatio (exclusive).
- **By convexity**. Extracted blobs have convexity (area / area of blob convex hull) between minConvexity (inclusive) and maxConvexity (exclusive).

Default values of parameters are tuned to extract dark circular blobs.

After detection of blobs, features are extracted which helps to identify the objects.

3.3.2 Probability of object matching calculation

Probability of object matching is calculated based on the feature matching between database objects and input object. We have created object databases using the measured features and stored it in the memory of the laptop. Each time when an input object is placed under the webcam, its feature is matched with the object database and probability of matched features are calculated and displayed in the monitor of the laptop.

We assume each object is defined as a set of measured features, *f*. Therefore, object at input and object in database can be formulated by

$$Obj[ID]_{input} = [f_a, f_b, f_c, f_d, \dots . f_z] \dots\dots\dots\dots\dots\dots\dots\dots\dots\dots\dots\dots (1)$$

$$Obj[ID]_{database} = [f_{a'}, f_{b'}, f_{c'}, f_{d'}] \dots\dots\dots\dots\dots\dots\dots\dots\dots\dots\dots\dots (2)$$

Therefore, the probability of matching feature *a* is calculated as

$$P_a = \frac{f_a}{f_{a'}} \dots\dots\dots\dots\dots\dots\dots\dots\dots\dots\dots\dots\dots\dots (3)$$

Other probabilities are calculated in the same way. The probability of object matching is then calculated as

$$P_{Obj[ID]} = \frac{P_a + P_b + \cdots .. P_z}{N} \times 100\% \dots\dots\dots\dots\dots\dots\dots\dots\dots (4)$$

Where, *ID* is the object name and *N* is the no. of feature considered.

3.3.3 Webcam Control: As shown the experimental setup, the motion of the webcam is controlled by a rack and pinion mechanism. A stepper motor is attached at the stand of the setup and moves a pinion which in turn gives a linear motion of the rack. A microcontroller (**AT89C51**) is used to drive the stepper motor. According to the program output the signal from the Laptop is fed through the USB port and connected to a microcontroller. The microcontroller sends the signal to the driver circuit of the motor and the motor drives accordingly. Initially the motor rotates to adjust the webcam so that the probability of identifying object reaches maximum. In the program we set the probability is 80% which means when an input object is matched 80% with the database object then the system will be stable and webcam will be fixed at that instant.

4. Results

Table 4.1: Probability of object matching for mobile and pen

Parameter	Object	Total	Probability
Area (A)	mobile	7745	0.14
	pen	1099	
Perimeter (P)	mobile	3797	0.14
	pen	546	
Bounding Box (B)	mobile	13958	0.38
	pen	5337	
Bounding Box ratio (BR)	mobile	131.808304	0.03
	pen	4.148256	
Density (D)	mobile	17.786625	0.05
	pen	0.881864	

Table 4.1 shows the probability of object matching for mobile and pen.The calculated value is

$$\text{Probability} = \left(\frac{0.14+0.14+0.38+0.03+0.05}{5}\right) \times 100\ \% = 14.2\ \%$$

Here we have found that the matching probability between the input image and database's image the probability value do not increase 80 % so the the input image is not pen.

Table 4.2 Probability of object matching for mobile and computer

Parameter	Object	Total	Probability
Area (A)	mobile	7745	0.65
	computer	11847	
Perimeter (P)	mobile	3797	0.65
	computer	2469	
Bounding Box (B)	mobile	13958	0.39
	computer	35720	
Bounding Box ratio (BR)	mobile	131.808304	0.02
	computer	2.518421	
Density (D)	mobile	17.786625	0.11

	computer	1.992728	

Table 4.2 shows the probability of object matching for mobile and computer.The calculated value is

$$\text{Probability} = \left(\frac{0.65+0.65+0.39+0.02+0.11}{5}\right) \times 100\% = 36.4\ \%$$

Since the matching probability value do not increase 80 % so the the input image is not computer.

Table 4.3 shows the probability of object matching for mobile and pen drive. The calculated value is

$$\text{Probability} = \left(\frac{0.7+0.48+0.48+0.09+0.20}{5}\right) \times 100\% = 39\ \%$$

Since the probability values do not increase 80 % so the input image is not pen drive.

Table 4.3: Probability of object matching for mobile and pendrive

Parameter	Object	Total	Probability
Area (A)	mobile	7745	0.7
	pendrive	11060	
Perimeter (P)	mobile	3797	0.48
	pendrive	1853	
Bounding Box (B)	mobile	13958	0.48
	pendrive	28974	
Bounding Box ratio (BR)	mobile	131.808304	0.09
	pendrive	11.807933	
Density (D)	mobile	17.786625	0.20
	pendrive	3.540914	

Table 4.4: Probability of object matching for mobile and mobile

Parameter	Object	Total	Probability
Area (A)	mobile	7745	0.98
	mobile	7912	
Perimeter (P)	mobile	3797	0.95
	mobile	3632	
Bounding Box (B)	mobile	13958	0.96
	mobile	14502	
Bounding Box ratio (BR)	mobile	131.808304	0.94
	mobile	140.0256	
Density (D)	mobile	17.786625	0.91
	mobile	16.26852	

Table 4.3 shows the probability of object matching for mobile and pen drive. The calculated value is

$$\text{Probability} = \left(\frac{0.98+0.95+0.96+0.94+0.91}{5}\right) \times 100\% = 95\ \%$$

The matching probability value increase 80% so the input image is mobile.

The program calculates the probability of matching for the input object with several objects in the database and show the results in the monitor. When the program finds the probability less than 80%, then it moves the camera ups and down to further calculate the value of probability. However, if the probability value is more than 80%, then the camera does not move which means it is stable.

5.**Conclusion**

We have successfully developed an automatic exploration system for object identification. This system is very simple and mimics an artificial intelligent system. However, the system needs lots of improvements. The system can only take images in 2D. Therefore, 3D objects cannot be processed with this system. The pose and orientation of the object is fixed in this system. In real world, object can be viewed in different poses and angles which give different recognition of the same object. Therefore, we need to build more robust system which can be developed with SIFT or SURF algorithms. There are lots of scopes are open for its development. The probabilistic object detection is very powerful method and works very well in the real world. Therefore, we can use Bayes Network to calculate probability for the object which will give better result. In conclusion, we have introduced a very simple system which solves automatic object exploration problem. This type of system is helpful in autonomous searching of objects, exploring un-identified objects, inspecting of products, collecting information from database and investigating of intelligent behavior in the research area of Artificial Intelligence (AI).

References

[1]Sao Mai Nguyen, Serena Ivaldi, Natalia Lyubova, Alain Droniou, Learning to recognize objects through curiosity-driven manipulation with the iCub humanoid robot, IEEE Third Joint International Conference on Development and Learning and Epigenetic Robotics (ICDL), 18-22 Aug.pp. 1-8, 2013

[2]S. Ivaldi, S. M. Nguyen, N. Lyubova, A. Droniou, V. Padois, D. Filliat, P.-Y. Oudeyer, O. Sigaud, Object Learning Through Active Exploration, IEEE Transactions on Autonomous Mental Development, Volume: 6, Issue: 1, pp.56 – 72, 2013

[3]Bo Gun Parka, Kyoung Mu Leeb, Sang Uk Leea, Jin Hak Leec, Recognition of partially occluded objects using probabilistic ARG (attributed relational graph)-based matching, Computer Vision and Image Understanding, Vol. 90, Issue 3, pp. 217–241, June 2003

[4]Tianyang Ma and L.J. Latecki, From partial shape matching through local deformation to robust global shape similarity for object detection, IEEE Conference on Computer Vision and Pattern Recognition (CVPR),2011, pages 1441 –1448, June 2011

[5]Biederman, I. Recognition-by-components: a theory of human image understanding. Psychological Review, Vol: 94, Issue: 2, pp.115‑147, 1987

[6]R.Muralidharan, Object Recognition Using K-Nearest Neighbor Supported By Eigen Value Generated From the Features of an Image, International Journal of Innovative Research in Computerand Communication Engineering Vol. 2, Issue 8, August 2014

[7]Daniel Kersten, Object Perception: Generative Image Models and Bayesian Inference, Chapter, Biologically Motivated Computer Vision, Volume 2525 of the series Lecture Notes in Computer Science, pp 207-218, 2002

[8] Leonardo Chang, Miriam Monica Duarte, Luis Enrique Sucar, Eduardo F. Morales, Object Class Recognition Using SIFT and Bayesian Networks, Proceedings of the 9th Mexican International Conference on Artificial Intelligence, MICAI, volume 6438 of the series Lecture Notes in Computer Science, pp. 56-66, Mexico, November 8-13, 2010

[9]Feng Jing, Mingjing Li, Member, IEEE, Hong-Jiang Zhang, and Bo Zhang, An Efficient and Effective Region-Based Image Retrieval Framework, IEEE Transactions on Image Processing, Vol. 13, No. 5, May 2004 pp. 699-709

[10]Kaichang Di, Zongyu Yue , Zhaoqin Liu, Automated Rock Detection and Shape Analysis from Mars Rover Imagery and 3D Point Cloud Data, Journal of Earth Science, Vol. 24, No. 1, pp. 125–135, February 2013

[11] Bradski, G, Kaehler, A "Learning OpenCV: Computer Vision with the OpenCV Library", O'Reilly Media, September, 2008

[12] OpenCV-3.0.0-dev, Simple blob detector-OpenCV documentation, retrieved 25 January 2014 from the web site http://docs.opencv.org/master/d0/d7a/ classcv_1_1SimpleBlobDetector.html

International Conference on Mechanical, Industrial and Materials Engineering 2015 (ICMIME2015)
11-13 December, 2015, RUET, Rajshahi, Bangladesh.

Paper ID: AM-10

Robotic Path Planning Algorithm as a Tool of Visualization of Characteristic Differences amongParticle Swarm Optimization,Artificial Bee Colony Algorithm and Firefly Algorithm

Md. Tajmiruzzaman[1], Md. Al-Mamun[2]
[1,2]Department of Industrial & Production Engineering, Rajshahi University of Engineering & Technology, Rajshahi-6204, Bangladesh
E-mail:taju_ipe09@yahoo.com
Cell: 01717718097

Abstract

Particle Swarm Optimization (PSO), Artificial Bee Colony (ABC) Algorithm and Firefly Algorithm are meta-heuristic optimization algorithms based on the intelligent behaviors of bird, honeybee and firefly swarms respectively. Although these three algorithms can deal with any number of dimensions (variables), Robotic Path Planning uses only two or three variables. The usage of these algorithms in Robotic Path Planning has been demonstrated in numerous research works. But in this paper, contrarily, a simple Robotic Path Planning algorithm is developed to demonstrate and visualize the characteristic differences among the three optimization algorithms. The shape, length, consumed time and straightness of the paths created separately by these algorithms are visualized and compared. Finally, it is shown that beside the conventional usage of standard benchmark functions to test the accuracy and convergence speed of an optimization algorithm, the proposed Robotic Path Planning technique can be successfully used either as an alternative or at least as a supplementary tool.

Keywords: Robotic Path Planning, Particle Swarm Optimization, Artificial Bee Colony Algorithm, Firefly Algorithm.

1. Introduction

Whenever a new Optimization algorithm is developed, researchers have to test its performance for different situations. In most cases, standard unconstrained benchmark functions such asRosenbrock, Rastrigin, Griewank, Schwefel, Sphere, Ackley functions are used [1]. Thereafter the algorithm needs to be tested in constrained as well as other dynamic environments to ensure its robustness for use.Robotic Path Planning algorithms can provide these constrained and dynamic environments [2], and beside this, some other inner characteristics of the Optimization algorithm may be visualized in this way.

Among the two broad categories of bio-inspired algorithms (Evolutionary algorithms and Swarm-based algorithms), the latter includes Particle Swarm Optimization, Ant Colony Optimization, Artificial Bee Colony algorithm, Firefly algorithm, Cuckoo Search, Bat algorithm etc. The idea of swarm intelligence was first introduced by G. Beni, in 1989 [3]. In this paper, Particle Swarm Optimization, Artificial Bee Colony Algorithm and Firefly Algorithm are considered to be tested in our proposed way.

The construction of this paper is as follows. In section-2, the three Optimization algorithms are described concisely. In section-3, the proposed Robot path planning algorithm and other details of it are depicted. Section-4 demonstrates experimental settings, computer simulation details and results of the work. Finally, section-5 will conclude the paper.

2.Overview of Optimization algorithms

2.1 Particle Swarm Optimization

PSO is a stochastic optimization technique developed by Eberhart and Kennedy [4]in 1995. It is inspired by social behavior patterns of organism that are live and interact within large groups. It incorporates Swarming behaviors observed in flocks of birds, school of fish or swarm of bees and even in human social behavior. The idea of PSO technique is that particles move through the search space with velocities which are dynamically adjusted according to their historical behavior. Therefore, the particles have the tendency to move towards better search space in the course of their search process. Particle swarm optimization algorithm start with a group of random particles and searches for optima by updating each generation. Each

particle is considered as a volume-less particle in the n-dimensional search space. The ith particle is represented as $x_i = \{x_{i1}, x_{i2},.., x_{iD}\}$. At each generation, each particle is updated by two best values. The first one is the best solution the particle has achieved by itself so far. This is known as p_{best}. The second one is the best solution obtained so far by all particles in the population. This best value is known as g_{best}. At each of the iterations, these two best values are combined to adjust the velocity along each dimension and that velocity is used to compute a new movement for the particle with the help of equations given below:

$$v_i = w \cdot v_i + c_1 \cdot rand_1 \cdot (p_{besti} - x_i) + c_2 \cdot rand_2 \cdot (g_{best} - x_i) \quad (1)$$

$$x_i = x_i + v_i \quad (2)$$

Where, c_1 and c_2 are cognitive parameter and social parameter respectively; $rand_1$ and $rand_2$ are two random numbers generated in range [0,1].The use of w, called inertia weight was proposed by Shi and Eberhart [5], in1998.Applying a high inertia weight at the start of the algorithm and making it decay to a low value through the PSO algorithm execution, makes the algorithm globally search in the start of the search, and search locally at the end of the execution.

2.2 Artificial Bee Colony (ABC) Algorithm

Artificial Bee Colony algorithm is an optimization algorithm first introduced by D. Karaboga [6], [7]. In the ABC algorithm, there are three types of bees: employed bees, onlooker bees, and scout bees. The employed bees search food sources around the positions initially and randomly located by the algorithm, and meanwhile they share the information of these food sources to the onlooker bees. The onlooker bees select good food sources from those found by the employed bees. The food sources with higher nectar amount (fitness) will have a large chance to be selected by the onlooker bees than the one of lower quality. When a food source is abandoned, the employed bee associated with it becomes a scout bee. The whole population of bees is called a colony. The first half of the colony turns into employed bees and the second half into the onlooker bees. The number of employed bees or the onlooker bees is equal to the number of solutions (the number of food sources).

The ABC generates a random initial population of SN solutions (food source positions), where SN denotes population size. Let $X_i = \{x_{i1},x_{i2},\ldots,x_{iD}\}$ represent the ith solution in the population, where D is the dimension size. Each employed bee X_i generates a new candidate solution V_i in the neighborhood of its present position as follows:

$$v_{ij} = x_{ij} + rand \cdot (x_{ij} - x_{kj}) \quad (3)$$

Where, X_k is a randomly selected candidate solution ($i \neq k$),j is a random dimension index selected from the set {1,2,…,D} and 'rand' is a random number within [−1, 1]. Once the new candidate solution V_i is generated, a greedy selection between X_i and V_i is used. If the fitness value of $V_i$is better than that of its parent X_i, then update X_i with V_i; otherwise keep $X_i$unchanged.

After all the employed bees complete the search process, an onlooker bee evaluates the nectar information taken from all employed bees and chooses a food source with a probability related to its nectar amount.

$$p_i = \frac{fit_i}{\sum_{i=1}^{SN} fit_i} \quad (4)$$

Where, fit_i is the fitness value of the ith solution in the swarm. The better the solution i, the higher the probability of the ith food source to be selected. And then onlooker bees find newer food sources around the more probable sources.

Being an iterative process, ABC algorithm repeats the upper mentioned process until it reaches the termination condition. If a food source position (solution) remains unchanged over a predefined number of iterations (called 'limit'), then this position is replaced by a random food source found by a scout bee.

2.3 Firefly Algorithm

The Firefly algorithm was propounded by Dr. Xin She yang [8] at Cambridge University in 2007 which was inspired by the mating behavior of tropical fireflies.

Firefly algorithm is established on three idealized rules [9]:i) artificial fireflies are unisex sothat sex is not an issue for attraction; ii) attractiveness is proportional to their flashing brightness which decreases as the distance from the other firefly increases due to the fact that the air absorbs light. Since the most attractive firefly is the brightest one that convinces its neighbors to move toward itself, so ultimately all other fireflies will coincide

with the brightest firefly (best solution). In case of no brighter one, it freely moves any direction; and iii) the brightness of the flashing light can be considered as objective function to be optimized.
For an optimization problem, the light intensity or brightness I_i of a firefly i is theobjective function or fitness value $f(x_i)$ and the position of it, x_i is a candidate solution.
The main steps of the FA start from initializing a swarm of fireflies;the initial positions of fireflies are generated randomly ($x_i \in [x_{min}, x_{max}]^D$), and the light intensity of each of the swarm is evaluated. And now, a loop of pairwise comparisons of light intensities (fitness values) is executed, where the firefly with lower light intensity will move toward the higher one.
The movement of a firefly i,attracted by another brighter firefly j (which has better fitness value $f(x_j)$), is determined as follows:

$$x_i = x_i + \beta_{i,j} \cdot (x_j - x_i) + \alpha \cdot \left(rand - \frac{1}{2} \right) \cdot |x_{max} - x_{min}| \quad (5)$$

Where, the second term is the attraction (movement of position) of firefly i towards the brighter firefly j. But this attraction is compromised by the third term which adds a random movement to the current position ofi. It is worth pointing out that, this second term performs exploitation whereas the third term performs exploration here.$\beta_{i,j}$is attractiveness parameter; α is the randomization parameter with 'rand' being a random number generator uniformly distributed in [0, 1].$\beta_{i,j}$is determined as follows:

$$\beta_{i,j} = \beta_{max} \cdot e^{-\gamma r_{i,j}^2} \quad (6)$$

Where, β_{max} is the maximum attractiveness when distance r = 0, and γ is absorption coefficient (of the air)which controls the speed of the convergence. Thus, the attractiveness will vary with the distance $r_{i,j}$between firefly i and j.

$$r_{i,j} = \|x_i - x_j\| = \sqrt{\sum_{d=1}^{D} (x_{i,d} - x_{j,d})^2} \quad (7)$$

After moving, the new firefly is evaluated and updated for the light intensity again. During pairwise comparison loop, the best-so-far solution is iteratively updated. Thispairwise comparison process is repeated until termination criteria are satisfied.

3. Robotic path planning

Path planning problem can be stated as: "Given a mobile robot R which is free to move in a two dimensional space V which holds some obstacles (static as well as moving) O whose shapes and trajectories are known to prior, and also given a source position S and target position T, robot path planning is to find an optimal path from S to T without any collision with obstacles, using a proper algorithm."
Now the algorithm which does this task we call it as 'Robot Path Planning algorithm' or RPP algorithm. An RPP algorithm does the task in many ways; one of the best ways to do it is to exploit a befitting optimization algorithm as GA [10], ACO [11], PSO [12] and ABC [13].
What these optimization algorithms do is that, parallel with their converging to optimum solution, they advance the robot towards its goal point. Butthe intrinsic exploration or randomization of an optimization algorithm may also cause the robot to deviate from the course and to wander in unusual trajectories. For this, the mother RPP algorithm makes some adjustments and adds other accessories to the optimization algorithm to make it work in proper ways. It also has to make provisions for dealing with the probable future obstacles. Sonow you see that, a good RPP algorithm takes an optimization algorithm and furnishes it with a whole accouterment; and if we take these trappings out of it, then the RPP algorithm will show us the inherent characteristics of the optimization algorithm it uses, and you can visualize these properties by the two dimensional paths it creates.

3.1 Proposed approach

The position of the robot is represented by Cartesian co-ordinates such as x- and y-coordinate positions.
The main steps of the proposed algorithm are as follows:

Step 1: An optimization algorithm is chosento be visualized.
Step 2: An initial population of particles (bees or fireflies) are generated around the robot's start position and within its sensing range in a circle.
Step 3: Each particle assumes a new position by the execution of an iteration of the optimization algorithm.

Step 4: All the particles are checked if they lies inside any obstacle or if the lines connecting the new positions of the particles to the robot's current position intersect any obstacle; if any particle lies inside or intersects any obstacle, then the particle is relocated to another new position and checked again and again until it finds a feasible position.

Step 5: The best particle (i.e., the one nearest to the goal and most distant from all the sensed obstacles) is found accordingly with the requirement. Move the robot onto it and go to Step 3.

Step 6: Perform Steps 3–5 until the goal is within the robot's sensing range and can be accessed via a straight line.

Step 7: If the robot's position is stuck in a local optimum other than the goal point, re-initialize the particles around the robot's position and go to Step 3.

Step 8: Trace all the successive point positions of the robot and process for visualize.

3.2 Fitness Function

In the step-5 of the proposed approach, we see that the best particle among all others is to be chosen. So every particle in its current position has to be evaluated over its fitness for it to be selected. So something is needed to be used as evaluator of every particle; this evaluator may be called as a fitness function.The fitness value of ith particle is determined as follows:

$$F = w_g \cdot \sqrt{(x_i - x_g)^2 + (y_i - y_g)^2} - w_o \cdot \sum_{o=1}^{M} \sqrt{(x_i - x_o)^2 + (y_i - y_o)^2} \quad (8)$$

Where (x_i, y_i) is current position of ith particle and (x_g, y_g) is co-ordinate of goal point and (x_o, y_o) is co-ordinate of the sensed obstacle, where o = 1, 2, 3,.., M; M being the number of sensed obstacles.

The first term is for measuring the Euclidean distance between the particle and goal point; the second term is for the cumulative distance of the particle from all the sensed obstacles. w_g and w_o are two weighing factor to balance the two terms.

4. Experiments and results

All the experiments are executed in a Fujitsu LH531 computer and the configuration of PC was Intel(R) Pentium(R) CPU B960 @ 2.20 GHz and 2 GB RAM.As RPP uses a two dimensional space, it is needless to say that, the dimension used for all the three algorithms, D=2. All the experiments are performed in a space of 200x200 square units. In the objective function, w_g and w_o are taken as 1 and 0.2 respectively. Maximum generation was kept as 100 for all. Number and shapes of obstacles in all the environments are uniform. To make a dynamic environment, some positions were assignedto the obstacles initially, before starting iterations, and then the obstacles move randomly in a range of (-1,1) for both x and y co-ordinates in each iteration.

Table 1. Length of the paths generated by PSO, ABC and FA

Particle No.	PSO			ABC			FA		
	Best	Worst	Mean	Best	Worst	Mean	Best	Worst	Mean
100	278.24	282.59	280.032	292.71	321.29	299.58	272.30	279.12	276.42
200	272.70	280.63	276.10	279.43	290.12	285.21	269.16	276.32	273.29
300	272.03	278.25	274.64	277.75	287.85	282.55	269.67	274.39	272.06
375	271.34	276.48	273.37	276.47	285.72	280.27	268.82	273.24	271.63
450	271.02	276.20	272.03	275.31	284.92	278.81	268.47	273.22	270.89

From Table 1andFig. 1(a) through Fig. 3(b), the larger are the particle (candidate solutions) numbers, the more the paths generated straighten. As the paths created by ABC algorithm are most curled up, it can be said that the algorithm has a larger exploration tendency and it lacks on convergence speed. The Firefly algorithm based pathis the most straightened all the time, so it can be assumed as the most converging algorithm but it is the most time consuming, as we can see in Table 2. PSO performs well and almost parallel with Firefly algorithm. It

should also be noticed that, all the algorithms succeed in making the robot reach the goal point after all, so they are all reliably usable in practical field.

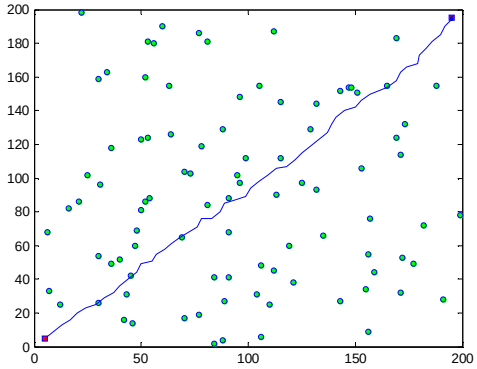

Fig. 1(a). Path by PSO for 100 particle

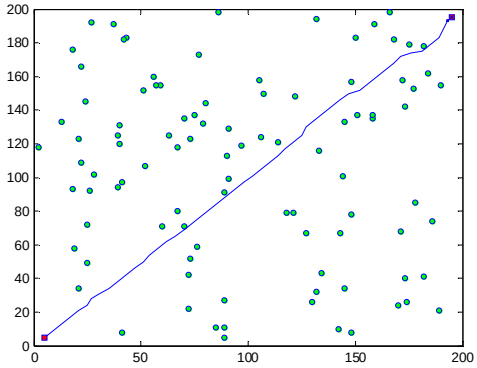

Fig. 1(b). Path by PSO for 300 particle

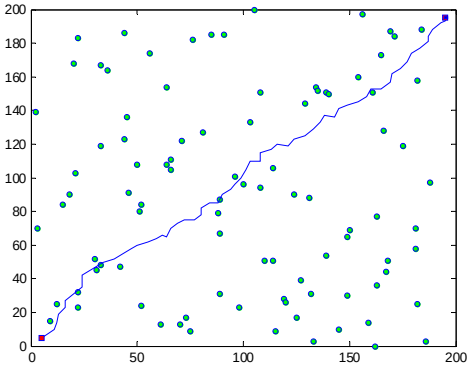

Fig. 2(a). Path by ABC for 100 particle

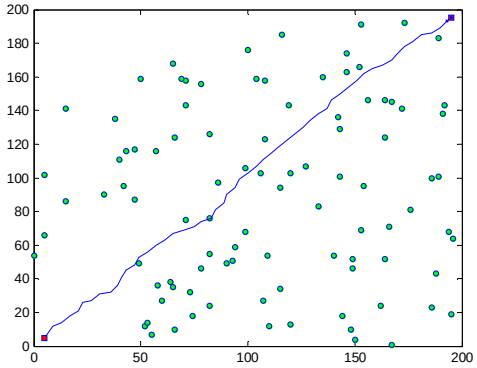

Fig. 2(b). Path by ABC for 300 particle

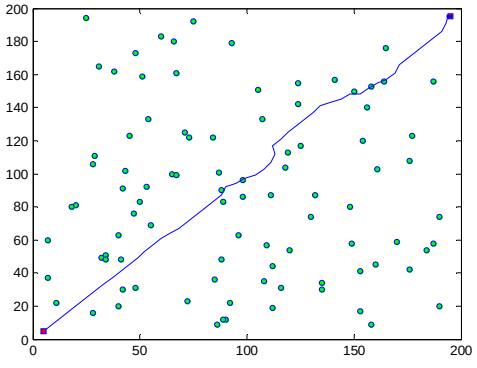

Fig. 3(a). Path by FA for 100 particle

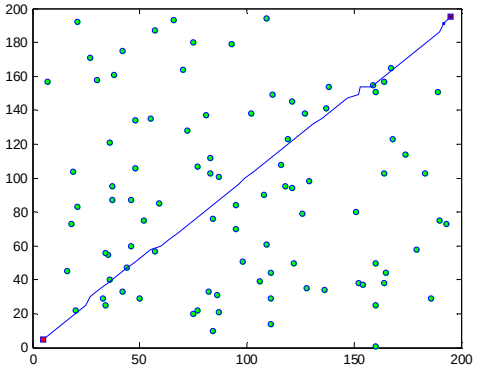

Fig. 3(b). Path by FA for 300 particle

Table 2. Processing time for the paths generated by PSO, ABC and FA

Particle No.	PSO			ABC			FA		
	Best	**Worst**	**Mean**	**Best**	**Worst**	**Mean**	**Best**	**Worst**	**Mean**
100	40.56	49.18	43.64	51.21	62.55	56.41	41.87	61.06	45.90
200	38.55	53.91	41.52	42.17	55.43	46.041	54.69	60.56	56.98
300	38.25	46.84	40.99	40.84	54.98	43.83	77.77	82.86	80.04
375	37.40	47.09	40.56	38.91	54.77	42.34	93.64	102.29	97.85
450	36.82	45.61	40.12	37.73	53.83	41.27	112.75	119.68	116.43

5. Conclusion

This work demonstrates just a new way to use the idea of robotic path planning. As in these cases: when the path is unnecessarily lengthy or roundabout, it can be assumed that the optimization algorithm has an excessive emphasis on exploration and has a lack on convergence capability; if the path is stuck on some point in the space and cannot be further extended despite the particle number being sufficiently large, then the optimization algorithm may be assumed as having a deficiency on exploration: the future researchers can use RPP algorithms in other advantageous ways as this work uses.

6. References

[1] Md. Tajmiruzzaman, Md. Asadujjaman,"Artificial Bee Colony, Firefly and Bat Algorithm in Unconstrained Optimization",*Proc. ofICMIEE,*Paper ID. ICMIEE-PI-140169, pp. 1-6, 2014.

[2] Md. Rakibul Islam, Md. Tajmiruzzaman, Md. MahfizulHaqueMuftee, Md. SanowarHossain, "Autonomous Robot Path Planning Using Particle Swarm Optimization in Dynamic Environment with Mobile Obstacles & Multiple Target", *Proc. of ICMIEE*, Paper ID. ICMIEE-PI-140282, pp. 1-6, 2014.

[3] G. Beni, J. Wang, "Swarm Intelligence in Cellular Robotic Systems", *Proc. of NATO Advanced Workshop on Robots and Biological Systems, Tuscany, Italy*, June 26–30, 1989.NATO ASI Series, Vol. 102, pp. 703-712, 1993.

[4] R. Eberhart and J. Kennedy, "A New Optimizer using Particle Swarm Theory", *Proc. of the Sixth International Symposium on Micro Machine and Human Science*, pp. 39-43, 1995.

[5] Y. Shi, and R. C. Eberhart, "Parameter Selection in Particle Swarm Optimizer", *Proc. of Seventh Annual Conference on Evolutionary Programming, Berlin: Springer-Verlag*, pp. 591-601, 1998.

[6] D. Karaboga, "An Idea Based on Honey Bee Swarm for Numerical Optimization", *Technical Report-TR06, Erciyes University, Engineering Faculty, Computer Engineering Department*, 2005.

[7] D. Karaboga, B. Basturk, "A Powerful and Efficient Algorithm for Numerical Function Optimization: Artificial Bee Colony (ABC) Algorithm", *Journal of Global Optimization*, Vol.39, pp. 459-471, 2007.

[8] X. S. Yang, "Firefly Algorithm, Stochastic Test Functions and Design Optimization", *International Journal of Bio-Inspired Computation*, Vol. 2, Paper No. 2, pp.78–84, 2010.

[9] X. S. Yang, "Nature-Inspired Metaheuristic Algorithms", *Luniver Press*, Second edition, pp. 81-96,2010.

[10] J. Solano, D.I. Jones, "Generation of Collision-free Paths by a Genetic Approach", *IEEE Colloquium on Genetic Algorithm for Control SystemEngineering*, pp. 5/1-5/6, 1993.

[11] H. Ying Tung, C. Cheng Long, C. Cheng Chih, "Ant Colony Optimization for Best Path Planning", *Proc. of IEEE/ISCIT*, Paper No.04, pp. 109-113, 2004.

[12] G. Z. Tan, G. J. Liu,"Global Optimal Path Planning for Mobile Robots Based on Particle Swarm Optimization", *Proc. ofApplications Research of Computers*, Vol. 24, Paper No.11, pp. 210-212, 2007.

[13] Qianzhi Ma,Xiujuan Lei, "Dynamic Path Planning of Mobile Robots Based on ABC Algorithm",*Lecture Notes in Computer Science,*Vol. 6320, pp. 267-274, 2010.

International Conference on Mechanical, Industrial and Materials Engineering 2015 (ICMIME2015)
11-13 December, 2015, RUET, Rajshahi, Bangladesh.

Paper ID: AM-12

Design and Development of a Mind-controlled Prosthetic Hand Using Electroencephalography Sensor

A H Khan[1], I Khan, Dr. M A R Sarkar
[1]Dept. of Mechanical Engineering, Bangladesh University of Engineering and Technology, Dhaka
E-mail: khanabidhossain@gmail.com

Abstract

The aim of this study is to develop a prosthetic hand in such a manner that the cost of production is drastically reduced and to make modern prosthesis available to people of third world countries. In this study, different designs are considered and compared to identify the suitable one. Also a new approach of using electroencephalography (EMG) sensor to control the prosthetic hand is introduced. This non-invasive technique allows detecting the attention level of human mind to activate the prosthetic hand and use it to grab or release an object. The possibility of eliminating surgery for prosthetic hand attachment is also investigated.

Keywords: *Prosthetic Hand, Electroencephalography, Brain signals, Beta wave*

1. Introduction

Many studies have been conducted for developing the design of human prosthetic hand. The development of modern prosthetic hand began with the invention of prosthetic hook by David Dorrance in 1912. It uses body power to open and close the hand to pick up an object. Since then, many designs were proposed for better efficiency and performance. Doshi, Yeh and LeBlanc designed a gloveless endoskeletal prosthetic hand in 1998 [1]. Massa, Roccella, Carrozza and Danio developed an underactuated prosthetic hand in 2002 which proposed a better degree of freedom of the hand [2]. Laurentis and Mavroidis developed a prosthetic hand which was shape memory alloy actuated [3]. Anthropomorphic artificial hand for prosthesis was proposed by Zollo, Roccella, Guglielmelli, Carrozza and Danio in 2007 [4]. Later, Dalley, Wiste, Withrow and Goldfarb designed a multifunctional anthropomorphic prosthetic hand with extrinsic actuators [5]. Also, most studies on prosthesis were based on EMG-based control but very few studies were conducted on the use of EEG brain signals for prosthetic hand control. Gagar, Harkam, Hertnaes and Pfurtscheller proposed prosthetic control by EEG-based human-computer interface in 1999 [6]. Mahmoudi and Irfanian then developed a single-channel EEG-based prosthetic hand grasp control for amputee subjects [7]. Our study is a unique approach where the human-computer interface is not required for prosthetic hand control; rather a microcontroller-based system is used for this purpose. Again, instead of using all EEG brain signal patterns, a specific brain wave called Beta wave, which is related to the attention level of human mind, was tracked with the electroencephalography sensor. The activity level of brain is measured with the help of Beta wave and this level is used to control the prosthetic hand.

2. Design considerations

While developing a suitable design for prosthetic hand, the first and foremost task is to design the fingers of the hand since the design of the fingers largely influence the number of motors used in the hand, thus cost of the total project. In this project, linkage mechanisms are utilized while designing the fingers so that only one motor is required to drive each finger. This highly limits the degrees of freedom of the finger segments but it also makes reduces the cost of the hand. In our study, three different possible designs of finger are presented and compared for advantages and disadvantages.

The first type of design of finger assembly with its kinematic diagram is shown in Fig. 1. From the figure, it is observed that the three finger segments ABCH, GCD and IDE are connected at points C and D. Also the three segments are interconnected with the help of two links FG and HI. These links make the movement of each segment interdependent. Thus using only one motor to apply force on extension A will allow the whole finger to create a curved shape and grab an object. So, the use of one motor for each finger is possible with this design.

The drawback of the design is that due to too many links and connections, it becomes extremely hard to avoid pressure development on the joints. Again, the design is such that one of the links is connected at a point H which is below the segment BC and CD. This extended part creates problems while grabbing an object.

To avoid this problem and keeping in mind that the topmost segment of the finger contributes very little on the overall force exerted for grabbing an object, the second type of design is suggested which is shown in Fig. 2

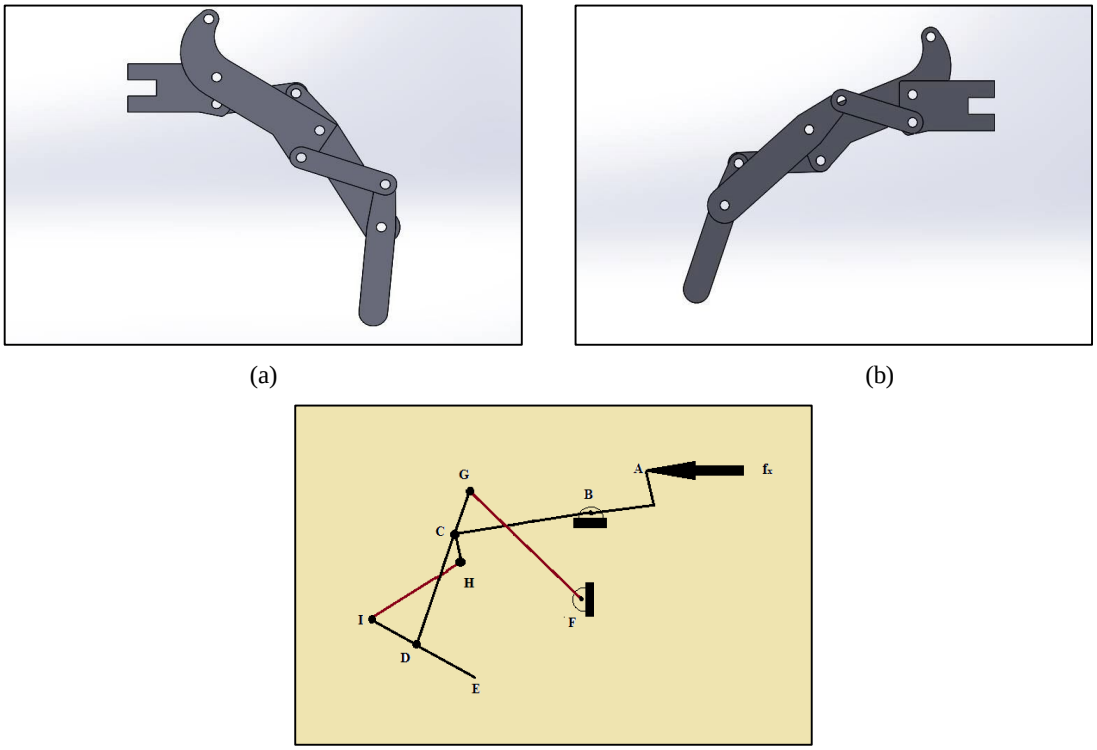

Fig. 1. Finger design of type 1; (a) left hand side view, (b) right hand side view, (c) kinematic diagram

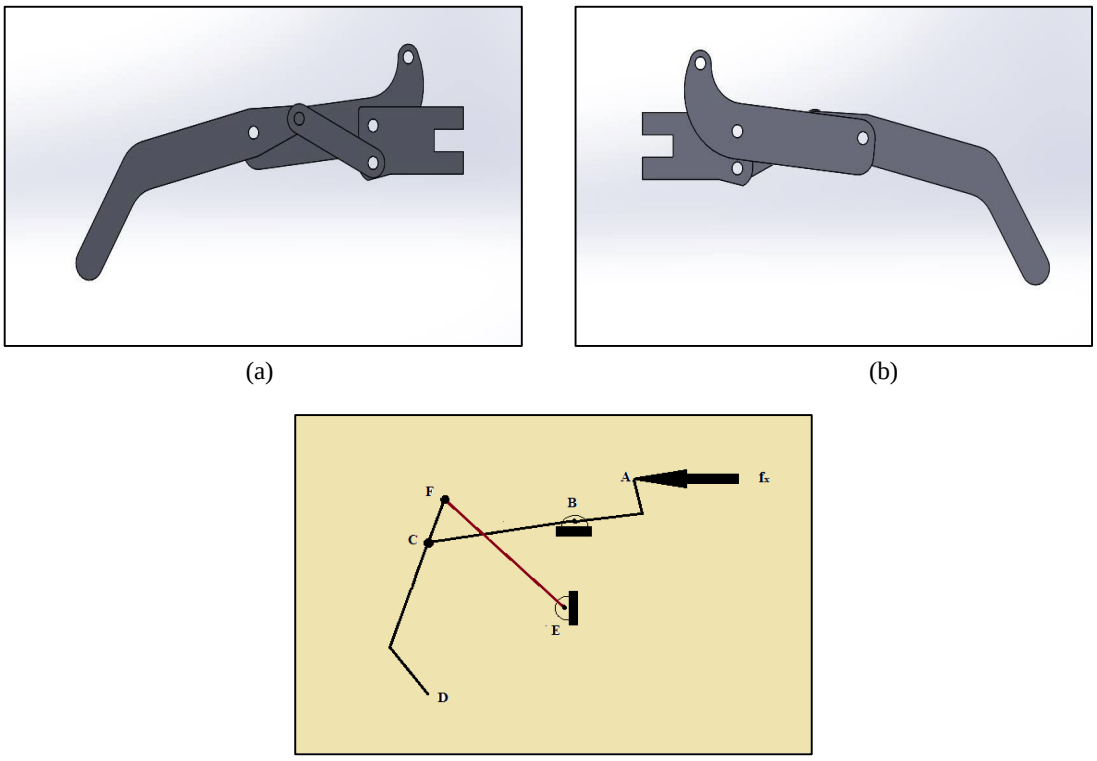

Fig. 2. Finger design of type 2; (a) left hand side view, (b) right hand side view, (c) kinematic diagram

In this design, the second and third segments of the finger are merged to form one single segment. So the number of segments is practically reduced to two, ABC and FCD and only one link is required which is EF. This not only solves the problem of interruptions while grabbing but also improves the performance of the hand. In the first design, due to too many links the power losses are greater. But in case of second design, these losses are much less.

Finally, the third type of finger design is shown in Fig. 3. This design is almost same as that of the second type but it is more compact. This is because the use of semi-circular slide ways instead of extensions at the end of the second segment has allowed the link to be placed more close to the joint between the two segments of the finger. This design can be useful because it can reduce the weight of each finger considerably. But the major drawback of the design is that the more the links are connected close to the joints, the greater is the torque required by the motor to exert sufficient force to grab an object. This is because a large force attend A will be reduced to a small force at the tip of the finger due to lever mechanism.

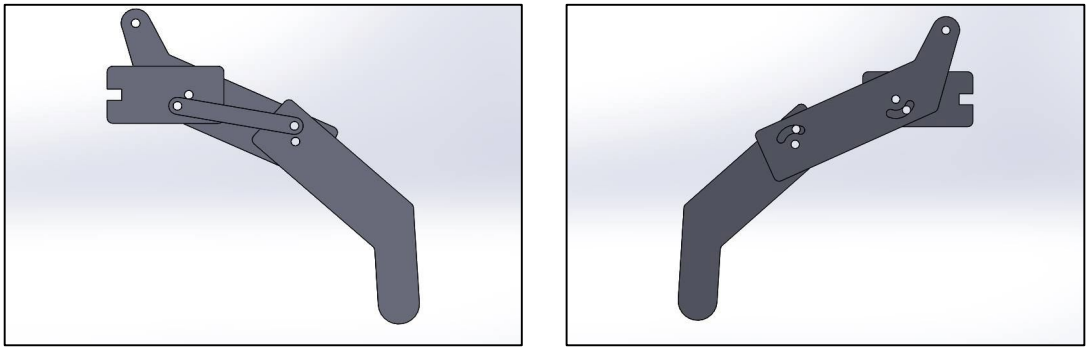

(a) (b)

Fig. 3. Finger design of type 2; (a) left hand side view, (b) right hand side view

Considering the advantages and limitations of the three designs, the second type is assumed to be appropriate for the prosthetic hand since it is a balance between the other two designs. So, in our prosthetic hand, the finger type 2 is used.

3. Material selection and manufacturing

The material of the prosthetic hand needs to be lightweight but strong enough to carry the load of the object. Carbon fiber is a good choice since it has both the qualities but it is very costly. Since the aim of this study is to develop a low cost prosthetic hand, plastic is a better option as material. Plastics are also lightweight and they also exhibit good strength. Also plastics can be easily processed. In our study, we have used acrylic plastic as the material which is available in the market at low price. This plastic is usually found in the form of plates or boards of different thickness. The prosthetic hand developed in this study uses 4mm thick acrylic boards.

The acrylic boards can be easily cut to desired shape in a laser cutting machine with high amount of accuracy. The laser cutting machines are provided with the two dimensional design of the parts to be cut and the machine follows the design to the scale. The machine used here has 0.25mm dimensional error. After cutting the parts in two dimensional planes, the parts are assembled to form the prosthetic hand.

4. Communication establishment with electroencephalography sensor

The process of communication establishment of the electroencephalography (EEG) sensor with the prosthetic hand is done through a microcontroller-based circuit. The microcontroller receives the data sent by the sensor and makes decision to operate the motors connected with each finger. For this, precompiled codes are loaded in the microcontroller. In this study, a microcontroller-based circuit called Arduino Uno is used.

The EEG sensor used in this project is manufactured by Neurosky and it is called Mindwave Mobile. The sensor is shown in Fig. 4.This sensor is a basically a headset which has three EEG probes to be placed at three different positions; one probe must touch the forehead, another at the ear and the third one at the side of the head. With the help of these probes, the sensor can measure the frequency of Beta, Gama and Delta- three different waves associated with human mind. In this study, only the Beta wave is taken into account.

Beta wave is closely related to the activity level of brain and indicated how much attentive a person is at a particular time. The frequency of the wave ranges from 12 Hz to 32 Hz. Low frequency indicates that the brain is at relaxed condition while higher frequency indicates high attention level. Mindwave mobile is provided with an in-built chip called Thinkgear which continuously interprets the frequency of Beta wave and sends a 170 bit data depending on it via Bluetooth.

The data sent via Bluetooth is received by the microcontroller with the help of a Bluetooth module that is paired with the sensor Bluetooth. Microcontroller then determines whether the person using the prosthetic hand wants to operate the hand or not. The microcontroller is coded in such a manner that if the person concentrates on an object that he wants to grab, then the microcontroller will send signal to the servo motors connected to each of the fingers. If the person wants to release the object, the person must remove his attention from the object. There is a threshold value of attention level for which the hand is activated. This threshold value is 60%. If a person has attention level more than 60%, then the prosthetic hand will be activated and the object will be picked up by the hand. The circuit diagram of the control system is shown in Fig. 5.

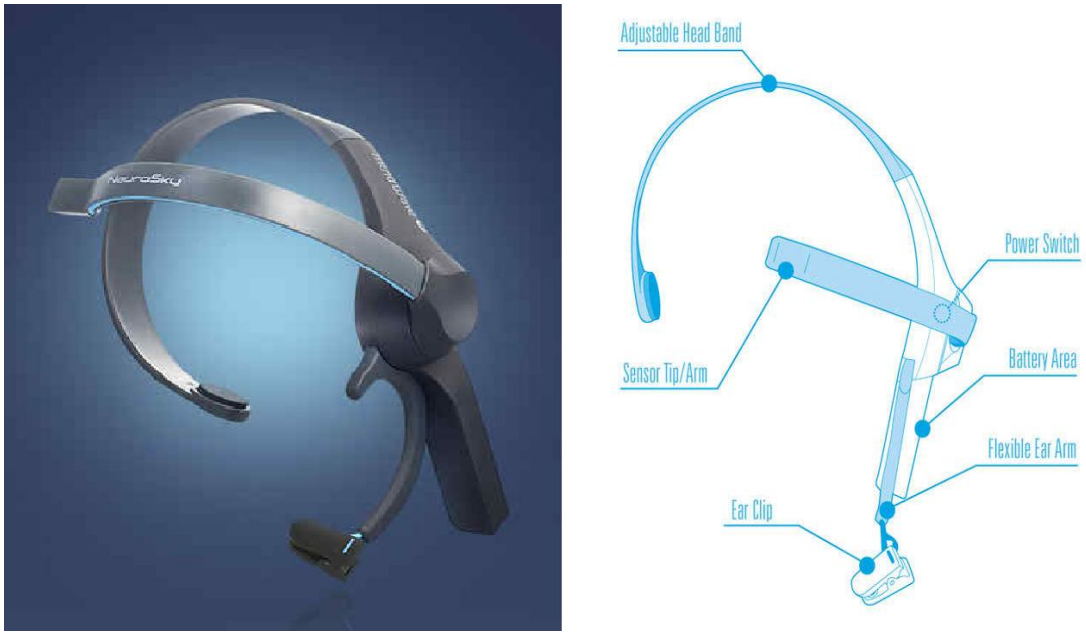

Fig. 4. EEG sensor headset

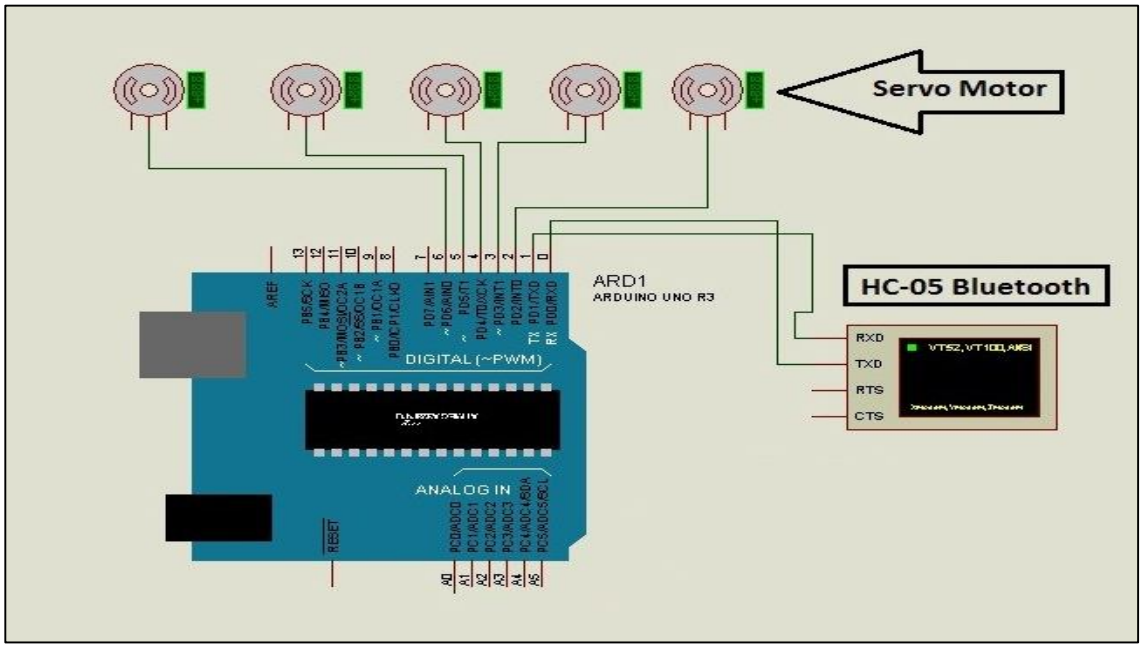

Fig. 5. Circuit diagram of the control system

The major success achieved in this study is that all the previous studies that used electroencephalography to control prosthetic hand required a human-computer interface but in our study computer has been replaced by microcontroller, thus making it portable. It has been possible since the complete EEG mapping of the brain is not done in this project to identify the EEG patterns for each movement pattern of the hand. Instead, only the attention level is measured, which reduces the amount of data to be processes, thus reducing the processor requirements. But the major drawback of this is that only one task is possible to do with the hand and that is grabbing or releasing an object. Still, the cost associated with computer interface is avoided, which makes the prosthetic hand low cost and affordable for people of third world country.

5. Final assembly of prosthetic hand

The fingers and motors operating the fingers are assembled together on an acrylic base. The base is cut in such a shape that there are slots for placing servo motors into specific positions. The servo motor used for each finger has a maximum torque limit of 2kg-cm. the motor horns are connected to the fingers with acrylic links. Fig. 6 shows the final assembly of the prosthetic hand.

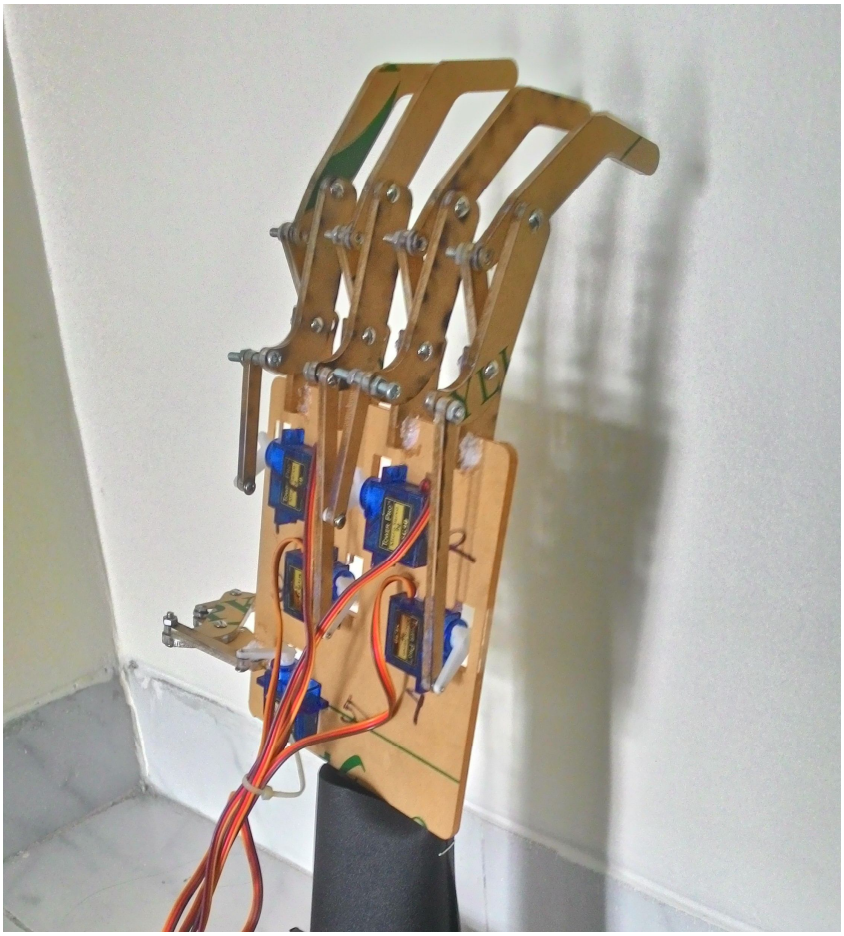

Fig. 6. Final assembly of prosthetic hand

In order to connect the prosthetic hand to a person's body, a plastic structure with screws is used which is designed after taking the measurements of the person. Since EG sensor is non-invasive in nature, surgical procedures may be avoided. But this type of joint is not suitable for lifting heavy objects with the hand. So, development of the design is necessary so that it can be attached to the body permanently with surgical procedures.

The power supply of the motors and the control circuit is done with the help of four Lithium-ion batteries which are small and compact but can supply high amount of energy for a long time period. The power supply system is placed inside the plastic structure. Thus, the power supply system contributes very little to the overall weight of the assembly.

6. Result and conclusion

The prosthetic hand was tested on 20 persons for analyzing the performance of the hand. The sensor worked well in almost 90% cases with few exceptions. Most of the people failed to raise their concentration level high enough to activate the hand in their first trial but they were able to control the hand properly after a few more trials.

Another important thing observed is the dependence of performance of the sensor on the weather. At higher humidity or lower temperature the performance of the sensor was pretty much low.

The metal gear servo motors connected to each finger can take around 2 kg loads, but due to linked structure of the finger, almost half of the energy is lost in the mechanism. And since only four fingers mainly contribute to holding an object while the other one is for support, the prosthetic hand can lift a maximum load of 4 kg if it is permanently attached to the bones. In case of a temporary joint of the hand, it is observed that a person feels pain if he tries to lift more than half kilograms.

The use of metal gear servo motors for finger control has a major drawback. The amount of force exerted on an object cannot be varied if servo motor is used, which is the case in the prosthetic hand developed in this project. Also they take up a significant amount of space which increases the size of the hand. If the servomotors are replaced by hydraulic muscles, these problems can be solved. But use of hydraulic muscle is very costly compared to servo motors. The decision may be taken depending on the targeted people for whom the hands are manufactured.

Again the use of attention level to activate the hand has some problems since continuously concentrating on an object will not be possible if the person wants to do two things at a time. For example, after lifting a glass of water, the moment he tries to drink water, the attention on the glass will be removed, and thus the hand will release the glass. This type of situation is undesirable. To avoid this problem, the reverse design of the system can be done so that when attention is given on an object, the hand opens wide and after removing the attention the hand closes. This may be a more practical system of controlling the hand.

Finally, the major limitation of the hand is that it has only one function and that is to grab an object. But human hand can perform so much more tasks and follow so many finger patterns. But in order to achieve that, each and every pattern of brain EEG signals needs to be mapped so that the prosthetic hand can identify and follow that pattern. This will lead to high cost of the hand, thus unaffordable for people third world country. Nevertheless, further studies are required for developing a better and more human-like prosthetic hand operated by Electroencephalography.

7. References

[1] R. Doshi, C. Yeh, and M. LeBlanc, "The design and development of a gloveless endoskeletal prosthetic hand", *Journal of Rehabilitation Research and Development,* Vol.35, No.4, pp. 388-395, 1998.

[2] B. Massa, S. Roccella, M.C. Carrozza, and P. Dario, "Design and Development of an Underactuated Prosthetic Hand", *Proc. of the IEEE, International Conference of Robotics and Automation, Washington,* pp. 3374-3379, 2002.

[3] K.J. De Laurentis, and C. Mavroidis, "Mechanical design of a shape memory alloy actuated prosthetic hand", *Technology and Health Care, IOS Press,* Vol. 10, pp. 91-106, 2002.

[4] L. Zollo, S. Roccella, E. Guglielmelli, M.C. Carrozza and P. Dario, "Biomechatronic Design and Control of an Anthropomorphic Artificial Hand for Prosthetic and Robotic Applications", *IEEE/ASME Transactions on Mechatronics,* Vol. 12, No. 4, pp. 418-429, 2007.

[5] S.A. Dalley T.E. Wiste, T.J. Withrow, and M. Goldfarb, "Design of a Multifunctional Anthropomorphic Prosthetic Hand with Extrinsic Actuation", *IEEE/ASME Transactions on Mechatronics,* Vol. 14, No. 6, pp. 699-706, 2009.

[6] C Guger, W. Harkam, C. Hertnaes, and G. Pfurtscheller, "Prosthetic Control by an EEG-based Brain-Computer Interface (BCI)", *Proc. aaate 5th European Conference for the Advancement of Assistive Technology,* pp. 3-6, 1999.

[7] B. Mahmoudi, and A. Erfanian, "Single-channel EEG-based prosthetic hand grasp control for amputee subjects", *Proc. of 2nd joint EMBS/BMES Conference,* Vol. 3, pp. 2406-2407, 2002.

International Conference on Mechanical, Industrial and Materials Engineering 2015 (ICMIME2015)
11-13 December, 2015, RUET, Rajshahi, Bangladesh.

Paper ID: AM-17

Vibration Monitoring and Condition Analysis of a 210MW Steam Turbine

I. Ahmed[*1], R. Islam[*2], M.A.R. Sarkar[*3], Ziaul Haq[**4]
[*] Department of Mechanical Engineering, Bangladesh University of Engineering and Technology, Dhaka 1000
[**] Superintendent Engineer, BPDB
E-mail: irfanahmed.me@gmail.com

Abstract

In this paper a description is given of the technique of vibration monitoring for condition analysis of steam turbine. Its value as a maintenance tool in the power plant is explained with examples of the type of faults which can be detected at an incipient stage without dismantling or taking the steam turbine off-line. For this purpose a steam turbine of model K-210-130-8 is monitored.
Many power generation steam turbines today are required in service well beyond their intended lifetimes. Dismantling for inspection is expensive and authority need to consider all relevant information in making the decision. Application of condition monitoring in all the applicable methods is justified, with each showing different degradation modes. Data obtained from tests before and after overhaul also reveal whether any restorative work achieved the expected improvements in performance. The paper outlined, with vibration monitoring and condition analysis of a 210MW steam turbine without dismantling it from its working condition.

Keywords: *vibration monitoring, condition analysis, steam turbine.*

1. Introduction

Engineering systems possessing mass and elasticity are capable of relative motion. If the motion of such systems repeats itself after a given interval of time, the motion is known as vibration. Vibration, in general, is a form of wasted energy and undesirable in many cases. It occurs in all mechanical equipment including steam turbines, nuclear power plants [1], pumps etc. Steam turbines are the mainstay of electricity production worldwide. Today's competitive electricity generation market has increased the pressure to keep power generation plant online as and when required. A contributing factor in providing ongoing assurance of acceptable plant condition is the use of vibration monitoring. Methods should be applied according to the modes of degradation expected. Vibration monitoring provides much of this assurance, and has developed such that access to on line vibration data is available to experts who may be located remote from the plant. Some degradation modes can be detected by visual inspection or non-destructive testing, eventually casings do require to be opened for inspection [2]. This is particularly so for the many large power generation machines continuing in service beyond their intended design life. Vibration monitoring can be applied to most plant. It is the one vibration analysis technique, which allows the optimum time for restorative maintenance to be determined, where the deterioration results in increased fuel consumption, or in reduced output, or both. It should be accepted that a turbine outage after a long time in service would probably take longer than if scheduled more frequently, as internal distortion is likely to have occurred. Also, parts such as casing will probably need replacement. Once a casing is opened and clearance measurements made, it is possible to estimate the performance improvements achievable by refurbishment and so justify the expenditure. However, it is clearly preferable to try to determine the internal condition first by testing. The overhaul decision should not be made unless there is a compelling technical or economic reason for opening a casing. Vibration monitoring has been used to extend time between openings of casings to up to 17 years, making its cost/benefits very favorable [3]. Vibration monitoring can also be used to evaluate the effect of maintenance or modification work on the steam path. This is of great benefit when justifying future work.

2. Vibration characteristics of common faults

Rotor imbalance

The key characteristics of the vibration caused by imbalance are (1) it is sinusoidal at a frequency of once per revolution (2) it is a rotating vector and (3) amplitude increases with speed. These characteristics assist in differentiating imbalance from faults that produce similar vibration. The vibration caused by pure imbalance is a once per revolution sine wave sometimes accompanied by low-level harmonics [3]. The faults commonly

mistaken for imbalance usually produce high-level harmonics or occur at higher frequency. In general, if the signal has harmonics above once per revolution, the fault is not imbalance. However, high level harmonics can occur with large imbalance forces, or when horizontal and vertical support stiffness differs by a large amount.

Oil whirl in fluid film bearings

Rotor supported by fluid film bearings are subject to instabilities not experienced with rolling element bearings. A basic difference exists between vibration due to oil film instability and vibration due to other faults, such as imbalance. The latter is a forced response to the imbalance force, occurs at the same frequency and is proportional to the size of the force. Oil film instability, on the other hand is a self-excited vibration that draws energy into vibratory motion that is relatively independent of rotational frequency. This is a highly complex study and further comment is outside the scope of a general paper.

Misalignment

Vibration due to misalignment is usually characterized by a 2 times running speed component and high axial levels. Misalignment takes two basic forms, (1) preload from a bent shaft or improperly seated bearings and (2) offset of the shaft centre-lines of machines or parts of machines in the same train. Flexible couplings increase the ability of the train to tolerate misalignment but are not a cure for serious alignment problems.

Mechanical looseness

Mechanical looseness usually involves bearing mounting housings or bearing caps; and almost always results in a large number of harmonics in the vibration spectrum. Components at integer fractions of running speed may also occur. Looseness tends to produce vibration that is directional, a characteristic that is useful in separating looseness from rotational defects such as imbalance [4]. Measured vibration will be highest in the direction and vicinity of the looseness. One characteristic of looseness is that the basic sinusoidal wave form is truncated or flat-topped, where the looseness is restricted and taken up at the end of travel.

Blades and vanes

Problems with blades and vanes are usually characterized by high fundamental vibration or a large number of harmonics near the blade passing frequency. Some components of blade passing frequency (number of blades X rpm) are always present and levels can vary markedly with load. This is especially true for high speed turbo-machinery and makes recording of operating parameters for historical data critical. It is important to establish base line spectra for several operating levels.

Resonance

Problems with resonance occur when natural frequencies of the shaft, machine housing or attached structures are excited by running speed or harmonics of running speed [7]. These problems are usually easy to identify because levels drop appreciably when running speed is raised or lowered. Spectral maps are especially useful in detecting resonance vibration because the strong dependence on running speed is readily apparent. Piping is one of the most common sources of resonance problems. When running speed coincides with a natural frequency, the resulting vibration will be excessive and strain on the pipe and machine will be excessive and
can lead to early failure.

.3. Description of Experimental Facility

Turbine

Specification of the turbine used in the experimental facility is as follows:

- Model No: K-210-130-8
- Type: Condensing type
- Capacity: 210 MW
- Inlet Pressure of Steam: 130kg/cm square
- rpm: 2500-4000

The turbine has total 29 stages. Low pressure cylinder has 6 stages, Intermediate pressure cylinder has 11 and High pressure cylinder has 12.

Vibro-Meter VM600

The Vibro-Meter VM600 is totally flexible both in terms of physical and system configuration. Its working range is from 5-50000Hz. In addition the use of VME hardware, [1] open architecture and industry standard communication protocols for data exchange, VM600 is modular and saleable. VM600 consists of a standard VME chassis (19”, 6U) with four types of Processing/communication cards:

- MPC4 - Machinery Protection Card
- AMC8 – Analogue Monitoring Card
- CPU-M card for configuration/display and network communications to other systems
- CMC16 – Condition Monitoring Card

VM600 is operated with Machinery Protection System 1(MPS1) software.

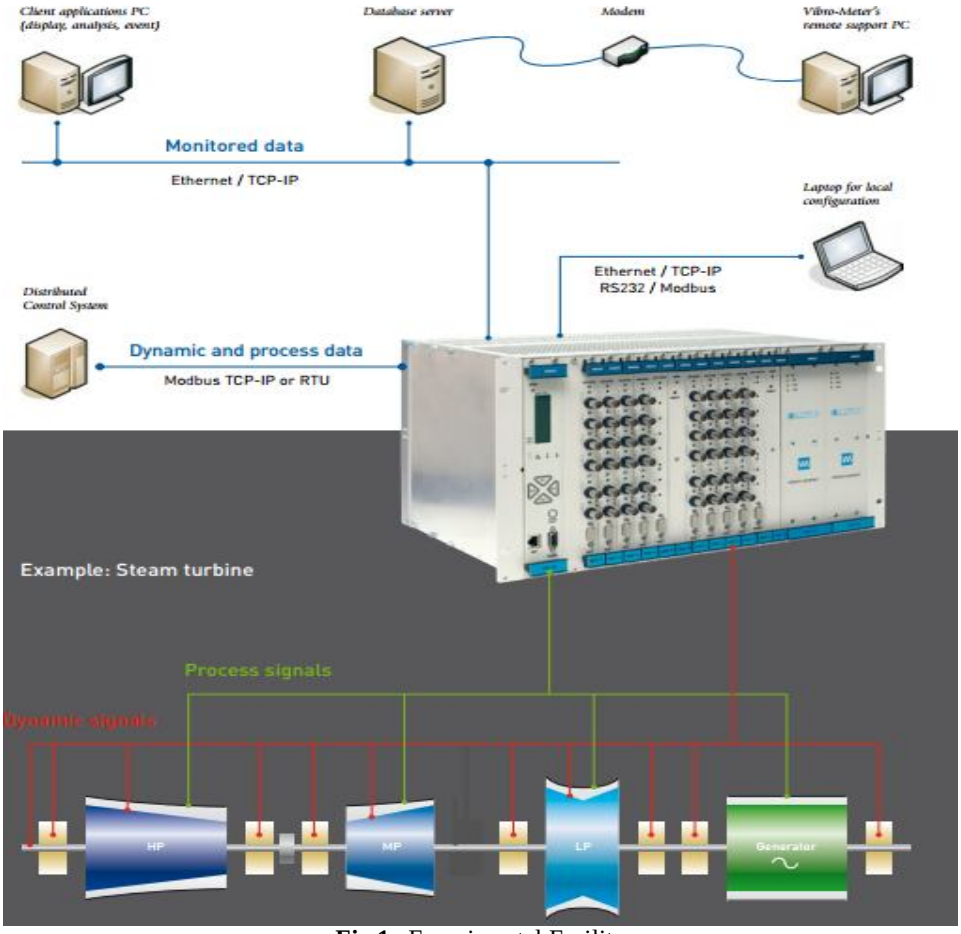

Fig.1 . Experimental Facility

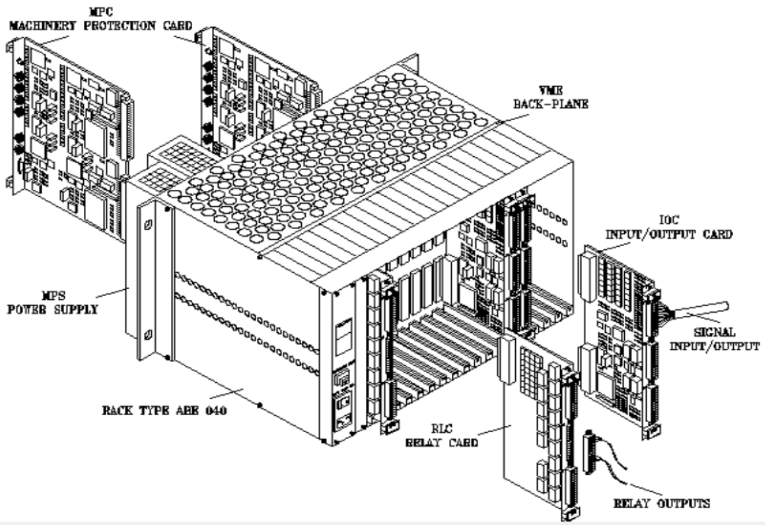

Fig.2 . Vibro-Meter (VM600)

Piezoelectric Accelerometer

Piezoelectric crystals are man-made or naturally occurring crystals that produce a charge output when they are stressed, flexed or subjected to shear forces. In a piezoelectric accelerometer a mass is attached to a piezoelectric crystal which is in turn mounted to the case of the accelerometer [7].

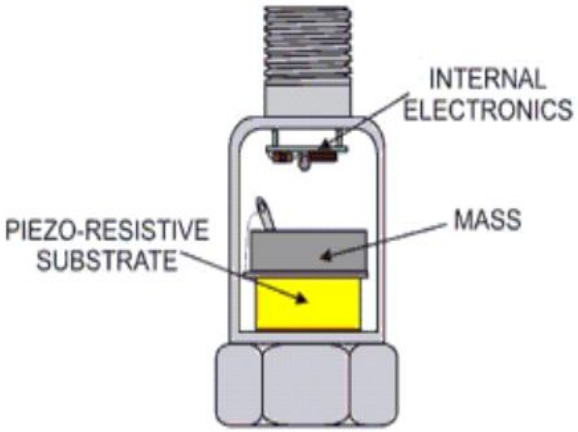

Fig. 3. A single ended compression accelerometer

When the body of the accelerometer is subjected to vibration the mass mounted on the crystal wants to stay still in space due to inertia and so compresses and stretches the piezoelectric crystal. This force causes a charge to be generated. As F=ma, this force is in turn proportional to acceleration. The charge output is either is converted to a low impedance voltage output by the use of integral electronics or made available as a charge output (Pico coulombs /g) in a charge output piezoelectric accelerometer [8]. In this system single ended compression accelerometers have been used. A single ended compression accelerometer is where the crystal is mounted to the base of the accelerometer and the mass is mounted to the crystal by a setscrew, bolt or fastener [8].

4. Methodology

For vibration monitoring three piezoelectric accelerometers have been installed on each of the seven bearings, present in the steam turbine [5]. The piezoelectric accelerometers are installed in three different directions, horizontal, vertical and axial. These accelerometers are used as input sources for Vibro-Meter VM600. So VM-600 is getting total twenty one inputs. VM-600 is getting input as acceleration and giving the output as velocity (mm/s) by integrating the input with respect of time in a definite range [6]. The output result is shown on the computer screen. If the output velocity reaches the value of 4.5 mm/s, the first alarm will be activated. After passing the value of 7.09 mm/s, the second alarm will be activated. After the second alarm, if necessary attempts are not taken for reducing the vibration or taking the output value below 7.09 mm/s; the turbine will shut down automatically. The vibration of the turbine is reduced by reducing or increasing the amount of fuel input and thus reducing or increasing the pressure.

6. Result and Analysis:

Data of vibration of the bearings were taken continuously for 10 days for analysis. From the collected data it has been found that the magnitudes of vibration are changing from time to time. Also the magnitudes are not same for the axial, vertical and horizontal accelerometers installed on the same bearing. For first to third bearings highest magnitudes have been found from axially installed accelerometers. For fourth to seventh bearings, highest magnitudes have been found from vertically installed accelerometers. The magnitudes of vibration of different bearings at a definite time have been provided in the table 1. From the table, the highest magnitude of vibration has been located at bearing no seven, which is also called the tail bearing. As the seventh bearing is located at the end part of the system, maximum instability as well as maximum amount of vibration was found there. So, the seventh bearing needs to be kept on continuous observation. Fig.4 is representing peak vibration vs. day for all the bearings. The peak vibration of a bearing indicates the highest magnitude of vibration which has been got on that day for the bearing. From Fig.4 it can be monitored that the magnitude of vibration is maximum at bearing no seven for each day. On fifth and sixth day the magnitude crossed the limit 4.5 mm/s. So the first alarm was activated on those days.

Table 1. Vibration Measured at a Specific Time

Bearing No	Output Vibration of Bearings (mm/s)		
	Axial (X)	Vertical (Y)	Horizontal (Z)
1	2.10	1.121	1.880
2	3.039	1.465	1.012
3	3.079	2.840	1.045
4	0.553	2.783	1.154
5	1.879	2.216	1.869
6	2.039	2.675	2.645
7	2.112	3.231	2.190

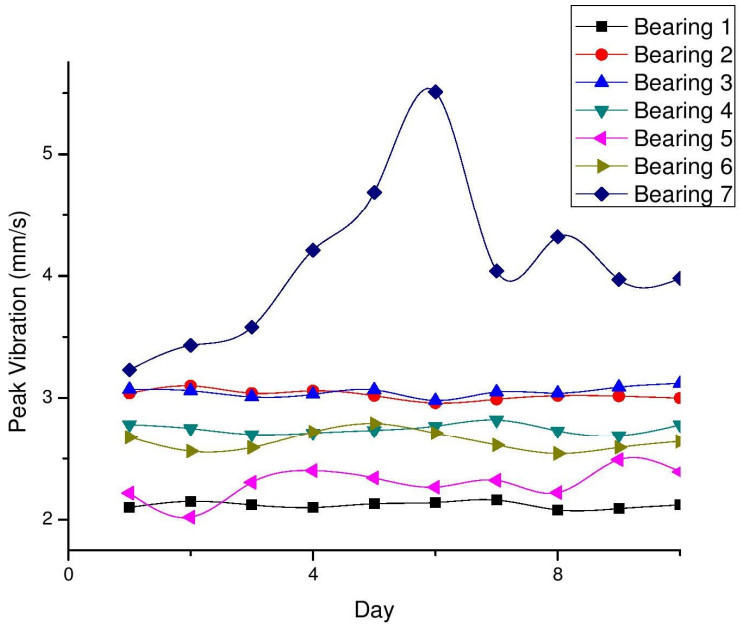

Fig.4 . Peak Vibration vs. Day

7. Summary and Closing Remarks

(1) Incorporation of VM600 system has made the condition monitoring process more reliable and more accurate.

(2) Vibration monitoring process should be imposed in all turbines for condition monitoring which will prevent the efforts of dismantling the turbine and loss of power generation.

(3) The visualization of the actual deformation of a structure under the operational unbalance force excitation gives a better insight in which modes are dominating the behavior at nominal speed. So it can be used in all kind of conditions.

(4) The most important future challenges for vibration monitoring lie in the integration with other condition monitoring techniques towards a reliable "residual lifetime monitoring", that will enable a safe and durable use of the assets in a flexible power generation portfolio.

(5) As magnitude of vibration is the maximum at seventh bearing, this one should be kept under continuous monitoring and observation.

11. References

[1] D.N. Brown, "Machine-Condition Monitoring Using Vibration Analysis; A case study from a nuclear power plant" pp.2-10, 2002.

[2] K. L. Mitra, R.J. Sing "Vibration Analysis Process and Its Implementation", *Sadhana*, Vol.13, Part.3, pp. 17-28, 2013.

[3] H. A. Searle, "Steam Turbine Condition Monitoring by Vibration Analysis",*PTSAST* , pp. 101-106, 2007.

[4] G. Boon, K. De Bauw " A journey through 30 years of vibration analysis on large turbines: a history of progress in technology and experience" *LABORELEC* , pp.111-126,2009

[5] Ray Beebe , "Condition Monitoring of Steam Turbine by Performance Analysis" *JQME*, Vol.9, No.2, pp.102-112,2003.

[6] M. J. Roemer, G.J. Kacprzynski, "Advanced Steam Turbine-generator maintenance planning using prognostic modes" *Proceedings of 54th Meeting of the Society for Machinery Failure Prevention Technology*, 2000.

[7] William T. Thomson, Marie Dillon Dahleh, Theory of Vibration with Applications, *Pearson Education*, 5th edition, pp. 160-213, 2011.

[8] William W. Seto , Mechanical Vibrations, *McGraw-Hill*, 2nd edition, pp. 2-42, 1995.

International Conference on Mechanical, Industrial and Materials Engineering 2015 (ICMIME2015)
11-13 December, 2015, RUET, Rajshahi, Bangladesh.

Paper ID: AM-19

Design, Simulation and Construction of an Automatic Wheelchair

Hasnayen Ahmed[1], Kazi Ehsanul Karim[2], Helal-An-Nahiyan[3]
[1,2,3]Department of Mechanical Engineering, Khulna University of Engineering & Technology, Khulna-9203, BANGLADESH
E-mail: riad.hasnayen@gmail.com , nahiyan.me@gmail.com

Abstract

Driving a manual wheelchair or crutches is a difficult task and past invented automatic wheelchair are not available in present market that can be bought and used for physically disable persons. The purpose of this research work is to propose of an automatic wheelchair system which facilitates the users. The proposed wheelchair has been implemented with design, simulation and construction of the whole body. Due to high sustainable stress, low cost and availability, Mild steel has been chosen over Aluminum, Cast iron, Stainless steel for frame material. The constructed wheelchair has a frame; four rear wheels with two shafts units; two front caster wheels for smooth turning and a chain driven gear train for power assist to rear wheel from motor shaft. The Sprocket gear is joined with chain which is connected with another smaller cassette that is mounted directly on motor shaft. In this wheelchair the chain is used to transmit power to drive wheel from the dc gear motor. Whenever the motor shaft rotates then the sprocket of rear spindle starts rotating and thus the wheel starts moving. Extensive testing was performed to ensure design integrity. This wheelchair has the potential to deliver increased freedom to a considerable consumer base.

Keywords: *Automatic Wheelchair, Sprocket Gear, Cost-Effective Electro-Mechanical.*

1. Introduction

An automatic wheelchair or electric-powered wheelchair is a wheelchair that is propelled by means of an electric motor rather than manual power. Automatic wheelchairs are useful for those who are not able to impel a manual wheelchair or who may need to employ a wheelchair for distances or over terrain which would be strenuous in a manual wheelchair. They may also be used not just by people with conventional mobility impairments, but also by people with cardiovascular and fatigue based conditions.

Today, worldwide there are around 600 million persons aged 60 and over; estimated one billion people live with disabilities. It is estimated that 16 million people in Bangladesh are living with disability (**Fig.1**) [1], whereas the actual scenario is much more acute. This is very frightening news, since aged people suffer from partial paralysis, trembling and usually unmovable problem.

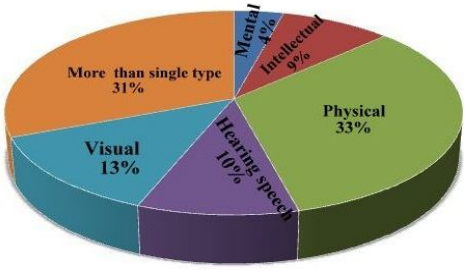

Fig. 1. Percentage of disable people in Bangladesh

Manual wheelchair and Automatic/Electric power wheelchair are available in current situation for assisting handicapped people. Manual wheelchairs can be operated by persons who have the use of their upper body or someone available to assist. But it only can move in limited surface only. In order to propel a manual wheelchair, a user not only has to move their weight, but they have to move the weight of the wheelchair as well. Some disabilities problems do not permit to move wheelchair manually. Most automatic wheelchairs are

implemented by modifying existing Powered Wheelchair systems. Examples include the Bremen Autonomous Wheelchair [2] and the Maid (Mobility Aid for Elderly and Disabled people) robotic vehicle [3]. These approaches arrange sensors and computing hardware around an existing infrastructure. They are able to take advantage of pre-built control and motor systems. One such project, the Tin Man wheelchair [4], uses servomotors to control the host chair through an unmodified joystick. Wheelchair equipment has also been designed from scratch. These devices enhance traditional designs in order to increase the possibilities of travel in challenging environments. They present complex control problems but can yield impressive results. One such project [5] proposes four hydraulic, wheeled, robotic legs. It aims to produce a device capable of ascending multiple stairs and lifting itself into vehicles. Another model [6], being developed by a commercial concern, can reputedly raise and balance itself on its rear wheels alone through the use of sophisticated gyroscopes and multiple Pentium processors.

Automatic wheelchairs, by their nature, demand specialized user interfaces. Whilst many projects do not address this issue directly, invariably using joysticks [2, 3, 5, 6], others do. One wheelchair [7] uses a visual display that shows a sequential scanning of commands (left, right, increase speed, stop, and etcetera). A highlighted command can be selected by pushing a button. Another design [9] uses natural language commands, such as "move forward" or "move left", though a headset microphone. More ambitious groups [4] have proposed commands such as "go to the kitchen" or "stop at the next door on the left". Other groups [10] have opted for voice recognition based on a user defined vocabulary and voice print techniques.

User uses the traditional wheelchairs need help from others or their own body power. Moreover physically weak users also face problems to grip joystick for moving the automated wheelchairs. In this circumstance, this project aims to design an automatic prototype wheelchair with button control which is fabricated from locally available resources and cheaper technologies that would be viable for disable person in the developing country like Bangladesh.

This project's wheelchair is distinguished from most other similar projects in its attempts to produce practical results using a minimum of equipment and computing power. These aims can be further defined through several distinct criteria;

a) Cost Effectiveness: This wheelchair will benefit the most individuals if the cost is not prohibitive. This factor is currently controlled by using locally available material and technology.

b) It must use practical components: Components should consider total system weight and dimensions. They should seek to maximize on-board battery life through power efficiency and minimize maintenance concerns through simplicity and durability.

c) It guarantees easy and comfortable driving.

d) It facilitates learning to handle the chair and obtaining maximum efficiency.

e) It should make the electronic system open to future additions.

f) It provides the ultimate easy movement & effortless independent operation without assistance by handicapped.

2. Material

Initially four materials were selected for frame. It was Aluminium 1060 alloy, Gray Cast Iron, Stainless Steel, Mild Steel and numerical analysis was done on it by Solidworks 2015. This simulation was done with 980N (User's Weight). Stress analysis on Alluminium, Cast Iron, Stainless, Mild steel is showed in **Fig. 2, Fig. 3, Fig. 4**, **Fig. 5** respectively. Stress, Strain, Displacement Result is showed in **Table.1**.

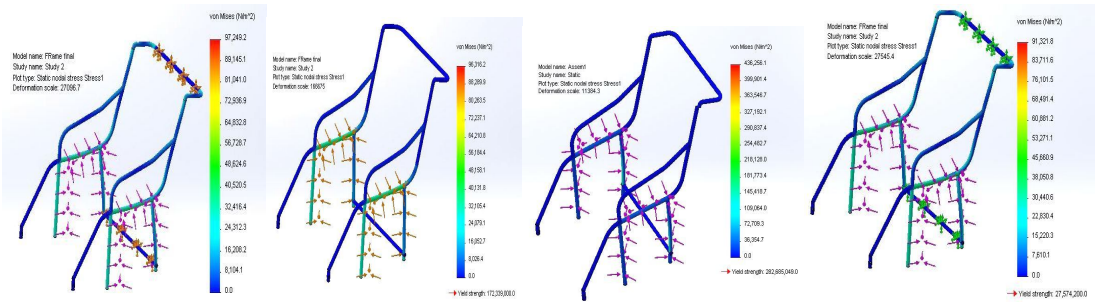

Fig. 2. Alluminum **Fig. 3.** Cast iron **Fig. 4.** Stainless steel **Fig. 5.** Mild steel

From Simulation result it is showed that Mild steel can sustain higher stress and it's Strain & displacement is very low than other material. Due to good simulation result, low market cost and availability Mild steel has been selected for frame material. The property of this material is given in **Table. 2.**

Table. 1. Stress, strain, displacement result by simulation

Material	Max. Stress (N/m^2)	Max. Strain	Max. Displacement (mm)
Alluminium	91321.8	1.136×10^{-6}	5.033×10^{-3}
Cast Iron	97249.2	1.167×10^{-6}	5.09×10^{-3}
Stainless Steel	96316.2	3.874×10^{-7}	6.987×10^{-4}
Mild Steel	436256.1	9.403×10^{-7}	1.101×10^{-2}

Table. 2. Property of mild steel

Property	Value	Unit
Elastic modulus	2.0499×10^{11}	N/m^2
Poisson's ratio	0.29	N/A
Shear modulus	7.9987×10^{10}	N/m^2
Mass density	7858	kg/m^3
Tensile strength	425000003.2	N/m^2
Yield strength	282685049	N/m^2
Thermal expansion Coefficient	1.2×10^{-5}	/K
Thermal conductivity	52	W/(m.k)
Specific heat	486	J/(kg.K)

3. Mechanical Design

The design of the wheelchair and stress & displacement analysis is done by using Solidworks 2015 software and the outlook view is generated with Keyshot4 software. Mild steel is used as material for simulation purposes. The design of the wheelchair is done by considering the maximum weight of the person is 100kg. So, the structure of the wheelchair has to be capable of carrying 980N load. Von Mises stress analysis and URES displacements indicate the validation of structure strength, using Mild steel under 980N load. Designed structure of the wheelchair is given in **Fig. 6**.

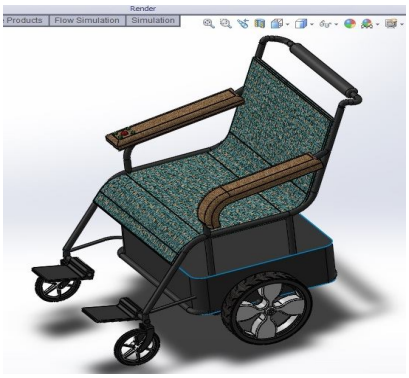

Fig. 6. Complete view of designed wheelchair

3.1 Von Mises stress analysis

Von Mises stress analysis is used to find the yielding criteria of isotropic or ductile materials under complex load. According to Von Mises yield criterion, it is independent of first stress invariant. But the ductile materials will exceed yield point when the second deviatory stress invariant will reach a critical value. The stress analysis of wheelchair frame, seat and rear shaft are given in the **Fig.7**, **Fig.8** and **Fig.9** respectively.

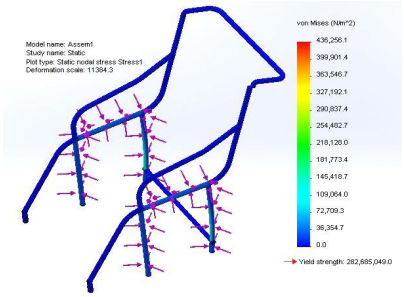

Fig. 7. Stress analysis on frame

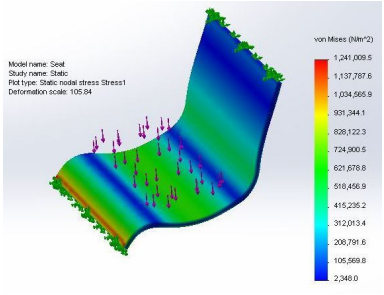

Fig. 8. Stress analysis on seat

From the stress analysis of the wheelchair frame, seat and shaft, it is found that the structures will sustain under the applied load.

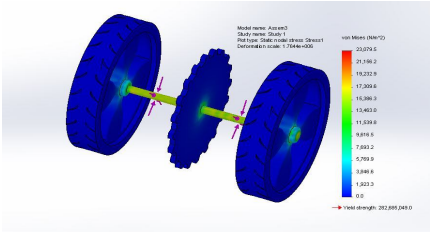

Fig. 9. Von Mises stress analysis on shaft

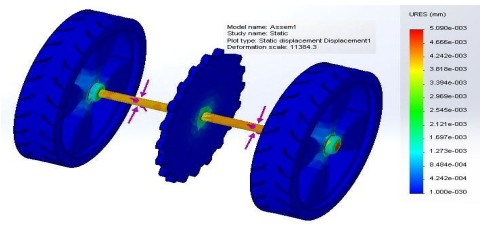

Fig. 10. URES displacement on shaft

3.2 Resultant displacement

The resultant URES displacement of Solidwork shows the average displacement of the wheelchair structure. It is found from the analysis that the highest deformation of the wheelchair frame is 0.001101mm under the applied load. The URES displacement of the wheel shaft, frame and seat are shown in **Fig.10**, **Fig.11**, and **Fig.12** respectively.

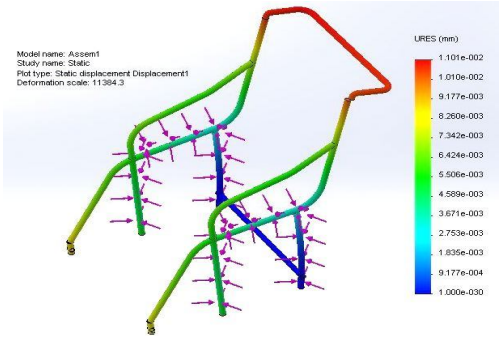

Fig. 11. URES displacement on wheelchair frame

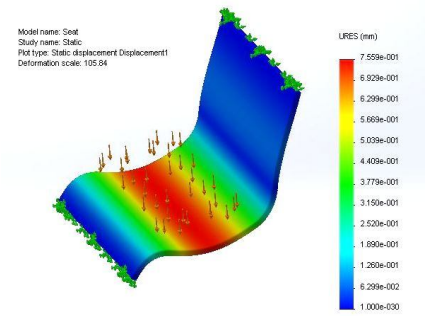

Fig. 12. URES displacement on wheelchair seat

4. Construction

The prototype wheelchair has been made with locally available material, such as; wood for seat, back rest and wheel, mild steel for frame, commercially available shaft & sprocket gear was used.

4.1 Rear shaft

Basically shaft carries the total load of a vehicle body. Major change is done in this structural construction. Instead of using common shaft, two modified axle usually called shaft is used in the automatic wheelchair's wheels which are not connected. Available wheel chair in present market has got 15.25 cm long and 12 mm diameter's axle in each rear wheel. But this construction has got 30 cm long and 2.5 cm diameter's axle. For easy unique controlling mechanism, two separate shaft has used. This shaft contains two wheels, bearing, bush, sprocket gear. The shaft with its component is showed in **Fig. 13**.

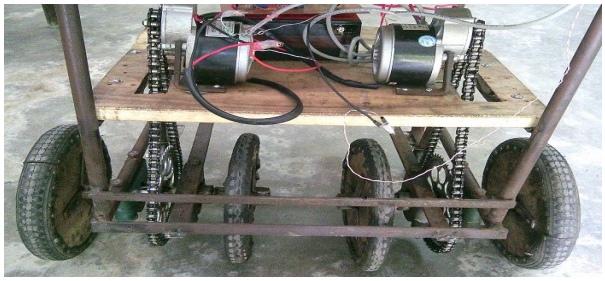

Fig. 13. Rear shaft mechanism

Fig. 14. Gear and chain drive mechanism

4.2 Gear and chain drive

Based on a top speed of five kilometer per hour and wheelchair wheels with a 25 cm radius, the output speed of the drive system had to at least equal 105 rpm. Chain drive has one main advantage over a traditional gear train.

Only two gear wheels and a chain are needed to transmit rotary motion over a distance. With a traditional gear train, many gears must be arranged meshing with each other in order to transmit motion. The Gear and chain drive mechanism is showed in **Fig. 14**.

4.3 Mechanism of automatic wheelchair

Major change is done in the structure and mechanism for this project. Two modified Shaft is used with sprocket. This Sprocket is joined with chain which is connected with another smaller cassette that is mounted directly on motor shaft. Whenever the motor shaft rotates then the sprocket of rear spindle starts rotating and thus the wheel starts moving. In this wheelchair the chain is used to transmit power to drive wheel from the dc gear motor. A wooden tray is attached underneath the seat to mount the dc gear motor and battery. Two dry cell batteries are used for power. The control circuitry is placed underneath the seat which is covered in a box. After completing the connection of the electro-mechanical equipment, the structure of wheel chair which is implemented is given in **Fig. 15**.

Fig. 15. Constructed automatic wheelchair

5. Result and Discussion

The expectation of this project was that a prototype would be produced that would conceptually prove that an effective automatic wheelchair could be designed that exceeded the performance of wheelchairs. These expectations were far exceeded as the finalized prototype performed exceedingly well in all aspects of the design specifications. Careful design and selection of mechanism and mechanical components combined to create a prototype that could meet the majority of wheelchair testing. Testing was conducted on the finalized prototype to ensure the design integrity. Integrity was determined by how well the wheelchair met the design specifications. Testing was performed with 100 kg a human occupant. Weights were added to the occupant to reach the required 980N weight to simulate a worst-case test scenario in all test scenarios. Stability testing was performed to ensure that the wheelchair could be proficiently operated in approved environments.

Dynamic stability testing was performed to ensure that the wheelchair could travel safely on flat ground. Wheelchair users could effectively move the wheelchair when required power applied to the motor.

The distance between the rear wheels was increased since the both motor-side wheel is located 15 cm further away from the wheelchair frame. The overall width of the wheelchair is 91 cm. This modification is slightly wide than existing wheelchair but it didn't so problem.

The automatic wheelchair prototype successfully allows a user to move without propelling the wheel by their arm. The power-assist motor completely replaces the function of the affected arm. In comparison with the existing dual-rim and lever-arm wheelchairs, the prototype clearly excels in maneuverability and no more arm strength required and the cost analysis also represents that it is going to be the cheapest wheelchair model (showed in **Table. 3**).

Table. 3 Cost analysis

Parts name	Quantity	Price in	Price	Parts name	Quantity	Price in	Price

		BDT	in $			BDT	in $
Steel pipe	10	1500	19	Bearing	2	300	3.8
Plain rod	5	250	3.17	Caster wheel	2	300	3.8
Wood	2	400	5.08	Screw and pin	-	200	2.53
Wooden wheel	4	350	4.43	Sprocket gear	2	300	3.8
Tire	2	200	2.53	Chain drive	2	200	2.53
Shaft	2	400	5.08	Mechanic's fee	-	1500	19
					Grand total	5900	74.75

6. Conclusion

A power-assist automatic wheelchair prototype that effectively meets the various transportation needs of individuals with hemiplegia or physical disabilities has been designed, manufactured, and tested. Intricate design detail and execution resulted in a visually simplistic design that promotes low cost and low maintenance. The modular aspect of the components allows the system to be retrofit to most manual wheelchairs with only minimal modifications. The main goal of replacing power lost by a user affected arm while maintaining maneuverability and transportability was successfully achieved. The overall dimensions of the constructed wheelchair and therefore maintains its ability to be transported in the trunk or backseat of a full sized car. The minimization of expense is pretty affordable for most of the people of Bangladesh and it can be even cheaper when taken for mass production.
This project can also be counted as a brilliant initiative for the betterment of physically handicapped and disabled people's lifestyle.

7. Acknowledgement

The authors are grateful to the Department of Mechanical Engineering, KUET, and the Khulna University of Engineering & Technology for providing the fund for the research work.

References

[1] P. Norek, M. Ahmed, et al, "Livelihood Challenges for Extremely Poor Disabled People in the Southwest Costal Region of Bangladesh", *Shiree working paper* 12, January 2013.
[2]T. Röfer, & A. Lankenau, "Ensuring Safe Obstacle Avoidance in a Shared-Control System'', *Proceedings of the IEEE/RSJ/GI International Conference on Emerging Technologies and Factory Automation 1999*, Vol. 2, 1405-1414, October 1999
[3]E. Prassler, J. Scholz, M. Strobel, & P. Fiorini, "An Intelligent (Semi-) Autonomous Passenger Transportation System'', *Proceedings of the IEEE/IEEJ/JSAI International Conference on Intelligent Transportation Systems Proceedings 1999*, 374-379, October 1999.
[4]D. Miller, & M. Slack, "Increasing Access with a low-cost Robotic Wheelchair'', *Proceedings of the IEEE/RSJ/GI International Conference on Intelligent Robots and Systems '94*, Vol. 3, 1663-1667, September 1994.
[5]M. Lawn, & T. Takeda, "Design of a robotic-hybrid wheelchair for operation in barrier present environments'', *Proceedings of the 20th Annual International Conference of the IEEE Engineering in Medicine and Biology Society*, Vol. 20, No 5,
[6]J. Hockenberry, (cited 20-May-2001) "A revolutionary new wheelchair'', NBC http://www.msnbc.com/news/285231.asp, June 2000.
[7]S. Fioretti, T. Leo, & S. Longhi, "A Navigation System for Increasing the Autonomy and the Security of Powered Wheelchairs'', *IEEE Transactions on Rehabilitation Engineering*, Vol. 8, No. 4, 490-498, Dec 2000.
[8]P. Trahanias, M. Lourakis, S. Argyros, & S. Orphanoudakis, "Navigational support for robotic wheelchair platforms: an approach that combines vision and range sensors", *International Conference on Robotics and Automation 1997*, Vol. 2, 1265-1270, April 1997.
[9]G. Pires, R. Araujo, U. Nunes, & A. Almeida, "RobChair-a powered wheelchair using a behaviour-based navigation", *International Workshop on Advanced Motion Control 1998*, 536-541, June 1998.
[10]N. Katevas, N. Sgouros, S. Tzafestas, G. Papakonstantinou, P. Beattie, J. Bishop, P. Tsanakas, & D.Koutsouris, "The Autonomous Mobile Robot SENARIO: A Sensor-Aided Intelligent Navigation System for Powered Wheelchairs'', *IEEE Robotics & Automation Magazine*, Vol. 4, Issue 4, 60-70, December-1997.

International Conference on Mechanical, Industrial and Materials Engineering 2015 (ICMIME2015)
11-13 December, 2015, RUET, Rajshahi, Bangladesh

Paper ID: AM-22

Identification of the location of any obstacle ahead of a running vehicle in a foggy and drowsy environment

Efat A. Haque[1], Jannatul J. Juthy[2] and Nirendra N. Mustafi[3]
[1,2,3]Department of Mechanical Engineering
Rajshahi University of Engineering & Technology, Rajshahi-6204, Bangladesh.
haque.efat@gmail.com

Abstract

The number of vehicle is increasing very fast worldwide and hence the occurrence of accidents is just following the trend. Many people are dying or becoming disabled in road accidents every day. Particularly in developing countries like Bangladesh, the scenario is really alarming. To decrease such unwanted road accidents is a declared target of modern Intelligent Transportation Systems. This paper illustrates a simpler approach to the avoidance of vehicle-vehicle collisions in a foggy and drowsy weather conditions. An intelligent system is planned to be developed using suitable sensors, named a Collision Warning System (CWS) for the drivers. The system will alert the driver in case of an impending collision to prevent or mitigate the crash. Ultrasonic sensors are selected to be used here, which can detect obstacles in a foggy and drowsy environment ahead of any running vehicle, and which can perform equally at day and night time in sensing the location of obstacles. The main purpose is of this work thus to design the systems and to test them in reality. The minimum distance that has to be maintained between vehicles in order to prevent an accident is determined by two second rule which is used worldwide. Whenever any obstacle or vehicle appears in front of the vehicle, the sensor will sense it and a speaker will alert the driver about its presence and let him know about an approximate location of the obstacle. The driver will then take the necessary safety measures to avoid the collision and will save the precious lives.

Key Words: Vehicle, Collision, Obstacle detection, Intelligent Transportation System, Ultrasonic sensor.

1. Introduction

In the modern era, road accident has become a burning issue worldwide. Day by day the rate of occurrence of road accident is increasing rapidly. Being a populated country, the rate of occurrences of road accidents in Bangladesh is really alarming. Despite of taking different measures by the government, the rate is not reduced appreciably due to the careless driving by the drivers. According to the Bangladesh Police Headquarters (FIR) report BRTA publishes statistical data on road accident every year. Table 1 presents such statistical data for years 2007-2014 [11]. It is said that the prevention is better than cure. Detecting an obstacle ahead of any vehicle can avoid the collision and thus can save human lives. To execute this, an advanced precise obstacle detection aptitude is needed. Vehicles on road may face human, animals, or any obstacle ahead of them and the estimation of the distance is done by the drivers own eyes which may lead to an accident eventually. This paper intends to find a technique to reduce the rate of occurrences of road accidents by installing a kit that helps the driver to detect the location of the obstacles ahead of the vehicle accurately. It's a technology based collision decreasing process and quite practical. This system will help the driver to remain alert about the vehicle coming

Table 1. Statistical data on road accident [11]

Year	Total accidents	Death	Injured	Total casualties
2007	4869	3749	3273	7022
2008	4427	3765	3284	7049
2009	3381	2958	2686	5644
2010	2827	2646	1803	4449
2011	2667	2546	1641	4187
2012	2636	2538	2134	4672
2013	2029	1957	1396	3353
2014	2027	2067	1535	3602

from the opposite end. Many efforts have been tested to design such an intelligent system for vehicles application published in the literature. An intelligent over speeding sensor was used to sense obstacle to reduce crash between two wheelers. The sensor used in [1] was able to work at speed above 25 kmph. S.P. Bhumkar presented a model at [2] to avoid accident by detecting the symptoms of fatigue of driver and control the speed the vehicle accordingly. In [3, 5] a passive Infra Red sensor was used for detecting obstacles. When the system in [3] was unable to avoid accident, the location was tracked by using GSM (Global System for Mobile Communication). Several vision based vehicle detection systems were reviewed in [4]. Pre-crash detection system was designed by Md. Maminul Islam at [6] using IR sensor. It also contained relay to protect the car from battery ignition and buzzer for making noise to inform the surrounded people when accident occurred. Sungji Han presented a vision based vehicle detection system was developed and decided whether that the obstacle is vehicle or non-vehicle [7]. Ultrasonic and Infra Red sensor were used simultaneously in paper [8] and properties of surface are calculated according to Phong Illumination Model. The main function of Phong model is to estimate the reflectance properties of any surface illuminated from the points on a surface. The aim of this paper is to design and develop a reliable, efficient and realistic detecting process to detect the obstacles for reducing road crush. The ultrasonic sensor is used here as it is very cheap and efficient to use in daylight and in any situation of weather, even in rainy and foggy weather when the driver might not be able to see obstacle within in two meter ahead of the vehicle. Then this arrangement will let the driver know about the almost exact location of any obstacle within 11 meter. This sensor provides precise data about the location of obstacles that are reliable enough to resist road accident in case of low speed vehicles. The voice alert keeps the driver alert and alertness of driver act as the main key to avoid road accident. This arrangement may be a life saver in practical field of application avoiding road accident on the highway.

2. Estimation of safe distance for stopping the distance

When a driver observes any other vehicle coming from the opposite side he needs some time to think and move his feet to accelerator for braking paddle. Stopping distance is the sum of the reaction distance and braking distance.

$$D= V^2/2\mu g$$

This equation implies stopping distance but in this case it's independent of driver's reaction time. Here, co-efficient of friction μ is varied with the condition of road surface. For normal surface μ is normally 0.8 and for wet surface it's 0.4 to 0.5.This paper also considers two second rule to avoid accident to alert the driver if any vehicle comes inside the safe distance. Two second rule is used worldwide to run the vehicles on the highway to maintain safe distance. According to this rule the driver has to stay two seconds behind of a vehicle running ahead of driver's vehicle. This rule is applicable for any type of vehicle for any speed. The driver has to face difficulties to measure the exact safe distance to maintain while driving. Two second rule solves this problem and lets the driver to observe how much the vehicle in front is moving forward in two second. These calculated data for stopping distance and safe distance according to two second rule are shown in Table 2.

Table 2. Data for stopping distance [10] and safe distance [12]

S.no.	Speed (km/h)	Stopping distance (good surface) M	Stopping distance (wet surface) m	Safe distance (m)
1	80	31	63	44.44
2	70	24	48	38.88
3	60	17	35	33.2
4	50	12	24	27.76
5	40	7	15	22.22
6	30	4	8	16.66
7	20	2	4	11.1
8	10	0.5	1	5.54

3. Methodology

At first an ultrasonic sensor is selected for this project of suitable range to use on a medium speed (20 to 30km/h) vehicle. The circuit is designed in PROTEUS design suit and program is written in Bascom AVR. Then all the necessary components are set into a PCB board according to the circuit diagram. After that audio sounds that tell about the measured distance are recorded in an Mp3 player and attached with the system. This will give an audio signal whenever the sensor senses any obstacle on the road. Finally after completing all the set up, the system is tested practically. Thus the desired kit is ready to install in any vehicle.

Block diagram of the system

The block diagram of the proposed system is presented in Fig.1.This diagram makes it possible to understand the whole procedure at a glance. A microcontroller controls the entire arrangement. Distance is measured by the sensor and this is displayed on the LCD screen by the help of microcontroller. The opto-couplers are used here for switching. Audio track is played according to distance shown in the LCD display. At the same time the driver hears the sound with the help of a speaker.

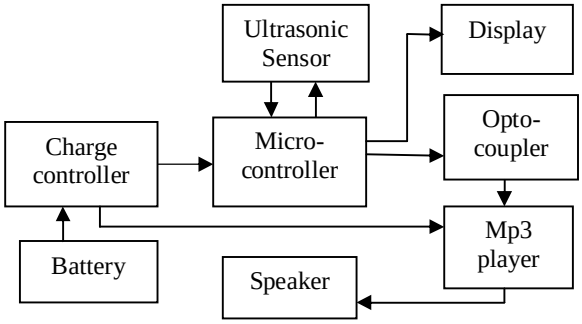

Fig. 1. Block diagram of the proposed system

Hardware description

Microcontroller ATmega32 acts as the brain of this project. It's an 8-bit microcontroller which is highly flexible and cost effective. Microcontroller with advanced RISC architecture consisting 32x8 general purpose working resisters. It consists high endurance non- volatile memory segments with 32kbytes of in-system self programmable memory which is flash program type and 1024bytes EEPROM. It's operated on 2, 7V-5.5V (ATmega32L) and 4.5V-5.5V (ATmega32). It consumes 1.1mA in active mode and 0.35mA in idle mode and less than 1μA in power down mode. Fig. 2 shows the pin configuration of ATmega32.

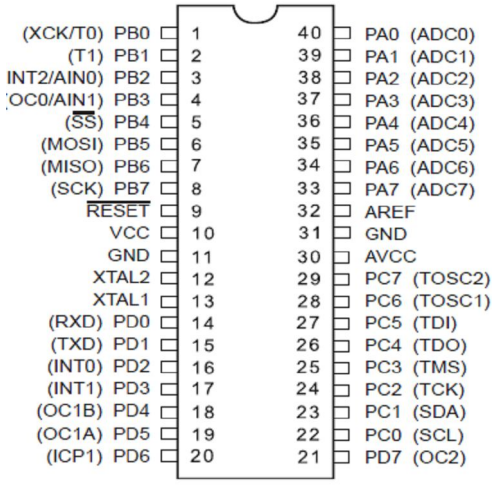

Fig. 2. Pin configuration of the microcontroller ATmega32 [9]

In this project an ultrasonic sensor US020 is used for measuring distance. The sensing range of this module is 11m. The static current of it is 3 mA. DC 5V power supply is needed to run it. This sensor emanates sound waves of high frequency which propagates at regular interval in the air. When this waves smack an obstacle, they are returned back as eco. For calculating the distance time interval between emitting the signal and receiving eco is measured by the microcontroller. Two regulators IC (Integrated circuit) 7805 and 7806 are used in this project .The main purpose of these regulator ICs are to carry on the accurate voltage from the power supply. In a circuit, the quantity of voltage from the source may swing and that's why fixed voltage supply may not be possible to maintain. This IC has three pins. Among them first one is input pin and third number is output pin. The name of middle pin is ground pin. The electronics semiconductor device named Opto-coupler PC817 is used here for transferring electrical signal within circuits. Through an optical transmission path it mainly connects two electrical detach circuits to keep them electrically isolated. Opto coupler can transfer electrical signal either digital or analogue. Along with microprocessor opto-coupler can be used for switching, signal isolation, pc communication and many other applications. In this project the opto-couplers are used for switching.

4. Experimental setup

Fig.3 represents the overall system arrangement. This circuit includes one ultrasonic sensor for detecting obstacles, one microcontroller ATmega32 to control the system, one LCD to show the measured distance and one Mp3 to give sound alert. An obstacle was kept at one meter distance, no.1 LED blinks, then the LCD displayed the measured distance as "1 met" and audio track from the Mp3 player is played accordingly. This procedure continues till the ultrasonic sensor gets any obstacle within the definite range of it.

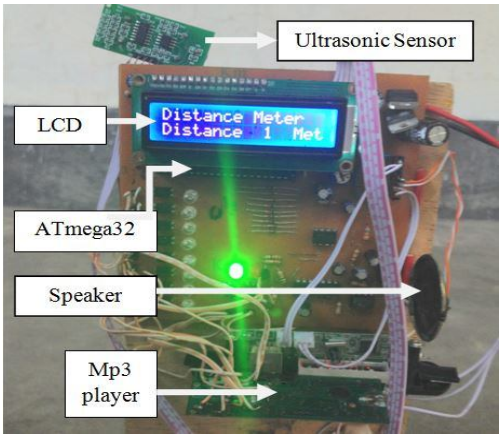

Fig. 3. Experimental setup of the system

The constructed circuit consists of one microcontroller ATmega32, one ultrasonic sensor, one LCD display (16*2), two regulator ICs, one charge controller, twenty two capacitors, and ten opto-couplers PC817. The entire circuit receives power to run from the vehicle battery via charge controller. The AN7805 is used to control the charge to the circuit and the AN7806 to the audio amplifier. The microcontroller contains the program to run the system. The program is written in Bascom AVR. At first all the pins used in this system are declared and mentioned which are for input and which are for output signal. Then the LCD part is described which controls the vision in the LCD monitor. After that the entire loop is described and according to the loop the pins become activate and inactive. The ultrasonic sensor throws a pulse of 40 kHz with the transmitter of the sensor, and then the receiver receives the eco of the transmitted ultrasound. The output of ultrasonic sensor is fed into the microcontroller as pulse in signal. The LCD monitor gets signal from the microcontroller and illustrate the distance measured by the sensor. The opto-couplers get signal from the microcontroller and work accordingly. When any obstacle is at 1 meter distance the first output pin of microcontroller becomes active while other pins remain inactive. Then the opto-coupler works and passes the signal to the Mp3 player where the 1st audio track is played and speaker make some sound which is amplified so that the driver of the vehicle can hear it. In the same procedure if the sensor senses any obstacle at 2 meter distance the 2nd pin becomes active and the first pin gets inactive so as the other pins on the microcontroller. Then 2nd audio track is played. The system works in the same way till the obstacle is within 11 meter. The circuit diagram of the system is shown in Fig. 4.

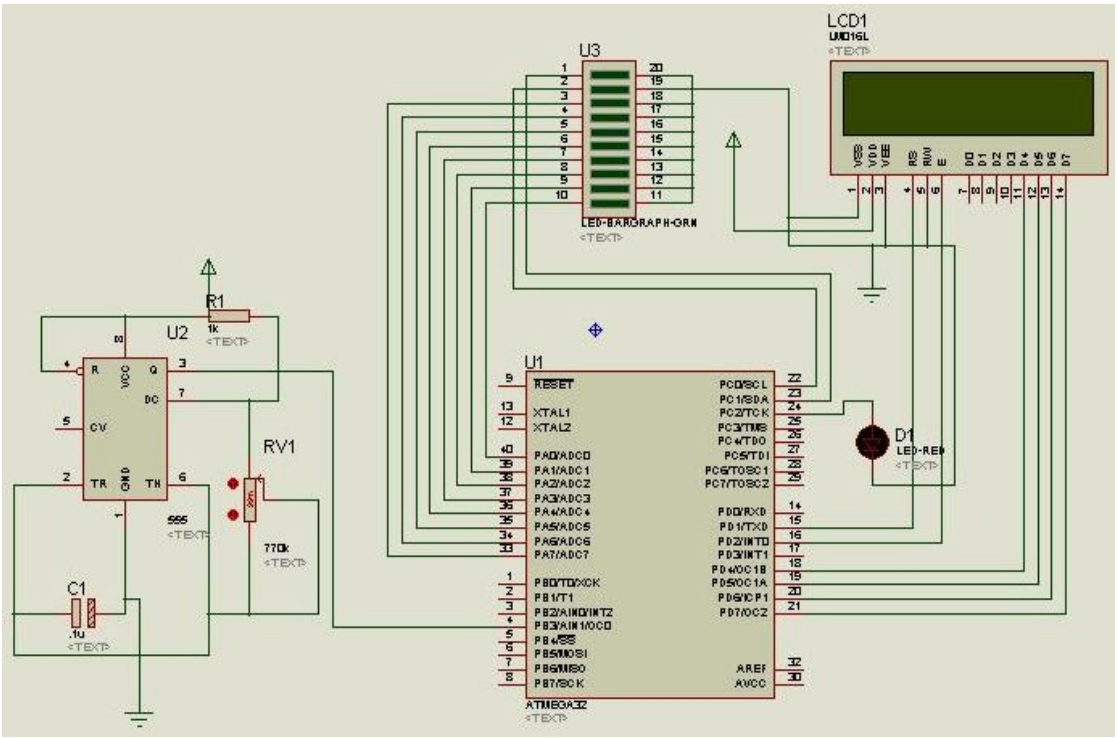

Fig. 4. Circuit diagram of the system

5. Results and discussion

At first the circuit was tested in stationary condition and then applied to a running vehicle. The constructed circuit performs well in both situations. The experimental data for stationary condition are accumulated in the Table 3. Deviations between the actual and displayed distance were noted during the tests. This is presented in the last column of the Table 3.

Table 3. Experimental data for stationary condition

S.no.	Actual distance (m)	Measured distance (m)	% Error
1	0.95	1	5.26
2	1.94	2	3.09
3	2.93	3	2.38
4	3.87	4	3.35
5	4.85	5	3.09
6	5.62	6	6.76
7	6.67	7	4.94
8	7.58	8	5.54
9	8.74	9	2.97
10	9.71	10	2.98
11	10.65	11	3.28

Fig. 5 shows the deviation between actual distance and measured distance graphically. The sensing range of ultrasonic sensor depends on some physical parameters such as temperature, external noise, shape of the surface and density or consistency of the material, humidity etc. By the effect of these factors measured values were deviated from the actual values in Table 3.

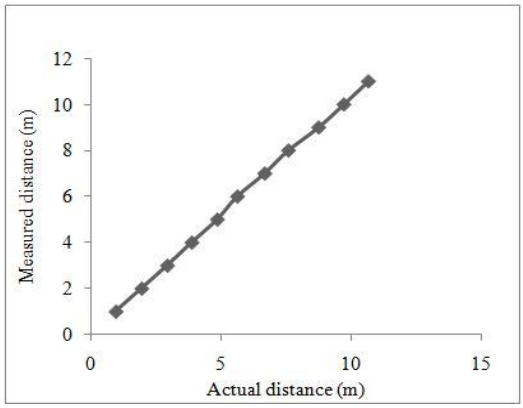

Fig. 5. Deviation between actual and measured distance

The results when the system was attached to a running vehicle are shown in Table 4. Fig.6 interprets the sensitivity of the system as a function of vehicle speed. It shows that the sensitivity decreased as the vehicle's speed increases.

Table 4. Experimental data for running condition

S.no	Speed (km/h)	Sensing range (m)
1	0	11
2	10	11
3	20	11
4	25	10
5	30	9
6	40	8
7	50	3

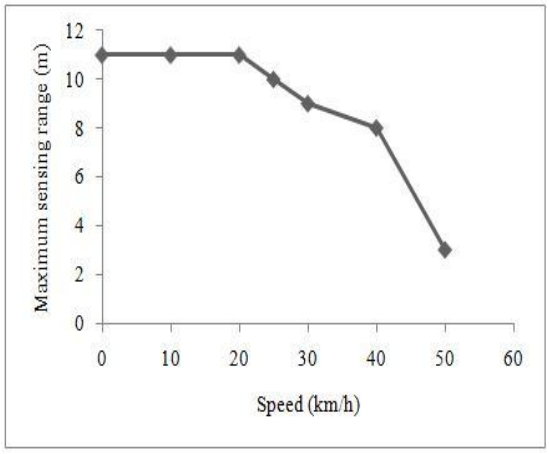

Fig. 6. Functionality of the system as a function of vehicle speed

After the system being applied on a running vehicle at a high speed, some errors took place in sensing obstacle at a long distance. It's been observed that the ultrasonic sensor used here can measure at its maximum range at 0-20 km/h and after that its sensing range decreases gradually.

6. Conclusions

After testing practically, it's confirmed that this project may be applied in vehicles running at low speed due to the range of the ultrasonic sensor used in this study. This system is applied to a local vehicle which normally

runs at a speed of 20 km/h – 30 km/h at busy roads. Considering safe distance and stopping distance, it's been seen that this system works successfully up to speed 20 km/h. In case of stopping distance the system works up to 45 km/h normal road surface and 35 km/h on wet road surface. Considering the speed of that vehicle, it's seen that this system is applicable for those types of vehicles which run at that speed on the highways. For further application on high speed vehicle, the sensor must be replaced with higher range ultrasonic sensor. The total cost of this project is approximately $35.32. This is quite economical to apply this system in practical field.

7. Future works

The limitations of the proposed system can be improved further in the following ways:

- High range ultrasonic sensor or possibly its amplification can be used so that it performs well for vehicles at high speeds.
- Despite of using the proposed system in a vehicle, a driver may not respond quickly in taking measures to avoid clashes. In this situation Auto Drive of the vehicle for a while after sensing the obstacle in front of it is quite important. That's why an Auto Drive system can be designed and integrated with this system to improve its reliability.

8. References

[1] Sonali.N, Maheswari.R, "An Intelligent Obstacle and Over Speeding Sensor to Prevent Dashing of Motorcycles", *International Journal of Soft Computing and Artificial Intelligence*, Vol.1, No.1, pp. 14-17, 2013.

[2] S.P. Bhumkar, V.V. Deotare, R.V.Babar, "Accident Avoidance and Detection on Highways", *International Journal of Engineering Trends and Technology*, Vol.3, No.2, pp. 247-252, 2012.

[3] Md.Khaled Hossain, Sayed Samial Haq, "Detection of Car Pre-Crash with Human, Avoidance System & Localizing through GSM", *International Journal of Scientific and Research Publications*, Vol.3, No.7, pp. 1-7, 2013.

[4] Zehang Sun, George Bebis, Ronald Miller, "On-Road Vehicle Detection: A Review'', *IEEE Transactions on Pattern Analysis and Machine Intelligence*, Vol.28, No.5, pp. 694-711, 2006.

[5] G. Benet, F. Blanes, J.E. Simo, P.Perez, "Using Infrared Sensors for Distance Measurement in Mobile Robots", *Robotics and Autonomous Systems*, Vol.40, No.4, pp. 255-266, 2002.

[6] Md. Maminul Islam, Md. Rabiul Hasan, Imran Chowdhury, Md. Towhid Chowdhury., "Internet of Car: Accident Sensing, Indication and Safety with Alert System", *American Journal of Engineering Research (AJER)*, Vol.2, No.10, pp. 92-99, 2013.

[7] Sungji Han, Youngjoon Han and Hernsoo Hahn, **"**Vehicle Detection Method using Haar-like Feature on Real Time System", *World Academy of Science, Engineering and Technology*, Vol.3, No. 11, pp. 375-379, 2009.

[8] Tarek Mohammad, "Using Ultrasonic and Infrared Sensors for Distance Measurement", *World Academy of Science, Engineering and Technology*, Vol.3, No.3, pp. 269-274, 2009.

[9] Atmega32 datasheet available at http://www.alldatasheet.com/datasheet-pdf/pdf/77378/ATMEL/ATMEGA32.html access in 9-15-2015.

[10] Vehicle stopping distance calculator available at http://www.csgnetwork.com/stopdistcalc.html access in 10-28-2015.

[11] Bangladesh Road Transport Authority- Road Safety available at http://www.brta.gov.bd/index.php/road-safety access in 9-15-2015.

[12] Two-second rule - Wikipedia, the free encyclopedia available at https://en.wikipedia.org/wiki/Two-second_rule access in 9-15-2015.

International Conference on Mechanical, Industrial and Materials Engineering 2015 (ICMIME2015)
11-13 December, 2015, RUET, Rajshahi, Bangladesh.

Paper ID: AM-23

Design and Construction of a Remote Controlled Fire Extinguishing Robot

Md. Rokunuzzaman[1], Md. Sharif Ahmed[2], Mustafa Muhibullah[2], Sourav Sarker[2], Md. Khursid Alam[2], Md. Sanower Hossain[2]
[1]Department of Mechanical Engineering, Rajshahi University of Engineering and Technology (RUET)
[2]Department of Mechanical Engineering, Rajshahi University of Engineering and Technology (RUET)
Email: souravsarkerjoy@gmail.com

Abstract

From the recent years, robotics has turned out to be an ingredient over which many people had shown their interest and gained popularity due to the advancement of many technologies. Therefore, it has been decided to design something that can make human life easier and comfortable and the interest of review is to make a fire extinguishing robot. Fire detection and extinguishment are perilous jobs that invariably put human lives (especially firefighters) in danger. The proposed fire extinguishing robot is designed for extinguishing fire in a small floor plan of a house, office or shopping mall of specific dimensions with the help of the CO_2 fire extinguisher which can be carried by the robot itself. Controlling of this robot demands of an operator who can easily control it from` remote location without being involved in firefighting. The remote control system for this project is based on conventional RF technology but with different approaches. Accuracy of the control system has been satisfactory throughout this project. The fire eliminating performance and the robot movement speed was closed to the aspiration.

Keywords: *RF, Tadpole, CO_2 fire extinguisher, DC motor.*

1. Introduction

The modern concept began to be developed with onset of industrial revolutions for the use of complex mechanics and subsequent introduction of electronics. A huge part of industrial revolutions has been accelerated in modern times due to the evolution of robotic science. Like other modules of technology, the fire extinguishing system has also put a significant effort to merge it with robotic science. Involvement of robots instead of humans has been practiced since the end of the last decade and through this project another solution is tried by developing a fire extinguishing robot which will be operated by human operator through remote controlled system from a safe distance. It performs the whole task by means of some mechanisms, e.g. driving system to move towards the fire striking zone and steering system to control the direction of robot. Moreover, to suppress fire, there is a methodical system which allows CO_2 gas to escape from the extinguisher which will be directed towards the source.

2. Background

The proliferation of robotic technology has put much gravity on fire extinguishing system and some researches over this particular are much noticeable e.g. Thermite, LUF, Tehzeeb, SAFFiR etc. Tharmite is based on technology developed for the U.S. Army, this squat little modular robot on tank treads is a small, powerful fire fighting machine that provides crews with a means for remote reconnaissance and fighting fires in hazardous areas safely and it is designed to be used in areas of extreme hazard, such as aircraft fires, refineries, chemical plants or nuclear reactors [1]. LUF is a radio controlled tracked vehicle or machine that clears the path for advancement of up to a distance of 1000 feet by incorporating a high capacity positive pressure ventilator and a “water beam” fog and this combination clears away smoke, heat, toxic gases and reduces the intensity of the fire, allowing firefighting and rescue teams to more safely approach the incident [2]. Tehzeeb is a type of rescuing robot that uses laser scanner module, a manipulator and map generation algorithms for localization and navigation in visually poor situation such as in dense smoke surrounding [3]. The Shipboard Autonomous

Firefighting Robot (SAFFiR), sponsored by the Office of Naval Research (ONR) is another type of bipedal, humanoid rescuing robot which uses thermal imaging to identify overheated equipment, and a hose to extinguish fire[4]. This robot is also capable of manipulating doors and fire hoses, and equipped with sensors to see and navigate through smoke.

3. Methodology

The implementation of this project involves the construction of fire extinguishing robot, interfacing with hardware such as motor driven circuitry, fire extinguisher pressing arm and steering system. Suppression is associated with involvement of a CO_2 fire extinguisher which is available in market. In this project there is a very little scope for human involvement-only for operating the remote control system. The entire system architecture of the fire extinguishing robot is shown in Fig.1.

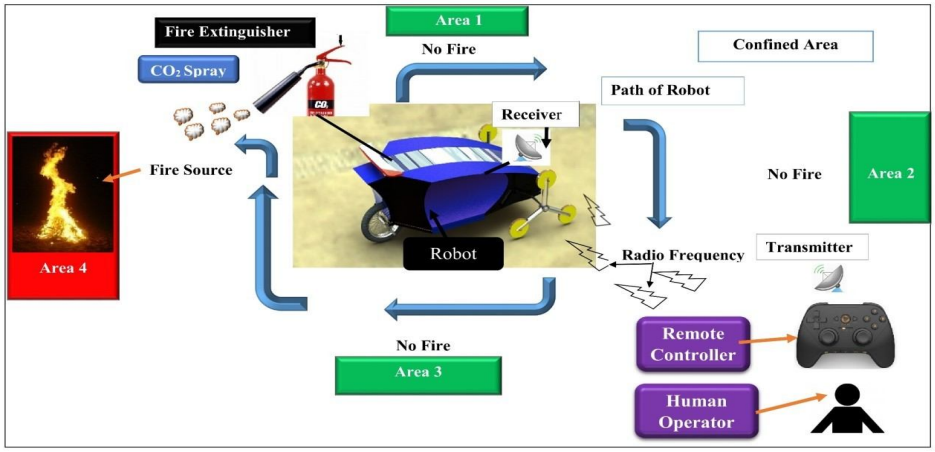

Figure 1: System architecture of the fire extinguishing robot

4. Design Methodology

Design of Chassis, Steering System and Protective body

A tadpole configuration (with two wheels out front and a driven one behind) has been inaugurated to minimize instability associated with motion [5]. In orthodox delta layout (one front wheel and two rear wheels), the vehicles center of gravity is not only high, but also well behind. In attempting to make a turn, the contraption becomes, in effect pendulum-albeit one swinging in a horizontal plane parallel to the road surface rather than vertically. And this yawing moment is amplified by gravity when heading downhill. The advantage of tadpole over conventional delta layout is that it puts center of gravity close to the steering axis, thus reduces its radius of gyration (i.e. the length of its imaginary pendulum arm) to something close to zero. This remarkably improves rollover resistance. In addition to this splendid configuration, the chassis of the robot is designed in such a degree that it could provide enough space to place fire extinguisher, batteries, circuit board, DC motors and other accessories. Moreover, a simple steering system has been designed for changing direction when necessary. This steering system comprised of riveted joints and knuckle joints at the two ends to ensure pliability. At the center of this system, there is a gear meshed with a pinion which will be driven by a DC motor controlled by a remote controller. The rotation of the gear makes the steering system twist. For instance, clockwise rotation of the gear can results in left turn while the anti-clockwise makes it to the right. Also, the robot will be driven by another DC motor connected with the rear wheel by a chain and sprocket mechanism. For forward and backward movements of the robot, this motor requires to be rotated in bi-directional too. Finally, a protective body has been provided to shield the fire extinguisher, circuit box, batteries, motors and other sensitive parts from the direct exposure of flame.

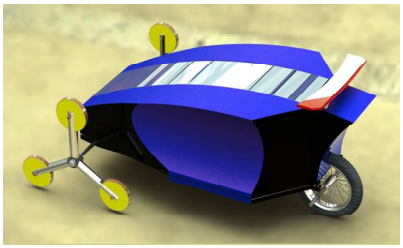

Figure 2a: Tadpole Configuration

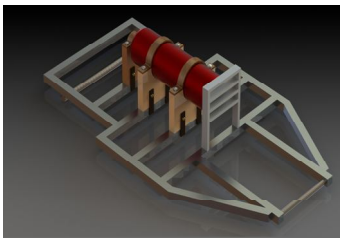

Figure 2b: Chassis Layout

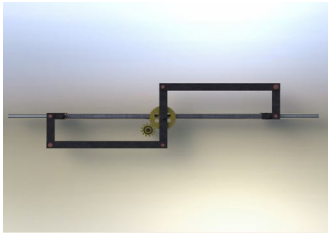

Figure 2c: Steering System

Design of the Fire Extinguishing System

This mechanism is mounted on the chassis and consists of a specially designed pressing arm (for pressing the top handle bar of extinguisher) in between two ball bearings housed over the chassis (Figure 3a). This allows the pressing arm to be rotated in 360̊, however, only if the DC motor shafted with it permits so. Also, this motor will be controlled by the same remote control system used for the steering motor and robot driving motor and provided with bi-directional rotation. In this case, reverse directional rotation is necessary to unleash the pressing arm (green colored) from the top handle bar of the extinguisher when CO_2 is not required (Figure 3b).

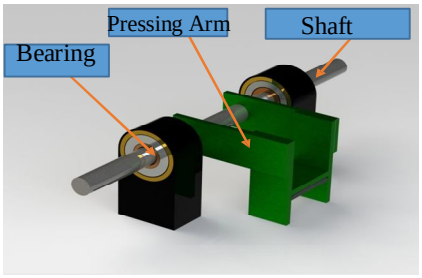

Figure 3a: Pressing Mechanism

Figure 3b: Pressing Mechanism with Extinguisher

This mechanism will be staged over the top handle bar of the fire extinguisher as shown in Figure 4:

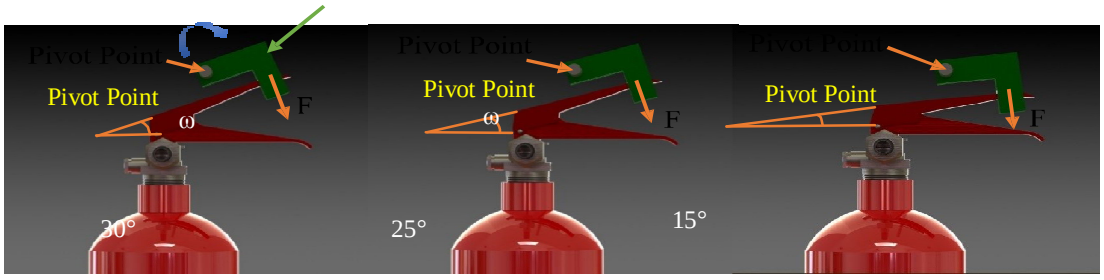

a) Stage 1 b) Stage 2 c) Stage 3

Figure 4: Progressive stages showing the pressing procedure of the top handle bar of a fire extinguisher by pressing arm mechanism

The torque required to press the top handle bar of the fire extinguisher is calculated by –

$$T = F \times r$$

Where, F=force required for pressing, r=turning radius.

5. Control System

The sole purpose of the control system is to control three distinct motors associated with the driving, steering and fire extinguishing mechanisms by a single remote controller. An overview of it can be shown by the following block diagram:

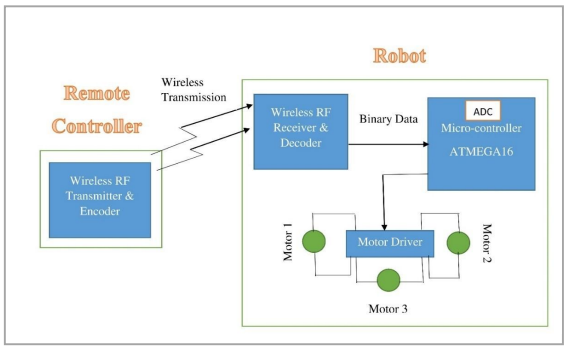

Figure 5: Block Diagram of Control

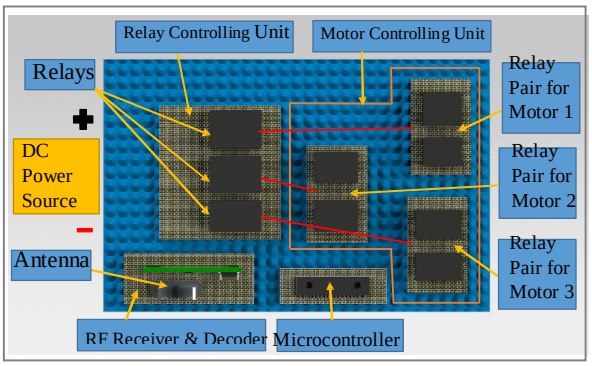

Figure 6: Relay Controlled Circuitry System

As mentioned earlier, the movement of the robot and fire extinguishing mechanism demand bi-directional rotation (table illustrates this) of the motors, it seems quite challenging to maneuver them via a single remote controlling unit. However, these difficulties had been eliminated by introducing a relay controlled circuitry system.

Table 1: Different type of movements produced with configuring all DC motors.

Rotation(+/-) of Motor1(Robot Driving Motor)	Movement of Robot	Rotation(+/-) of Motor2(Steering System Motor)	Movement of Robot	Rotation(+/-) of Motor3(Fire Extinguisher Pressing Motor)	CO_2 Spray
Clockwise(-)	Forward	Clockwise(-)	Right Turn	Clockwise(-)	Yes
Anti-Clockwise(+)	Backward	Anti-Clockwise(+)	Left Turn	Anti-Clockwise(+)	Release the arm

The relays in controlling unit had shown in the diagram act as switches for the motor controlling unit (figure 6). This is because each of the motors needs to be commenced individually when required. This is done by the conversion of binary data into electric pulses in the microcontroller of the circuit panel where it receives its data from the RF receiver and decoder. The RF receiver gets its signals from the RF transmitter and encoder which is melded with the remote controller.

The motor controlling unit constitutes of three pairs of relays assigned for three motors mentioned above. They act as final switches for the motors for deciding in which direction these motors will be revolved based on the data available in the receiver.

6. Expression for Calculating Success Rate of the Control System

Success rate can be defined as the ratio of total number of successful trials to the total number of trials performed.

$$\text{Success rate} = \frac{\text{Total no. of successful trials}}{\text{Total no. of trials performed}}$$

7. Experimental Setup and Construction

The final construction of the prototype of the robot is shown below (Fig. 7 and Fig. 8). For this prototype, the microcontrollers are coded with C programming language.

Figure 7: Photograph of the robot

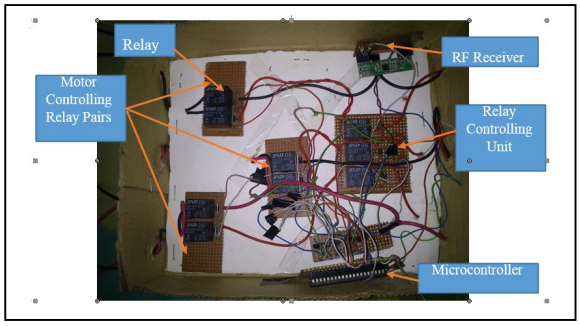

Figure 8: Photograph of the Circuit Board

8. Experimental Results and Discussion

Velocity of the robot = 1.9669125 ms^{-1}.

Discharge rate of CO_2 gas from the fire extinguisher = 0.8658 cm^3/s.

Torque required to press the main arm of the CO_2 fire extinguisher = 100 kg-cm.

An experiment has been performed to observe the extinguishment of fire by testing on some materials like papers, woods, plastics, clothes etc. and the time required for suppression was calculated which the table below illustrates:

Table 2: Measurement of time regarding extinguishment of fires associated with different types of objects.

No. of trial(s)	Type of object(s)	Average time of fire extinguishing (sec)
1	Cloth	2.8
2	Plastic	2.4
3	Paper	2.6
4	Wood	5.8
5	Kerosene	9.0

From the observation, it can be noticed that requirement of time was quite lesser for the objects mentioned except for kerosene. For measuring control systems' success rate, twenty five trials had been performed regarding three major systems followed.

Table 3: Measurement of success rate of control system on different parameters.

Success Rate of Control System	Percentage (%)
Robot driving system	88
Steering System	80
Pressing Arm	92

9. Conclusion

The technologies has been used to develop this firefighting robot are literally familiar but the implementation was unalike. RF module has been tactfully merged with the control system to make it much utilitarian operating system. The response area is larger than conventional fire extinguishing robot because of radio frequency module. Although there were many constraints, the robot can extinguish fire spraying CO_2 into the explosive area. The purpose of this research on this fire extinguishing robot is to nurture the knowledge of engineering in robotics that would be a convenient application for a real-world robot in extinguishing fire with efficacy and save more innocent people's lives in future. For future enhancement of this project, some supplementary attributes may be added by assimilating stair climbing feature to this robot and in this case Wearable Depth

Sensor can be used to detect obstacle like stairs. Thermal imaging technology can also be incorporated for detecting objects in highly heat concentration zone.

References

[1] Szondy, D. (October 5, 2012). Thermite fire-fighting robot removes fire fighters from harm's way. Available at http://www.gizmag.com, Retrieved: October 2014.

[2] www.nrt.org/production/NRT/RRT3.nsf/Resources/May2009ppt2/$File/LUF-60_Presentation_to_ Chiefs-2.pdf. Retrieved: June 2014.

[3] Young-Duk Kim; Yoon-Gu Kim; Seung-Hyun Lee;Jeong-Ho Kang; Jinung An; "Portable Fire Evacuation Guide Robot System", Intelligent Robots and Systems, IEEE/RSJ International Conference, 11-15 October 2009. Pages: 2789-2794.

[4] White, T.(April 2, 2015). Marketing Sailors 'SAFFiR'- Navy Unveils Firefighting Robot Prototype at Naval Tech EXPO. Available at www.navy.mil. Retrieved: July, 2015

[5] Gulati Vikas, Mehta Sameer, Kashyap Ankur, Pawar Kartik. (2012). Design and FEA of a Recumbent Trike. Indian Journal of Applied Engineering Research, ISSN 0973-4562. (Vol. 7) No. 11.

International Conference on Mechanical, Industrial and Materials Engineering 2015 (ICMIME2015)
11-13 December, 2015, RUET, Rajshahi, Bangladesh

Paper ID: AM-24

MMS Based Car Security System

Utsha Barua[1], Mohammed Badsha Alamgir[2], Mohammed Liaket Ali[3]
[1,3]Department of Mechanical Engineering,
[2]Department of Computer Science and Engineering,
[1-3]Chittagong University of Engineering and Technology.
E-mail: [1]*utshabarua10@gmail.com* [3]*mohammedliaketcuet10*@gmail.com
[2]*Badsha.bdmap@gmail.com*

Abstract

With the growing number of automotive vehicles and their improvements, the primary concern of the owners is the security. In this paper, an automatic security system is developed by applying GSM technology along with a prototype camera (OV7670). This system uses light sensor in the vehicle's door which is used to send a signal in the devolopment board (Arduino mega2560) that the car door is closed. If the thief enters wrong passcode, the door will be automatically locked in this case with the help of a solenoid lock. Simultaneously, the GSM module (SIM900) will send a MMS that the vehicle is under attack along with a photo of the thief to the vehicle owner's mobile. There is also a buzzer to alert the people around the vehicle. In a word it will be a bad decision for the thieves to try to breakdown in this type of secured vehicle.

Keywords: *GSM system, MMS, prototype camera (OV7670), Solenoid lock,* Arduino mega2560.

1. Introduction

For a relaxed parking experience without any type of unwanted occurrences, one needs to have a superb anti-theft system as now-a-days car theft has become a common types of criminal activity. And with the improvement of anti-theft vehicle security system, thieves are also using updated technology for stealing vehicles. Therefore, it is necessary to introduce more compact and multi-stage security system in the vehicle for demotivating the thieves. Especially it will be a nightmare for the thief if he or she is locked inside the car while trying to steal the vehicle along with a blaring sound of buzzer. With this feature, the new addition is the camera which will capture the image of the thief and with the help of GSM module that image will be sent instantly to the vehicle owner's mobile.[1,2] A message will be send to the police station so that police can locate the Car position. By that image send by the GSM it will be a matter of time to detain the thieves. There is a 4 ×4 keypad for inputting passcode to verify authentic user of the vehicle. An LCD display will show the entered passcode. The whole system will be powered by a separate power source and certainly not from the vehicle's main battery so that merely cutting the wire from vehicle's battery won't dismiss the main security system. Along with those extra features it is a bit expensive compared with the local limited feature anti-theft system but the fact is this system enables the user to get the image of the thief immediately during the stealing attempt and due to the door locking mechanism, vehicle's owner will get enough time to reach the vehicle or to take any kind of steps he wants to take. And for the further legal action by the police, that image will act as an evidence.

2. System structure and working principle

In this paper only one kind of sensor is used. We used LDR sensor in the vehicle door.[3] When the doors are closed, the light sensors will detect darkness to activate the ON/OFF switch of the solenoid lock.The keypad will be activated for passcode input. LDR resistance which varies according to amount of light falling, So the LDR will send signal to the microcontroller that the doors are closed when they detect darkness. The LCD screen will then ask for a passcode. If the passcode that is entered is wrong then there will be a second chance to enter the correct passcode. If the passcode is wrong again, the microcontroller will activate the solenoid lock.The vehicle's door will be locked. The microcontroller will simultaneously raise an alarm. The camera module will receive a signal to capture an image and the GSM module is set to a specific number so that it will send a MMS to the owner's number. If it's applicable for the country concerned, then the GSM module can also make a call to the Police station automatically. The locked door can be opened by inputting the correct passcode.

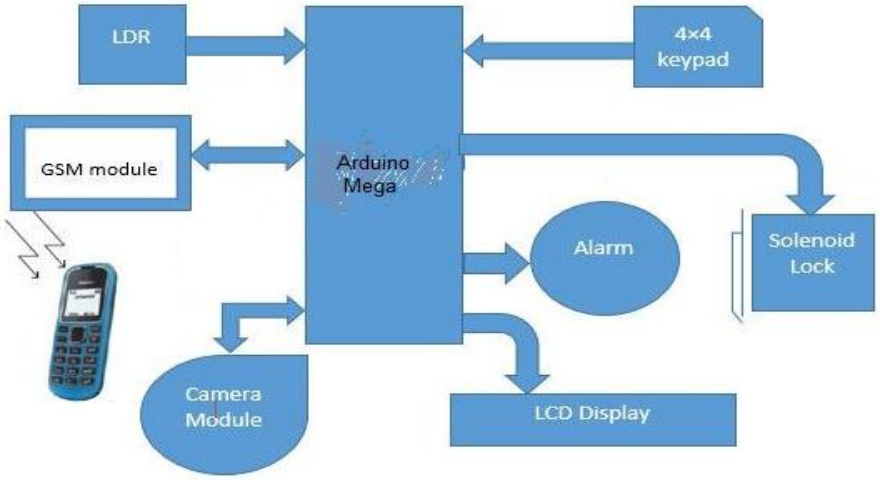

Fig. 01. Structural Diagram

3. Selection and design of system hardware

A. Arduino mega2560:

Arduino Mega 2560 is well known for its simplicity. It is a board based microcontroller on the ATmega2560. This high performance, low power 8-bit microcontroller combines 8KB SRAM, 4KB EEPROM, 256KB ISP flash memory, 32 general purpose working registers, 86 general purpose I/O lines, real time counter, six flexible timer/counters compare modes, PWM, 4 USARTs, 16 channel 10-bit A/D converter, a JTAG interface for on-chip debugging and byte oriented 2-wire serial interface. Most sheilds designed for Arduino, the Mega is very compatible . This device achieves a throughout approaching 1 MIPS per MHz and runs between 4.5-5.5 volts when executed a single clock cycle powerful instruction. It can operate simply by a battery or by connecting it to a computer with USB cable or by an AC to DC adapter.

B. GSM module:

In our system we used a SIMCOM SIM900 GSM module. It is used to send a MMS to the owner's mobile. It's used to have RS232 serial interface. This module operates on four frequencies - 850,900, 1800, 1900 MHz called as Quad-Band. RS232 allows connecting to PC and also with microcontroller. We have used AT commands to configure GSM module to send MMS. In this module baud rate is configurable from 9600-115200 through AT commands. We used 19200 as baud rate. The range of reception is good as well as good receiving facility. The protocol used by GSM for control and setup depends on AT command set. The GSM modem offers different services. Since this project is concerned about sending MMS, only a few subsets of AT-command sets are needed to be implemented. Some of the AT-command sets are given below.

Table 01. AT command sets

Command	Description
AT	Check if serial interface and GSM modem is working.
AT+CMMSCURL	Set the URL of the MMS center.
AT+CMMSPROTO	Set the protocol parameter and MMS proxy.
AT+CMMSCID	Set the networks parameter for MMS.
AT+CMMSSENDCFG	Set the parameters for sending MMS.

C. Liquid crystal display (LCD) unit

In our project we used a 16×2 character line LCD module which is a parallel port module. This program must interact with the outside world using I/O devices that communicate directly with human being. LCD requires 3 control line as well as 8 I/O lines for the data bus. So there is in total 11 data lines. Three control lines are referred to as EN, RS, RW. Three control line are used to tell the LCD that data is someone is sending data. The EN line is called "Enable". As data is supplied to data pins, high to low pulse has to be be applied to this EN pin so that the data present at the data pins can be latched. The RS line is called "Register Select" line. The "RW" line is the "Read/Write" control line.

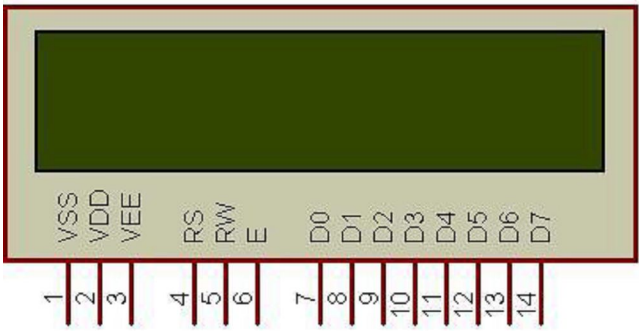

Fig. 02. Schematic diagram of LCD

When RS is low, that means 0, it is considered as a command or a special types of instructions like clear screen, position cursor. On the contrary when RS is high that means 1, it is a text data and it is going to be displayed on screen. When RW is low (0) then the information on the data bus is being shown on the screen. As RW is high (1), the system is effectively querying the LCD. For reference purpose, some commands given below.

Table 02. LCD command codes

Code (Hex)	Command to LCD instruction Register
1	Clear display screen
2	Return Home
80	Force cursor to beginning of 1st line
0C0	Force cursor to beginning of 2nd line

D. 4×4 matrix keypad

The most widely used I/O devices are keypads and LEDs. For microcontroller projects this 16 button keypad provides a human interface component. Its simple adhesive type back part enables it to mount in a variety of applications. Its other benefits are excellent price performance ratio, easy communication with any microcontroller, ultra-thin design.

Key specifications:

- Max Rating: 24 VDC, 30 mA
- Operating temperature range: 32 to 122°F(0 to 50°C)
- Interface: 8-pin access to 4×$ matrix
- Dimensions: Keypad(2.7×3.0 inch), Cable: (0.78×3.5 inch)

E. Camera module

We used an OV7670 camera module. It has a digital image processing chip-OV706, which is specially designed for image acquisition and processing application. Most important fact is that it is very convenient to connect with Arduino controller, can read image and data via UART serial port. After that it performs some image processing such as AWB (Auto White Balance), AGC (Automatic Gain Control) AE (Automatic Exposure).

This module can produce a high quality digital video signal with the help of a standard CCIR656 interface It can do real time encoding for collected image. External controller can easily read M-JPEG video streams. It's also capable of self-defining detection area and sensitivity. So in a word it's very competent to do our work. There is an external SD card module to store the pic that is captured by the camera. There are 4 terminals in both SD and camera module. The assigned port for SD module is 50,51,52,53 in Arduino mega and the RX, TX is connected with 25 and 23 respectively. Port configurations are depicted below.

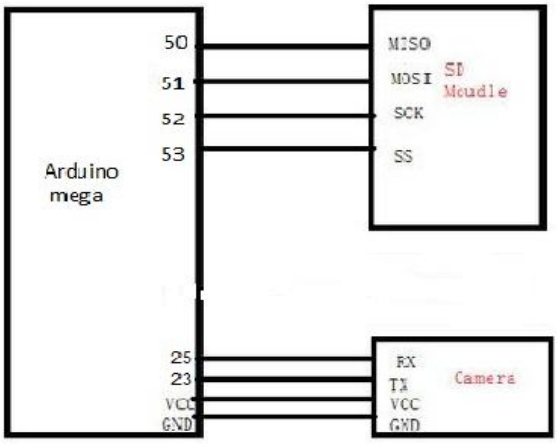

Fig. 03. Schematic diagram of Camera Setup

F. Solenoid lock

A simple circuit like below can be used to control a solenoid lock. But this circuit can be replaced by a relay. It's worth noting that a solenoid lock requires more current than an Arduino can provide directly from its output pins. We will use an alternative power source for solenoid due to its large power consumption. It will be driven by a TIP120 transtor.

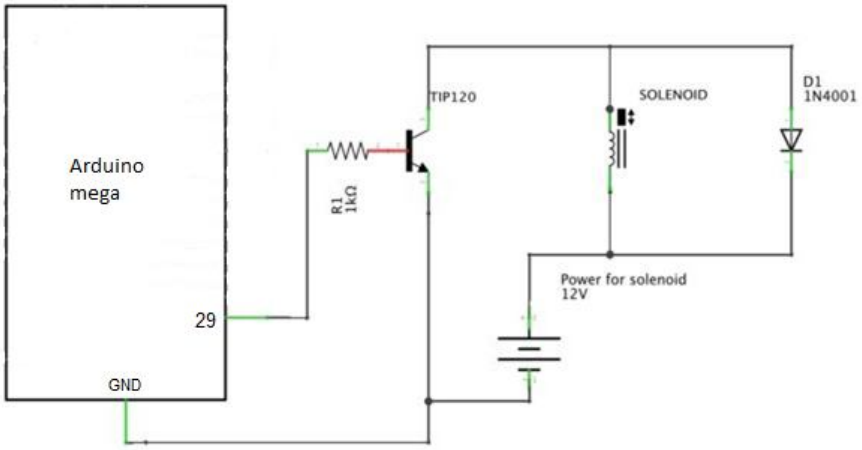

Fig. 04. Solenoid circuit

G. Buzzer

A simple buzzer is used in our project. Buzzer is actually an audio signaling device which can be mechanical, electrical, electro-mechanical. An auxiliary battery can be used so that it can operate if the main battery connection is cut down. A direct current of range 1.5V to 12.0V can be used as voltage supply to ensure smooth operation. As the voltage rises, the magnitude of sound of the buzzer becomes much louder.

4. Flowchart of the whole system

The whole system is described step by step in the flowchart. This system works on the basis of some logic. This flowchart represents those logic and decision making process. It shows all the possible outcomes of the system.

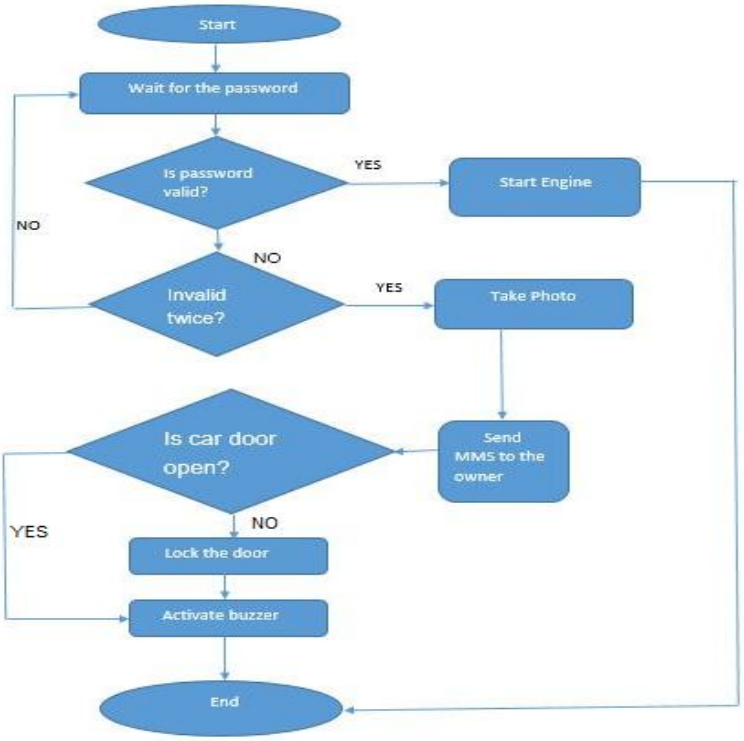

Fig. 05. Flowchart

5. Circuit diagram

The overall diagram of the circuit is just like the picture given below. This circuit diagram is developed in Fritzing circuit maker. It's a bit clumsy in this figure but PCB will make the appearance simple. Here Arduino is used for test basis.

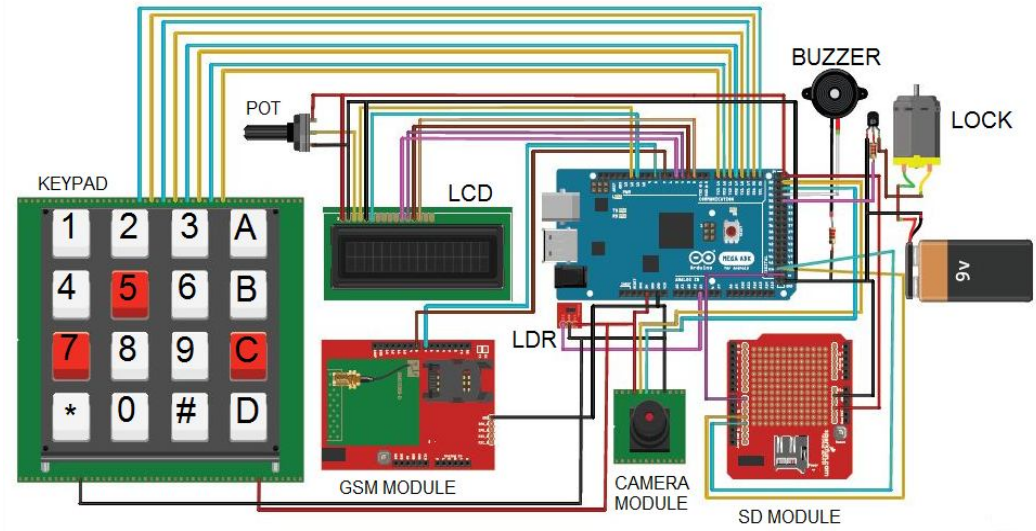

Fig. 06. Circuit Diagram

6. Test and result

The system is tested several times and each time it produced satisfactory result. Every single time when the entered password is wrong for twice, the solenoid lock and the camera acted simultaneously. And the GSM module sent MMS to the owner's mobile. LCD showed whether the system is blocked or ON.

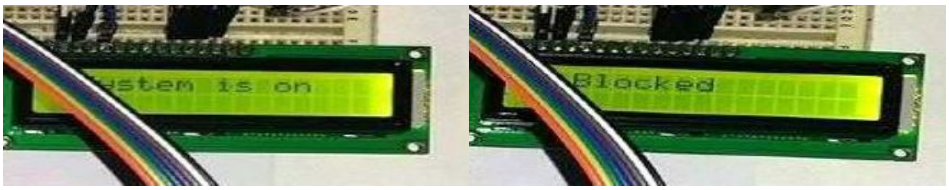

Fig. 07. Password varification output in the LCD

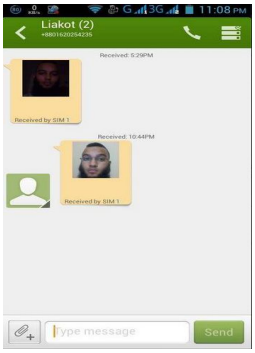

Fig. 08. MMS received in the owner's mobile

7. Conclusion

This project is so designed to make an anti-theft system in the vehicle. With this smart kit in the vehicle it is almost impossible to steal a vehicle. Besides, the owner can instantly get the picture of the thief so the Police can take a real effective step. This picture also works as an evidence against the thief. In near future, there is no doubt that all the vehicles will be embedded with this security system.

8. References

[1] Mohd Helmy Abd Wahab, IAEng Member, Suresh P. Gopalakrishna, Ayob Haji johari, "Speed Trap Image Transfer through GSM Network", *Proceedings of the World Congress on Engineering and Computer Science*, WCECS 2008, October 22-24, 2008, San Francisco, USA.

[2] B.G Nagaraja, Ravi Rayappa, M. Mahesh, Chandrasekhar M. Patil, Dr. T.C. Manjunath-"Design & Development of a GSM Based Vehicle Theft Control System" 978-0-7695-3516-6/08©2008 *IEEE*, DOI 10.1109/ICACC.2009.154, pp.148-152.

[3] D. A. Devi and A. Kumar, Design and Implementation of CPLD based Solar Power Saving System for Street Lights and Automatic Traffic Controller, *International Journal of Scientific and Research Publications*, Vol. 2, Issue11, November 2012.

[4] Mohammed Abuzalata, Muntaser Momani, Sayel Fayyad and Suleiman Abu-Ein, "A Practical Design of Anti-Theft Car Protection System Based on Microcontroller" *American Journal of Applied Sciences* 9 (5): 709-716, 2012, ISSN 1546-9239 © 2012 Science Publications.

[5] Mohammad Syuhaimi Ab-Rahman, Aminatul Hidayah Asmir, Kasmiran Jumari1, "Development of camera and GSM interfacing system for home security surveillance", Vol. 8(38), pp. 1858-1871, 11 October, 2013, DOI 10.5897/SRE11. 1807, ISSN 1992-2248 © 2013 Academic Journals.

[6] Vikas Singh, Prof. S.P.Karmore, "GSM and GPS BASED VEHICLE SECURITY and CONTROLLING SYSTEM", *International Journal of Engineering Research and Applications (IJERA)* ISSN: 2248-9622, International Conference on Industrial Automation and Computing (ICIAC- 12-13th April 2014)

[7] Ruchita J. Shah, Anuradha P. Gharge, "GSM Based Car Security System", *International Journal of Engineering and Innovative Technology (IJEIT)*, Volume 2, Issue 4, October 2012, ISSN: 2277-3754, ISO 9001:2008 Certified.

[8] Hnin Pwint Han, Hla Myo Tun, "Advanced Car Security System Using GSM", *International Journal of Scientific and Research Publications*, Volume 4, Issue 5, May 2014 1, ISSN 2250-3153.

[9] SIM900 MMS AT command manual V1.01,SIMCOM tech.

[10] http://www.instructables.com/id/Vehicle-security-with-GSM/

[11] Boylsted (2003), Electronic Device and Circuit Theory, Chapter-17, Linear-digital IC, page-742

[12] http://www.atmel.com/devices/atmega2560.aspx?tab=tools.